Thesis

Cytotoxicity of neuropathy-causing lipids 1-deoxy-sphingolipids

GALIH, Augustinus

Abstract

Hereditary sensory and autonomic neuropathy type IA and IC (HSAN IA/IC) are caused by autosomal dominant mutations that lead to the accumulation of atypical lipids called 1-deoxy-sphingolipids. How the lipids perturb the physiology of the cell are largely unknown. By combining genetics, lipidomics, and chemical proteomics approaches in the budding yeast, our study showed that there are two sequential and overlapping events in the cell. The first event comprises perturbations of actin organization, alteration of the shape of mitochondria, and formation of hydrophobic bodies by 1-deoxy-sphinganine. These aberrations, however, are not sufficient to kill the cell. The second event is the toxicity of C26 1-deoxy-ceramide. The lipid might directly inhibit a multisubunit essential protein that has broad impacts, directly inhibit multiple essential proteins, or perturb the structure of cellular membranes. Each of these perturbations is sufficient to kill the cell.

Reference

GALIH, Augustinus. *Cytotoxicity of neuropathy-causing lipids 1-deoxy-sphingolipids*. Thèse de doctorat : Univ. Genève, 2018, no. Sc. 5207

URN : urn:nbn:ch:unige-1045192
DOI : 10.13097/archive-ouverte/unige:104519

UNIVERSITÉ DE GENÈVE

Section de chimie et biochimie
Département de biochimie

FACULTÉ DES SCIENCES
Professeur Howard Riezman

Cytotoxicity of Neuropathy-causing Lipids 1-deoxy-sphingolipids

THÈSE

présentée à la Faculté des sciences de l'Université de Genève
pour obtenir le grade de Docteur ès sciences, mention biochimie

par

Augustinus GALIH

de

Yogyakarta (Indonésie)

Thèse N° 5207

GENÈVE

Atelier Repromail

2018

UNIVERSITÉ
DE GENÈVE
FACULTÉ DES SCIENCES

DOCTORAT ÈS SCIENCES, MENTION BIOCHIMIE

Thèse de Monsieur Augustinus GALIH

intitulée :

«Cytotoxicity of Neuropathy-causing Lipids 1-deoxy-sphingolipids»

La Faculté des sciences, sur le préavis de Monsieur H. RIEZMAN, professeur ordinaire et directeur de thèse (Département de biochimie), Monsieur R. J. LOEWITH, professeur ordinaire (Département de biologie moléculaire) et Monsieur T. HORNEMANN, professeur (Institute for Clinical Chemistry, University Hospital Zurich, Switzerland), autorise l'impression de la présente thèse, sans exprimer d'opinion sur les propositions qui y sont énoncées.

Genève, le 4 mai 2018

Thèse - 5207 -

Le Doyen

N.B. - La thèse doit porter la déclaration précédente et remplir les conditions énumérées dans les "Informations relatives aux thèses de doctorat à l'Université de Genève".

To my parents

Table of Contents

Résumé 1

Summary 4

Introduction 7

1. Sphingolipid homeostasis 7

1.1. Sphingolipid metabolism 7

1.2. Regulation of biosynthesis 10

1.3. Regulation of trafficking and degradation 13

2. Modes of action of sphingolipids 15

2.1. Sphingolipids as components of cellular membranes 15

2.2. Sphingolipids as direct modulators of protein functions 19

3. Hereditary sensory and autonomic neuropathy type IA and IC 22

Materials and Methods 27

Results 37

1. 1-deoxy-sphingolipids are toxic to the budding yeast 37

1.1. 1-deoxy-ceramides are the main toxic lipids 37

1.2. Toxicity of 1-deoxy-ceramide depends on the length of its acyl chain 38

1.3. 1-deoxy-ceramide has distinct biological properties 40

2. Genetic screens reveal the natures of the toxicity of 1-deoxy-sphingolipids 43

2.1. 1-deoxy-sphingolipids disrupt multiple cellular processes 43

2.2. Toxicity of 1-deoxy-sphingolipids involves inhibition of nuclear migration 47

2.3. Sap190 ensures the normal proportion of C_{24} to C_{26} fatty acyl-CoA 51

3. Features of the toxicity of 1-deoxy-sphingolipids 55

3.1. 1-deoxy-sphinganine disrupts the organization of actin 55

3.2. Toxicity of 1-deoxy-sphingolipids does not involve oxygen-dependent functions of mitochondria 57

3.3. 1-deoxy-sphinganine induces the formation of hydrophobic bodies 65

4. Chemical proteomics captures potential targets of 1-deoxy-ceramide 69

5. *C. elegans* model of hereditary sensory and autonomic neuropathy type IA 73

General Discussion 78

Conclusions 89

Perspectives 90

References 91

Acknowledgements 106

Résumé

La neuropathie héréditaire sensorielle et autonome (HSAN) de type IA et IC sont des maladies neurologiques héréditaires qui affectent les fonctions sensorielles et autonomes du système nerveux périphérique. Les maladies sont causées par des mutations dominantes dans les gènes qui codent pour la sérine palmitoyltransférase (SPT), qui est la première enzyme dans la voie de la biosynthèse des sphingolipides *de novo*. Les mutations améliorent la promiscuité du SPT du substrat, conduisant à une augmentation de la synthèse des 1-désoxy-sphingolipides (1-doxSphs). Depuis 1-doxSphs sont métaboliquement piégés, ils ont tendance à s'accumuler au fil du temps. Comment les niveaux élevés de 1-doxSphs perturbent la physiologie de la cellule et comment ces perturbations émergent comme HSAN IA/IC chez l'homme sont largement inconnues.

Nous avons utilisé la levure bourgeonnante comme système modèle pour étudier le mécanisme de la cytotoxicité des 1-doxSphs puisque la levure produit également de faibles niveaux de 1-doxSphs au cours de sa croissance normale. Les 1-doxSphs sont constitués de bases 1-désoxy-sphingoïdes (1-doxSB) et de 1-désoxy-céramides (1-doxCers). En surexprimant la céramide synthase, nous pourrions déterminer que les 1-doxCers sont les principaux lipides toxiques. Les 1-doxCers sont constitués de 1-désoxy-céramide (1-doxCer) et de 1-déoxyméthyl-céramide (1-doxmetCer). Nous avons décidé de nous concentrer sur 1-doxCer car nous avons réussi à sensibiliser la levure à 1-doxCer plus qu'à 1-doxmetCer. Des tests de croissance et des analyses lipidomiques ont montré que la toxicité du 1-doxCer dépend de la longueur de sa chaîne acyle. De plus, son mécanisme de toxicité est distinct de ceux des autres lipides.

Pour élucider le mécanisme de la cytotoxicité de 1-doxCer, nous avons réalisé trois criblages génétiques à l'échelle du génome. Les écrans ont révélé que le 1-doxCer pouvait - du

mécanisme le plus probable - inhiber directement une protéine essentielle multisubunitaire dont l'inhibition conduit à des défaillances dans de multiples processus cellulaires, inhibe directement plusieurs protéines essentielles impliquées dans divers processus cellulaires ou perturbe la structure des membranes cellulaires. De plus, la toxicité de 1-doxSphs implique l'inhibition de la migration nucléaire. Les cribles ont également révélé Sap190 comme une nouvelle protéine qui assure la proportion normale d'acyl-CoA gras en C_{24} à C_{26}. Comment Sap190 réalise cette fonction reste à étudier.

Nous avons ensuite examiné si les cellules de levure présentaient également les mêmes phénotypes que les cellules de mammifères après l'accumulation de 1-doxSphs. La microscopie de différentes souches comprenant des mutants résistants révélés par les criblages a montré que la 1-désoxy-sphinganine (1-doxSa) provoque des perturbations de l'organisation de l'actine pouvant conduire à l'inhibition de la migration nucléaire. Il a également montré que 1-doxSa modifie la forme des mitochondries. Cette altération n'était pas accompagnée d'une inhibition des fonctions clés des mitochondries. De plus, il a montré que 1-doxSa induit la formation de corps hydrophobes distincts des gouttelettes lipidiques canoniques.

Pour rechercher les cibles moléculaires de 1-doxCer, nous avons adopté une approche de protéomique chimique en utilisant des analogues de lipides photoréticulables et cliquables. L'approche a capturé deux cibles potentielles de 1-doxCer. Ce sont des vésicules COPII qui sont nécessaires pour le transport vésiculaire de l'ER vers le Golgi et le complexe T contenant de la chaperonine (CCT) qui est nécessaire pour le repliement de nombreuses protéines dans le cytosol.

Pris ensemble, notre étude a montré qu'il y a deux événements séquentiels et se chevauchant dans la cellule. Le premier événement comprend les effets de 1-doxSa qui comprennent les perturbations de l'organisation de l'actine, l'altération de la forme des mitochondries et la formation de corps hydrophobes. Ces aberrations, cependant, ont des

impacts mineurs sur la physiologie de la cellule. Le deuxième événement est la toxicité de 1-doxCer qui a des impacts majeurs sur la physiologie de la cellule. Nous proposons que ce dernier événement est réalisé par l'inhibition d'une protéine essentielle multi-sous-unité, telle que le manteau de vésicule COPII ou CCT.

Enfin, pour étudier les rôles des 1-doxSphs dans des organismes plus complexes, nous avons établi un modèle de *C. elegans* de HSAN IA. La combinaison de la mutation HSAN IA dans SPT et d'une mutation dans une céramide synthase (*hyl2(tm2031)*) qui augmente l'accumulation de 1-doxCer, réduit la capacité des vers à capter la chaleur de l'environnement et les sensibilise à l'anoxie.

Summary

Hereditary sensory and autonomic neuropathy (HSAN) type IA and IC are inherited neurological diseases that affect the sensory and autonomic functions of the peripheral nervous system. The diseases are caused by dominant mutations in the genes that encode for serine palmitoyltransferase (SPT), which is the first enzyme in the *de novo* sphingolipid biosynthesis pathway. The mutations enhance the substrate promiscuity of SPT, leading to increased synthesis of 1-deoxy-sphingolipids (1-doxSphs). Since 1-doxSphs are metabolically trapped, they tend to accumulate over time. How elevated levels of 1-doxSphs perturb the physiology of the cell and how these perturbations emerge as HSAN IA/IC in humans are largely unknown.

We used the budding yeast as a model system to study the mechanism of cytotoxicity of 1-doxSphs since the yeast also produces low levels of 1-doxSphs during its normal growth. 1-doxSphs consist of 1-deoxy-sphingoid bases (1-doxSB) and 1-deoxy-ceramides (1-doxCers). By overexpressing ceramide synthase, we could determine that 1-doxCers are the main toxic lipids. 1-doxCers consist of 1-deoxy-ceramide (1-doxCer) and 1-deoxymethyl-ceramide (1-doxmetCer). We decided to focus on 1-doxCer as we managed to sensitize the yeast to 1-doxCer more than to 1-doxmetCer. Growth assays and lipidomic analyses showed that the toxicity of 1-doxCer depends on the length of its acyl chain. Moreover, its mechanism of toxicity is distinct from those of other lipids.

To elucidate the mechanism of cytotoxicity of 1-doxCer, we performed three genome-wide genetic screens. The screens revealed that 1-doxCer might - from the most probable mechanism - directly inhibit a multisubunit essential protein whose inhibition leads to failures in multiple cellular processes, directly inhibit multiple essential proteins implicated in diverse cellular processes, or perturb the structure of cellular membranes. Moreover, the toxicity of 1-doxSphs involves inhibition of nuclear migration. The screens also revealed Sap190 as a novel

protein that ensures the normal proportion of C_{24} to C_{26} fatty acyl-CoA. How Sap190 achieves this function remains to be investigated.

We then examined whether yeast cells also exhibit the same phenotypes as mammalian cells following 1-doxSphs accumulation. Microscopy of different strains including resistant mutants revealed by the screens showed that 1-deoxy-sphinganine (1-doxSa) causes perturbations of actin organization which might lead to inhibition of nuclear migration. It also showed that 1-doxSa alters the shape of mitochondria. This alteration was not accompanied by inhibition of key functions of mitochondria. Moreover, it showed that 1-doxSa induces the formation of hydrophobic bodies that are distinct from the canonical lipid droplets.

To hunt for the molecular targets of 1-doxCer, we took a chemical proteomics approach using photocrosslinkable and clickable lipid analogs. The approach captured two potential targets of 1-doxCer. They are COPII vesicle coat which is required for vesicular transport from the ER to the Golgi and chaperonin-containing T-complex (CCT) which is required for folding of many proteins in the cytosol.

Taken together, our study showed that there are two sequential and overlapping events in the cell. The first event comprises the effects of 1-doxSa which include perturbations of actin organization, alteration of the shape of mitochondria, and formation of hydrophobic bodies. These aberrations, however, have minor impacts on the physiology of the cell. The second event is the toxicity of 1-doxCer which has major impacts on the physiology of the cell. We propose that this latter event is achieved by inhibition of a multisubunit essential protein, such as COPII vesicle coat or CCT.

Finally, to study the roles of 1-doxSphs in more complex organisms, we established a *C. elegans* model of HSAN IA. The combination of the HSAN IA mutation in SPT and a mutation in a ceramide synthase (*hyl2(tm2031)*) that enhances the accumulation of 1-doxCer,

reduced the ability of the worms to sense heat from the environment and sensitized them to anoxia.

Introduction

Sphingolipids compose a group of diverse metabolites that carry a sphingoid base (also called long-chain base) as a backbone of their molecules (**Fig. 1**). Sphingolipids are exceptionally versatile lipids as they are able to serve as structural components of cellular membranes and as direct modulators of protein functions in the cell. As a consequence, they play roles in a wide range of cellular processes. Furthermore, the cell must precisely regulate their levels as imbalances in sphingolipid levels lead to disabling diseases with complex clinical manifestations in humans [1,2].

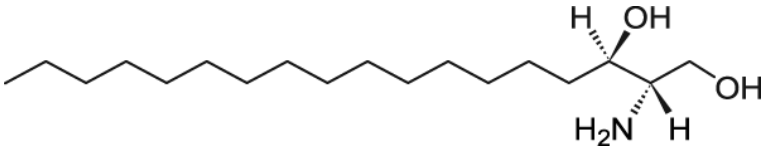

Figure 1. Chemical structure of a sphingoid base.

1. Sphingolipid homeostasis

1.1. Sphingolipid metabolism

Sphingolipids are essential for survival for most organisms. Significant fractions of sphingolipids in these organisms are derived from *de novo* biosynthesis consistent with the finding that the activity of the first enzyme of the pathway, serine palmitoyltransferase (SPT) is indispensable. The main pathways of sphingolipid metabolism are highly conserved from yeast to human. Most enzymes in the biosynthetic and degradation pathways are distributed along the secretory and endocytic pathways, respectively [3]. As a consequence, many sphingolipids are transformed into more complex or simpler sphingolipids as they are transferred along the secretory or endocytic pathway, respectively. *De novo* biosynthesis of sphingolipid requires serine, whereas degradation of sphingolipid produces hexadecenal and

phosphoethanolamine that are used for the production of another category of lipid, glycerolipid (**Fig. 2**). Sphingolipid metabolism, therefore, links amino acid metabolism to glycerolipid metabolism [4,5]. For more detailed and extensive review on sphingolipid metabolism, readers are referred to these publications [6,7].

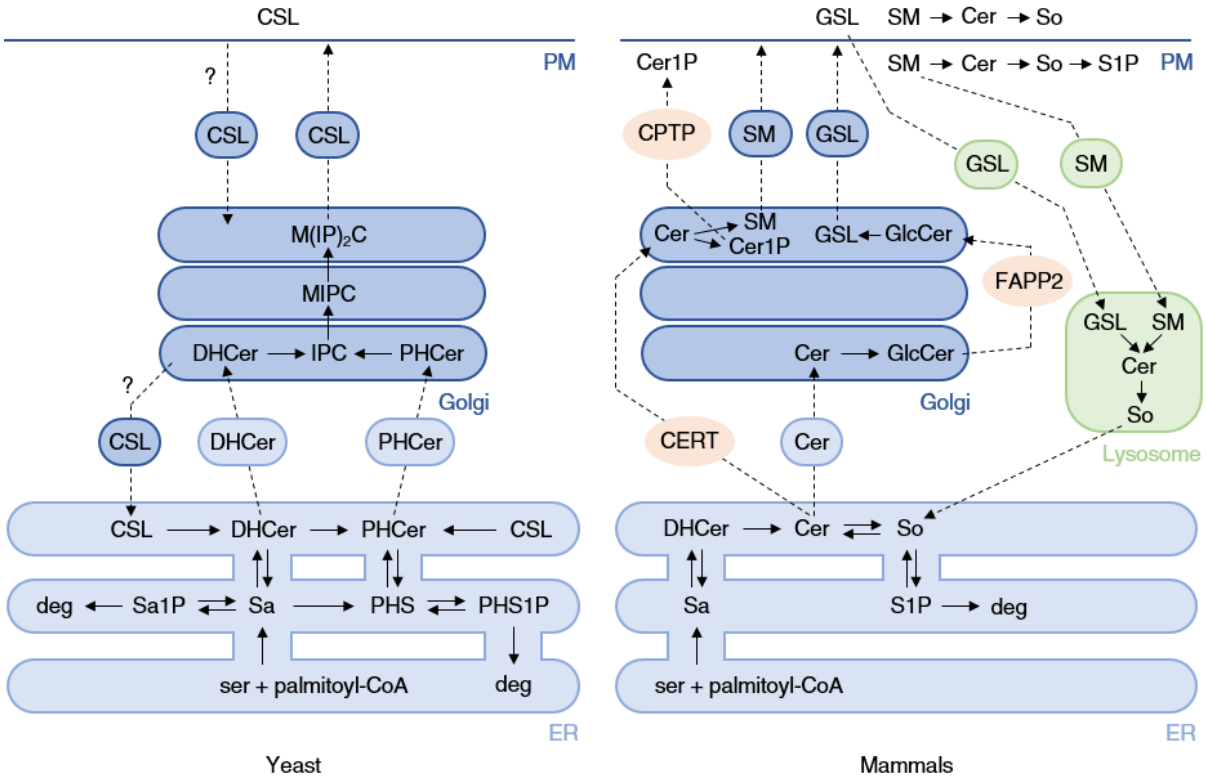

Figure 2. Overviews of sphingolipid metabolic pathways in yeast and mammals. ser: serine, Sa: sphinganine, Sa1P: sphinganine 1-phosphate, PHS: phytosphingosine, PHS1P: phytosphingosine 1-phosphate, So: sphingosine, S1P: sphingosine 1-phosphate, DHCer: dihydroceramide, Cer: ceramide, PHCer: phytoceramide, IPC: inositol-phosphoceramide, MIPC: mannose-inositol-phosphoceramide, $M(IP)_2C$: mannose-(inositol-P)$_2$-ceramide, CSL: complex sphingolipids (IPC, MIPC, $M(IP)_2C$), GlcCer: glucosylceramide, GSL: glycosphingolipid, SM: sphingomyelin, Cer1P: ceramide 1-phosphate, deg: degradation.

The first step in *de novo* biosynthesis of sphingolipid is the condensation of serine with palmitoyl-CoA by SPT at the cytosolic leaflet of the endoplasmic reticulum (ER) membrane. This reaction produces a sphingoid base, 3-ketosphinganine which rapidly undergoes reduction to form sphinganine [8]. In the budding yeast, most sphinganine is hydroxylated to form

phytosphingosine. Next, sphinganine or phytosphingosine is coupled with very long-chain fatty acyl-CoA to synthesize dihydroceramide or phytoceramide, respectively [9]. In mammals, sphinganine is coupled with fatty acyl-CoA by a family of enzymes, ceramide synthase (CerS) to produce dihydroceramide which is then desaturated to form ceramide [10]. The bulk of ceramide is directly transferred to the *trans*-Golgi network (TGN) by a dedicated ceramide transfer protein CERT [11]. At the TGN, the headgroup of ceramide can be phosphorylated by ceramide kinase to form ceramide 1-phosphate [12] or alternatively can be linked to phosphorylcholine by sphingomyelin synthase to form sphingomyelin [13]. Smaller fractions of ceramide in the ER membrane may be carried by anterograde vesicular transport to the *cis*-Golgi network. Part of this pool of ceramide could be converted to glucosylceramide which is then delivered to the TGN by a glucosylceramide transfer protein FAPP2 [14,15] for the synthesis of more complex glycosphingolipids [16]. From the TGN, ceramide 1-phosphate is delivered by a dedicated transfer protein CPTP [17], whereas the other complex sphingolipids are carried by vesicles to the plasma membrane (PM) [18].

The degradation routes for most sphingolipids are in the opposite direction of their biosynthesis routes as most biosynthetic reactions have opposing reactions, most often by specific enzymes rather than reversal of the biosynthetic enzymes. For example, the most abundant complex sphingolipid in humans, sphingomyelin is degraded through the hydrolysis of its headgroup generating ceramide and free phosphocholine instead of phosphatidylcholine which is the substrate used in its synthesis. The reaction is catalyzed by the sphingomyelinase enzyme family. The enzymes are classified based on their cation dependence and pH optima of activity into acid, neutral, or alkaline sphingomyelinase. The main enzymes are acid sphingomyelinase in lysosomes or in the extracellular space (secreted) and neutral sphingomyelinase in various cellular compartments [19,20,21]. Next, ceramide is deacylated by ceramidases releasing sphingosine. Ceramidases are also classified based on their pH optima

of activity into acid, neutral, or alkaline ceramidase [22]. The released sphingosine is either fed into the salvage pathway or phosphorylated to form sphingosine 1-phosphate (S1P) [23]. S1P is then irreversibly degraded by S1P lyase in the ER to generate hexadecenal and phosphoethanolamine. S1P lyase has broad substrate specificity and therefore it can degrade all phosphorylated sphingoid bases in mammals [24].

1.2. Regulation of biosynthesis

The focal point of regulation of global sphingolipid levels is SPT since it catalyzes the first and rate-limiting step of the *de novo* biosynthesis pathway. There are two ER transmembrane protein families that negatively regulate the activity of SPT, Orm and Nogo-B. In the budding yeast, Orm1/2 physically associate with SPT as parts of the SPOTS complex. Orm1/2 directly inhibit the activity of SPT when the cell has sufficient levels of sphingolipid. The extent of the inhibition correlates with the inverse of the degree of Orm1/2 phosphorylation which is modulated by sphingolipid levels. The nature of this inhibitory mechanism enable homeostatic regulation that is rapid, sensitive, finely tuned, and responsive to multiple cues [25]. Orm1/2 are inhibited by Npr1 via the target of rapamycin complex 1 (TORC1) signaling pathway following nutrient starvation [26] or by Ypk1 via the TORC2 signaling pathway following sphingolipid depletion [27] or heat stress [28]. In mammals, ORMDL1-3 redundantly inhibit the activity of SPT in response to elevated levels of ceramide and more complex sphingolipids [29]. The regulation of the inhibition is still largely unknown since the phosphorylation sites of Orm1/2 in yeast are not found in ORMDLs. Several single-nucleotide polymorphisms in ORMDL3 gene have been associated with the risk of childhood asthma [30], although this association is not due to altered sphingolipid levels [31,32]. Another regulator of SPT, Nogo-B is expressed in both endothelial and smooth muscle cells. It forms a complex with SPT and ORMDLs and selectively inhibits the activity of SPT in endothelial cells to

control vascular function, blood pressure [33], and heart function [34]. However, not all organisms bearing SPT have Orm or Nogo-B protein (e.g. *C. elegans*), suggesting that there are other possible mechanisms of SPT regulation.

The production of ceramide as the central metabolite in sphingolipid metabolism is also subjected to regulation. The regulation of CerS is achieved via phosphorylation, protein turnover, and controlling the availability of its substrates. In the budding yeast, CerS comprises homo- and/or hetero-dimer of Lag1 and Lac1 with at least two essential regulatory subunits Lip1 [35,36]. The optimal activity of CerS requires C_{26} fatty acyl-CoA and phosphorylation in its conserved C-terminal regions by casein kinase 2 (CK2) [37,38]. Following sphingolipid depletion or heat stress, TORC2 promotes Ypk1 to phosphorylate the N-terminal regions of CerS to enhance ceramide production [39]. The involvement of CK2, which has broad roles in cell growth and proliferation as well as TORC2, which regulates cell growth in response to nutrient availability in the regulation indicate that ceramide level is subjected to constant adjustments for optimum cell growth. In mammals, there are six CerSs that are expressed at different levels in different tissues. They have strong yet overlapping preferences for different lengths of fatty acyl-CoA. CerS are mainly regulated post-translationally since their mRNA levels do not always reflect the profile of ceramide species in the tissue [40]. CerS1 is structurally distinct among CerSs [41] and regulated by a distinct mechanism. It has a short half-life that is regulated by the opposing actions of p38 mitogen-activated protein kinase (MAPK) as a positive regulator and protein kinase C (PKC) as a negative regulator. Its turnover requires its activity, indicating a negative feedback mechanism for its regulation [42]. The activities of CerS2-6 are stimulated by phosphorylation in the C-terminal regions. Except for CerS3, the phosphorylation is mediated by CK2, suggesting a conserved regulatory mechanism for ceramide synthesis [43].

Another key point of regulation is sphingosine kinase (SK) that phosphorylates sphingosine to form S1P. The activity of SK contributes to the delicate balance between the level of death-promoting ceramide and the level of growth-promoting S1P. This balancing mechanism is referred to as the "sphingolipid rheostat" [44]. S1P may act as a direct modulator of intracellular proteins or as a signaling molecule that functions in an autocrine and/or paracrine fashion. The latter mechanism is mediated by G-protein-coupled receptors, S1P1–5 at the cell surface [45,46]. These receptors, however, are not found in the budding yeast. The function of SK is regulated by modulation of their catalytic activity and subcellular localization [47]. The activity of SK1 is increased upon phosphorylation of its Ser225 by extracellular signal-regulated kinase 1 and 2 (ERK1/2). The phosphorylation is also required for translocating SK1 from the cytosol to the cytosolic leaflet of the PM. This translocation might direct SK1 to the available pool of sphingosine and localize the production of S1P [48]. Cytosolic SK1 is bound by a Ca^{2+}-myristoyl switch protein CIB1 in a Ca^{2+}-dependent manner and ferried to the PM [49]. Once on the PM, only phosphorylated SK1 is retained via its physical interaction with phosphatidylserine [50]. In most cases, the increased activity of SK1 is transient since phosphorylated Ser225 is rapidly dephosphorylated by protein phosphatase 2 [51]. Similar to that of SK1, the activity of SK2 is also enhanced upon phosphorylation by ERK1/2, albeit at different sites. ERK1/2 phosphorylate SK2 at Ser351 and Thr578 [52]. SK2 can also be phosphorylated by protein kinase D (PKD) at either Ser383 or Ser385 within its nuclear export signal sequence to promote its exit from the nucleus to the cytosol [53], therefore relieving its inhibition on DNA synthesis [54]. The fact that the cell employs ERK1/2 as main regulators of SK activity indicates that the level of S1P is adjusted in accordance with various extracellular stimuli that modulate cell proliferation, differentiation, and survival.

1.3. Regulation of trafficking and degradation

The intracellular trafficking of most sphingolipids relies on membrane vesicle trafficking and cytosolic lipid transfer proteins (LTPs) [3]. Since LTPs have specificities for lipid clients and operate at particular subcellular compartments, the regulation of LTPs provides means for modulating particular routes in sphingolipid metabolism. Among those that transfer sphingolipids in mammals, CERT and its regulation are best understood. CERT has three functional regions; a PH domain that binds phosphatidylinositol 4-phosphate at the cytosolic leaflet of the TGN, an FFAT motif that binds to VAP-A at the ER membrane, and a START domain that binds ceramide [11]. The function of CERT is suppressed by phosphorylation of the serine-repeat (SR) motif at the C-terminal side of the PH domain as it induces an interaction between the PH and the START domains. The phosphorylation is reduced following sphingomyelin or cholesterol depletion, suggesting that the function of CERT is regulated in response to sphingomyelin or cholesterol levels [55,56]. Two kinases have been shown to phosphorylate CERT at the SR motif; PKD (PKD1/2) and CKIγ2 [57,58]. PKD inhibits the function of CERT, thus reducing the synthesis of sphingomyelin at the TGN. Since the synthesis of sphingomyelin releases diacylglycerol which can activate PKD, its inhibition suppresses further activation of PKD. This series of events creates a negative feedback mechanism for regulating the function of CERT [57]. In contrast, the function of CERT is enhanced upon dephosphorylation by PP2Cε [59] or phosphorylation at Ser315 at the N-terminal side of the FFAT motif [60].

The degradation of complex sphingolipids and ceramide in mammals releases sphingosine which is routed either to irreversible degradation or to the salvage pathway. The latter route can contribute 50-90% towards sphingolipid biosynthesis when measured in various cell lines [61,62]. In addition, the cell needs to coordinate the *de novo* biosynthesis with the degradation of sphingolipid for optimum growth and survival as has been shown in

the budding yeast during nutrient limitation [63] or heat [64] stress. In human myotubes, the coordination might involve a phasic mechanism since the levels of dihydroceramide and ceramide peak at different times of the day [65]. Despite its significance, the regulation of sphingolipid degradation is largely unknown. Nevertheless, many factors affecting the functions of sphingomyelinase and ceramidase have been characterized. Acid sphingomyelinase (a-SMase) is targeted either to lysosomes or to the extracellular space depending on *N*-glycosylation [66], phosphorylation [67], and its signal peptide [68]. In response to ionizing radiation stress, protein kinase C-δ (PKCδ) binds to and phosphorylates a-SMase at Ser508. The phosphorylation promotes the translocation of a-SMase from the cytosol to the PM and increases its activity [69]. Neutral sphingomyelinase 2 (n-SMase2) is the predominant n-SMase [70,71]. Its activity is enhanced by several stimuli. The inflammatory cytokine tumor necrosis factor-α (TNFα) induces the translocation of EED from the nucleus to the PM, where it physically links n-SMase2 to the TNF-R1•FAN•RACK1-complex, resulting in the activation of n-SMase2 [72,73]. Oxidative stress induces the degradation of calcineurin that binds to n-SMase2, thereby allowing phosphorylation of the enzyme by p38 MAPK and protein kinases Cs to increase its activity [74,75]. Anionic phospholipids, especially phosphatidylserine and phosphatidic acid [76] bind to specific regions of the enzyme and promote its activity [77,78]. In addition, *in vitro* study showed that the activity of n-SMase is modulated by sphingomyelin/ceramide molar ratio of the membrane, suggesting a feedback loop mechanism for its regulation [79]. Alkaline sphingomyelinase (alk-SMase) is present in the intestinal tract and human bile [21]. High-fiber diet increases its activity, whereas high-fat diet greatly reduces it [80,81,82].

Human acid ceramidase is synthesized as a polypeptide which undergoes self-cleavage producing the α and ß subunits of the enzyme. The self-cleavage occurs most rapidly at acidic pH, indicating that generation of the active water-soluble heterodimeric enzyme takes place

mainly in endosomes and/or lysosomes where it exerts its function [83,84]. The efficient degradation of ceramide by acid ceramidase in lysosomes requires sphingolipid activator proteins (saposins) [85,86], anionic lysosomal phospholipids, and high membrane curvature [87]. The anionic phospholipids might promote the association between acid ceramidase and the membrane. Subsequently, saposins might perturb lipid packing in the membrane, thereby facilitating the enzyme to get a better access to its hydrophobic substrate [87]. Neutral ceramidase is localized at the PM as a type II integral membrane protein. The *O*-glycosylation of the mucin-like domain in the N-terminal region is required for retaining the enzyme at the PM [88]. On the other end, conserved amino acid residues in the C-terminal region are essential for the proper folding, trafficking, and activity of the enzyme [89]. The degradation rate of the enzyme by the ubiquitin/proteasome complex is increased in response to a diffusible intercellular messenger, nitric oxide [90]. This event is antagonized by PKC [91]. The most studied alkaline ceramidase, alkaline ceramidase-2 (ACER2) resides at the Golgi membrane and requires Ca^{2+} in the Golgi lumen for its activity [92]. The activity of ACER2 is increased following the activation of a proto-oncogene c-Src [93]. In mesangial cells, the activity of alkaline ceramidase is enhanced by platelet-derived growth factor [72]. Besides dedicated ceramidase, other proteins with intrinsic ceramidase activity also contribute to the degradation of ceramide. The adiponectin receptor 1/2 degrades ceramide upon adiponectin binding, thereby tipping the balance of the "sphingolipid rheostat" in favor of sphingosine and S1P to increase insulin sensitivity, decreases inflammation, and promotes cell survival [94,95].

2. Modes of action of sphingolipids

2.1. Sphingolipids as components of cellular membranes

The lipid component of cellular membranes is composed mainly of glycerolipid, followed by sterol, and sphingolipid. Sphingolipids affect the properties of the membrane

where they reside in several ways due to their unique properties. Compared to the major glycerolipids, ceramide and complex sphingolipids have a longer and more saturated acyl chain [96]. They are also more rigid because of the configuration of the amide group and the presence of a double bond at position 4-5 of sphingosine. In addition, they are more capable of forming hydrogen bonds with other sphingolipids or with cholesterol [97,98]. These properties enable them to promote tighter lipid packing and thereby increasing the thickness and rigidity of the membrane. Furthermore, they drive lipid phase separation in artificial membranes by forming a liquid-ordered (L_o) phase together with cholesterol or a gel-phase together with other sphingolipids in the midst of a liquid-disordered (L_d) phase of glycerolipids [99,100,101] (**Fig. 3a**). These abilities make them suitable as components of hydrophobic physical barriers.

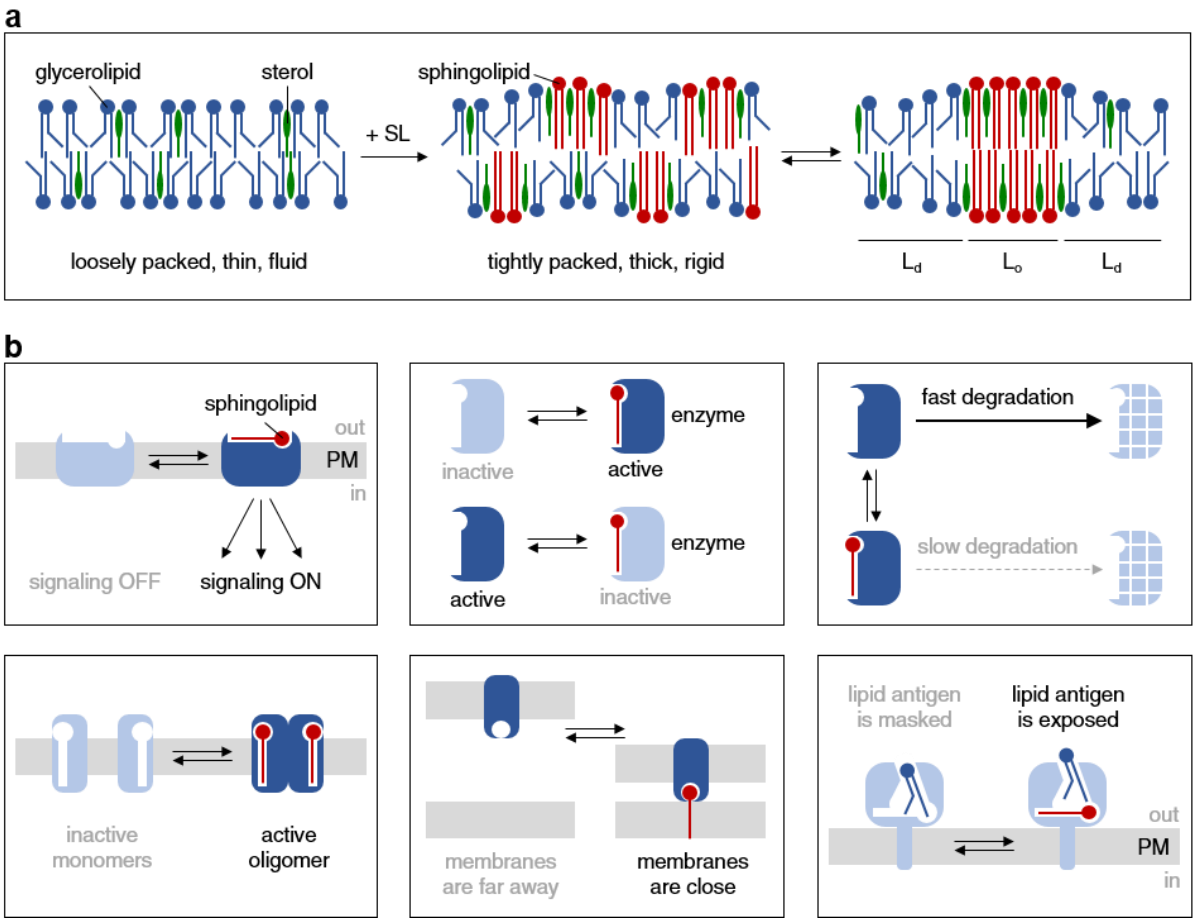

Figure 3. Modes of action of sphingolipids in the cell. (**a**) Impacts of sphingolipids on the properties of the lipid bilayer. (**b**) Sphingolipids as direct modulators of protein functions.

In the budding yeast, sphingolipids constitute a barrier at the ER membrane in the bud neck. The barrier hinders the diffusion of misfolded proteins associated with the ER membrane from the mother cell to the daughter cell and thereby protecting the daughter cell from their adverse effects [102]. In mammals, the PM of intestinal cells is polarized into apical and basolateral domains with distinct lipid composition. Glycosphingolipids are enriched at the expense of glycerolipids in the apical PM. Such enrichment was thought to stabilize the membrane to cope with conditions in the external environment that are harsher than those in the internal milieu [103]. Indeed, depletion of the main mammalian ceramide synthase causes disruptions to colon barrier function and epithelial integrity in mice [104]. In humans, ceramide represents about 50% of lipid in the extracellular matrix of corneocytes in the stratum corneum of skin [105]. Since the stratum corneum protects the body from exsiccation and infection [106], disruption of genes involved in the biosynthesis of skin ceramide leads to fatal consequences in mice [107,108] and humans [109].

The preferential associations of sphingolipids with cholesterol and other lipids bearing saturated acyl chains led to a notion that these lipids form micron-sized clusters termed “lipid rafts” within cellular membranes. Lipid rafts were originally postulated as platforms for lipid-driven sorting of lipids and proteins destined to the apical PM at the TGN of polarized epithelial cells. The function of lipid rafts was later extended beyond membrane trafficking to include signal transduction at the PM [103,110]. Immunoisolated vesicles budded from the TGN using artificial or natural PM proteins as baits in the budding yeast are enriched with sphingolipids and sterol [111,112]. Furthermore, sphingomyelin is enriched in a subset of TGN-derived vesicles that are also enriched with a glycosylphosphatidylinositol(GPI)-anchored protein, but not with an integral membrane secretory protein (CD8α) in a human cell line [113]. In addition, glycosphingolipids are required for maintaining apicobasal polarity in *C. elegans* [114]. These data together indicate that sphingolipids play a key role in the sorting of lipids and proteins

destined to the PM at the TGN. However, direct evidence of the existence and the physiological relevance of lipid rafts at the PM has yet to be obtained [115]. Direct observations of lipids or GPI-anchored proteins using Förster resonance energy transfer (FRET) [116,117,118], high-speed imaging and single-molecule tracking [119,120], or stimulated emission depletion (STED) nanoscopy-fluorescence correlation spectroscopy (FCS) [121,122] at the PM of living mammalian cells showed non-homogenous and dynamic lateral distribution of lipids and lipid-anchored proteins. Furthermore, such distribution is not only a consequence of the intrinsic properties of the lipids, but also their interactions with transmembrane proteins and the cortical actin meshwork [123,124]. This more elaborate organization of the PM is expected to serve physiological functions [125].

A type of distinct region that is enriched with sphingolipids and cholesterol at the PM is caveolae. Caveolae have a flask or an open cup shape of 60-80 nm wide where the opening faces towards the extracellular space. They are marked by oligomeric membrane-associated proteins named caveolins. Caveolae have been implicated in endocytosis, metabolic regulation of lipids, signal transduction, and mechanosensation, depending on the cell type and organ system [126,127,128]. As part of their mechanosensation function, caveolae were thought to serve as membrane reservoirs that immediately flatten upon acute mechanical stress induced by osmotic swelling or by uniaxial stretching, thereby allowing PM expansion and preventing PM rupture. Once the stress is relieved, caveolae are formed again in an ATP- and actin-dependent manner [129,130]. The PM of the budding yeast also has furrows that have a similar shape to caveolae. They are occupied by transporters, including the arginine permease Can1 [131] and generated by large protein complexes named eisosomes [132]. Besides providing a similar mechanosensation function to that of caveolae [133], the furrows are implicated in the regulation of sphingolipid levels. Following sphingolipid depletion, the furrows have been postulated to flatten and therefore liberate BAR domain-containing proteins, Slm1/2 that were

associated with them. The released proteins remain attached to the cytosolic leaflet of the PM and become available for TORC2. In turn, this newly assembled complex activates Ypk1/2 kinases to phosphorylate Orm proteins, thereby relieving their inhibition on SPT and increasing the rate of sphingolipid biosynthesis [134].

2.2. Sphingolipids as direct modulators of protein functions

Sphingolipids can also exert their roles by directly modulating the functions of proteins in several ways (**Fig. 3b**). First, sphingolipids function as ligands for receptors at the cell surface to initiate intracellular signaling cascades. S1P generated inside the cell targets different proteins [135] to promote cell proliferation and to suppress apoptosis [136]. Alternatively, S1P can be secreted as a signaling molecule that functions in an autocrine and/or paracrine fashion termed "inside-out" signaling. The mechanisms of S1P secretion are different in different cell types. Mast cells secrete S1P in an ATP-dependent manner [137], zebrafish yolk syncytial layer cells and mouse endothelial cells passively secrete S1P through a transporter [138,139], whereas erythrocytes and platelets are able to secrete S1P by both mechanisms [140,141]. In the circulation, S1P binds to either apolipoprotein M in high-density lipoprotein particles or albumin, generating two distinct pools of S1P for different physiological roles [142]. Extracellular S1P binds to five specific seven transmembrane-spanning G-protein-coupled receptors, S1P1–5 at the cell surface and stimulates their activities. Each receptor is coupled to a defined yet overlapping set of G-proteins that function in a wide range of cellular processes. The net result of S1P signaling via the S1P receptors affects cell survival, proliferation, migration, and differentiation [45,46]. Since aberrant S1P signaling has been implicated in cancer, atherosclerosis, inflammation, and multiple sclerosis, it has been targeted for therapy [143,144]. Another sphingolipid that can function as a ligand for a receptor at the cell surface is ceramide. Ceramide binds to CD300f (also called LMIR3) which is an inhibitory receptor of

mast cells activation. CD300f contains two immunoreceptor tyrosine-based inhibitory motifs (ITIMs) and a single immunoreceptor tyrosine-based switch motif (ITSM) in its cytoplasmic region. Deficiency of CD300f aggravates mass cell-dependent allergic responses in mice, including anaphylaxis, airway inflammation, and dermatitis [145]. In a mouse model, ceramide binding to CD300f inhibits IgE- or ATP-mediated mast cell activation via its ITIMs and ITSM, in allergic responses or colitis, respectively [146,147]. In addition, it also inhibits LPS-induced skin inflammation, indicating that CD300f is also a negative regulator of Toll-like receptor 4 signaling [148].

Second, sphingolipids function as modulators of enzymes. S1P has been implicated in the signaling pathway initiated by TNF-α binding to TNF receptor (TNFR). A key component of the pathway, TNFR-associated factor 2 (TRAF2) binds to SK1. S1P presumably produced by SK1 binds to TRAF2 as a cofactor for its E3 ligase activity and prevents the binding of its inhibitor TRIP. Activated TRAF2 increases polyubiquitination of RIP1, leading to the activation of the transcription factor NF-κB that executes a pro-survival program [149,150]. However, this model has been challenged since SK1/2 were later found to be dispensable for TNF-α-mediated responses [151,152,153]. S1P is also involved in epigenetic regulation of gene expression. Nuclear SK2 is associated with specific promoters, such as those for the genes encoding the cyclin-dependent kinase inhibitor p21 and the transcriptional regulator c-fos. Following stimulation by PKC, SK2 produces S1P that in turn binds to histone deacetylases HDAC1/2 in the vicinity. S1P binding inhibits their activity and therefore enhances transcription of the genes [154]. In telomere maintenance, S1P binding mimics protein phosphorylation of the catalytic subunit, human telomerase reverse transcriptase (hTERT) at the nuclear periphery. It stabilizes hTERT by inhibiting MKRN1-dependent hTERT ubiquitination and degradation, and therefore delaying cell senescence [155]. On the other end of "sphingolipid rheostat", ceramide induces cell cycle arrest by directly activating PKCζ.

Activated PKCζ interacts with MEKK1, SEK, and SAPK to inhibit insulin-like growth factor-1-induced cell growth [156]. This sphingolipid function also plays roles in the etiology and development of diseases. In Alzheimer's disease (AD), ß- and γ-secretases sequentially cleave amyloid-ß precursor protein to generate amyloid-ß peptide whose accumulation in the brain is linked to the pathogenesis of AD. S1P contributes to the pathogenesis of AD by binding to the major ß-secretase BACE1 and stimulating its activity [157]. In Gaucher's disease (GD), glucosylceramide and glucosylsphingosine might leak from lysosomes and be degraded by ß-glucosidase GBA2 at the cytosolic surface of the ER and *cis*-Golgi membranes. GBA2 produces sphingosine which has been proposed as the toxic metabolite in GD. Sphingosine prevents further cytotoxicity by binding to GBA2 and inhibiting its activity presumably by extracting it from the membrane [158].

Third, sphingolipids function as modulators of protein assemblies. At the *cis*-Golgi membrane, p24 is a transmembrane protein involved in the formation of COPI vesicles during retrograde transport. The vesicles are depleted from cholesterol and most sphingomyelin species except for C_{18} sphingomyelin (SM 18) [159]. SM 18 binds to the transmembrane domain of p24 and promotes a shift from its inactive monomeric to active oligomeric state, thus promoting COPI-dependent transport [160]. In mitochondria, oligomerization of activated BAK or BAX at the outer membrane forms pores that allow cytochrome-*c* to leak from the intermembrane space into the cytosol to execute apoptosis. Ceramide that arrives to the outer membrane from other organelles can be metabolized further to produce S1P and hexadecenal. Subsequently, S1P and hexadecenal lower the threshold of apoptosis by inducing the activation and oligomerization of BAK and BAX, respectively [161]. These findings contradict the general notion of S1P as an anti-apoptotic metabolite [44]. The presence of ceramide, specifically C_{18} ceramide, in the outer membrane has also been associated with cell death via lethal autophagy. Following Drp1-mediated mitochondrial fission, C_{18} ceramide is recognized

by LC3B-II and therefore targeting LC3B-II-containing autophagolysosomes to the mitochondria. This mitophagy inhibits mitochondrial function and oxygen consumption, leading to cell death [162]. At the cell surface, CD1 molecules bind and present lipidic antigens to T cells. Among the four isoforms of CD1, CD1b has the largest volume of cavity for carrying the antigen [163]. It relies on diacylglycerol and an atypical sphingolipid, 1-deoxy-dihydroceramide as scaffolding lipids to present much of its antigens [164].

3. Hereditary sensory and autonomic neuropathy type IA and IC

Hereditary sensory and autonomic neuropathy (HSAN) is caused by missense mutations in genes encoding for SPT. HSAN type IA and IC are caused by mutations in *SPTLC1* [165,166] and *SPTLC2* [167,168,169], respectively (**Tab. 1**). Each of the mutations increases the use of alanine or glycine by SPT as a substrate along with serine, therefore increasing the production of atypical sphingoid bases, 1-deoxy-sphinganine (1-doxSa) or 1-deoxymethyl-sphinganine (1-doxmetSa), respectively [170,171] (**Fig. 4a**). Higher levels of 1-deoxy-sphingolipids (1-doxSphs) correlate with the severity of HSAN I. Mutations associated with the mild and severe forms of HSAN I were predicted to affect amino acid residues around the active site and on the surface of SPT, respectively [172]. The most common mutation, *SPTLC1*-C133W was proposed to allow bound alanine to react with the acyl-CoA, not to facilitate alanine binding [171]. Another mutation in *SPTLC2*, S384F was proposed to disrupt a putative phosphorylation site that is involved in regulating substrate specificity [168]. The absence of a hydroxyl group at the first carbon prevents the conversion of 1-deoxy-sphingoid bases (1-doxSB) into complex sphingolipids and their degradation via the canonical sphingolipid degradation route by SPL. Since 1-doxSB are metabolically trapped, they tend to accumulate in the cell (**Fig. 4b**). Although 1-doxSB can also be readily acylated by CerS [173], they seem to have distinct metabolic routes. The most abundant native 1-deoxy-sphingosine

(1-doxSo) carries a *cis*-Δ^{14} double bond, in contrast to sphingosine which bears a *trans*-Δ^{4} double bond [174]. Moreover, the aliphatic chain of 1-doxSB can be hydroxylated at various positions by cytochrome P450 (CYP)4F enzymes.

Table 1. Clinical information about HSAN IA and IC

OMIM	**HSAN IA**: 162400 **HSAN IC**: 613640
Affected Gene	**HSAN IA**: *SPTLC1* [165,166] **HSAN IC**: *SPTLC2* [167,168,169]
Mutation (DNA / Amino acid)	**HSAN IA**: 398G>A / C133Y; 399T>G / C133W [165]; 431T>A / V144D [166]; 992C>T / S331F [175] **HSAN IC**: 1075G>A / V359M; 1145G>T / G382V; 1510A>T / I504F [167]; 1151 C>T / S384F [168]; 547C>T / R183W [169]
Affected Enzyme	Serine palmitoyltransferase
Impact on Sphingolipid	Increased synthesis of atypical sphingoid bases, 1-deoxy-sphinganine and 1-deoxymethyl-sphinganine [170,171]
Inheritance	Autosomal dominant
Onset	Varies between the first and fifth decades of life [176,177,167,169]
Clinical Manifestation	**HSAN IA**: Predominant loss of pain and heat sensation; severe shooting, burning and lancinating pains; ulcerative mutilations; hypohydrosis (if present); variable distal motor involvement [178,176] **HSAN IC**: Similar to HSAN IA but without autonomic signs [167]
Disease Management	Oral L-serine supplementation [179,180]; cleaning and protecting wounds on neuropathic limbs; eradication of infection; combination of an anti-epileptic drug and an anti-depressant drug for shooting pains [176,181]

The hydroxylation is slow (several days) which is a characteristic of a detoxification process. Therefore, it was proposed as a part of a non-canonical degradation route for 1-doxSphs [182]. In addition to HSAN I, 1-doxSphs have been implicated with several medical conditions, such as diabetes, non-alcoholic steatohepatitis (NASH), defective serine biosynthesis, and TNF-dependent toxicity [183].

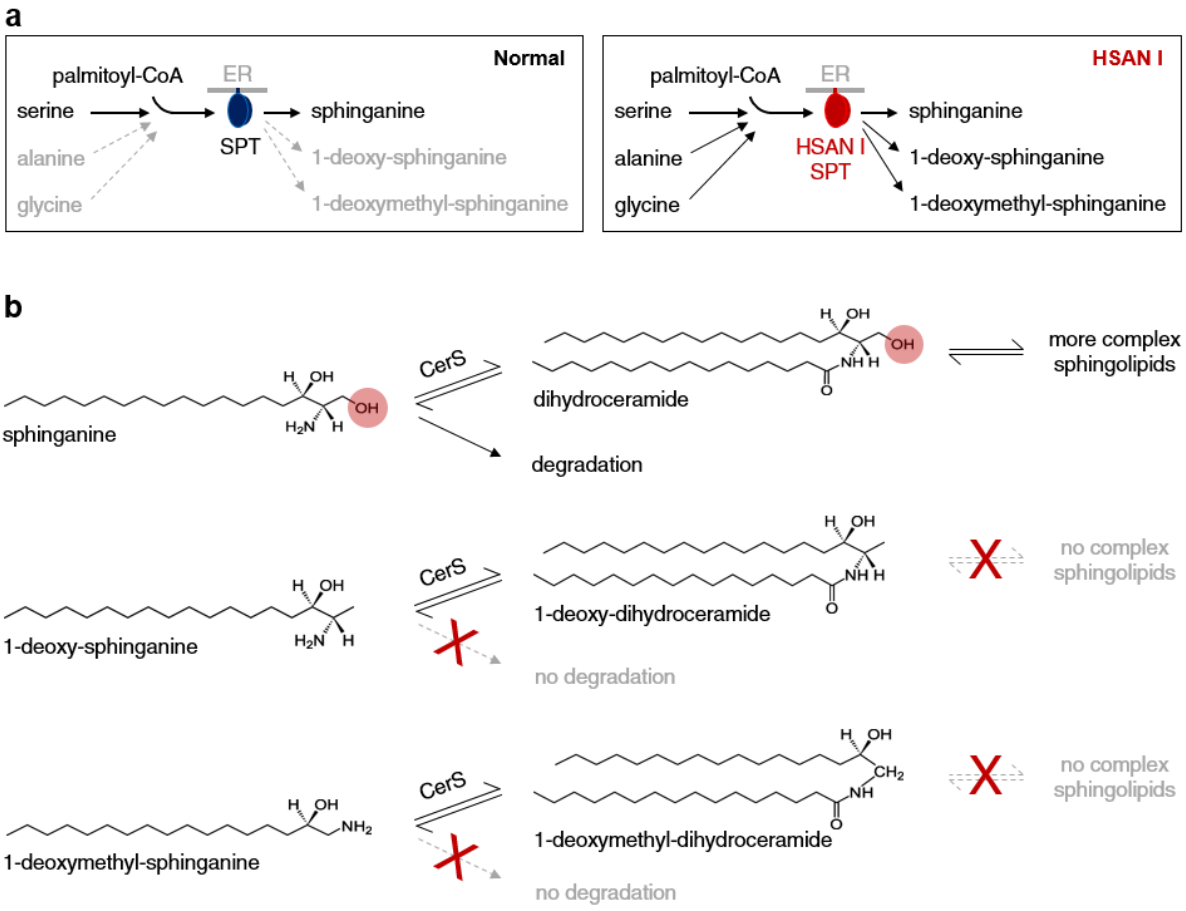

Figure 4. Aberrant sphingolipid metabolism underlying HSAN I. (**a**) Impacts of HSAN I mutations on the function of serine palmitoyltransferase (SPT). (**b**) Metabolic fates of typical and atypical sphingoid bases. The red circle highlights the missing hydroxyl group in the atypical sphingoid bases. CerS: ceramide synthase.

How the accumulation of 1-doxSphs disrupts the normal physiology of the cell and leads to HSAN I are largely unknown. 1-doxSa causes a reversible loss of actin stress fibers of a mammalian cell line. The effect could be partially suppressed with a Rho activator lysophosphatidic acid, suggesting that the effect involves inhibition of Rho proteins [184].

Prolonged incubation with 1-doxSa induces cell death through complex mechanisms, including ER stress [185], apoptosis, senescence, and necrosis [186,187,188]. The execution of apoptosis is independent of the common apoptotic machinery, and therefore it was proposed via an atypical apoptotic pathway [186]. The toxicity of 1-doxSa can be alleviated by a ceramide synthase inhibitor Fumonisin B1 (FB1), indicating that 1-deoxy-ceramide (1-doxCer) also contributes to the toxicity of 1-doxSphs [187,188]. The chemotherapy agent paclitaxel induces peripheral neuropathy as its major side effect in patients and the accumulation of 1-doxSphs in the cell. Among 1-doxSphs measured in the plasma of the patients with peripheral neuropathy, C_{24} 1-doxCer has the highest association with the incidence and severity of neuropathy, particularly motor neuropathy. These data suggest that different 1-doxSphs species have different degrees of toxicity [189]. The subcellular localization of 1-doxSphs was studied using an analog of 1-doxSa onto which a fluorophore can be attached by click chemistry. The analog accumulates mostly in mitochondria and causes mitochondrial fragmentation and dysfunction such as swelling, rounding up, cristae lost, and reduced respiration. These effects could be reduced by FB1 treatment. Moreover, direct 1-doxSa treatment to isolated mitochondria did not lead to a loss of mitochondrial membrane potential. These data provide further evidence of the major roles of 1-doxCer in the toxicity [185]. Another mechanism of the toxicity might involve perturbations of membrane structure since high concentrations of 1-doxCer disrupt giant unilamellar vesicles and 1-deoxymethyl-ceramide (1-doxmetCer) cannot form monolayers at the air-water interface [190].

In this study, we used the budding yeast as a model system to investigate the molecular mechanisms by which elevated levels of 1-doxSphs perturb the physiology of the cell. We chose the yeast since it naturally produces low levels of 1-doxSphs and it is amenable to genome-wide genetic manipulations. We started by characterizing the toxicity of 1-doxSphs to the cell to uncover the main toxic lipids, the role of acyl chain length in their toxicity, and their

biological properties compared to other lipids. Next, we performed genome-wide genetic screens to reveal cellular processes that are inhibited by 1-doxSphs and key proteins that are required for the toxicity. We then employed resistant mutants found in the screens to characterize the toxicity further and to compare it with that in mammalian cells. Features that we characterized were the effects of 1-doxSphs on actin and mitochondria, as well as the involvement of oxygen, the mitochondrial genome, and hydrophobic bodies in the toxicity. In addition to the genetic approaches, we also took a chemical proteomics approach using photocrosslinkable and clickable lipid analogs to hunt for potential targets of 1-doxSphs. Finally, we created and characterized a *C. elegans* model of HSAN IA to explore the roles of 1-doxSphs in more complex organisms. The worms carry an extra copy of the worm gene for the subunit 1 of SPT with the most commonly found HSAN IA mutation in human patients. We also examined the impacts of the HSAN IA allele on their ability to sense heat in the environment and their sensitivity to anoxia.

Materials and Methods

Yeast strains

N°	Name	Genotype	Source
1	WT (yMS721)	MATα *his3Δ1 leu2Δ0 lys2+/lys+ met15Δ0 ura3Δ0 can1Δ::STE2pr-sp HIS5 lyp1Δ::STE3pr-LEU2*	Maya Schuldiner
2	yMS721 LAG1	yMS721 *TDH3pr-LAG1-CYC1term URA3*	This study
3	yMS721 LAC1	yMS721 *TDH3pr-LAC1-CYC1term URA3*	This study
4	yMS721 LIP1	yMS721 *TDH3pr-LIP1-CYC1term URA3*	This study
5	yMS721 LAG1 LIP1	yMS721 *TDH3pr-LAG1-CYC1term TDH3pr-LIP1-CYC1term* (tandem) *URA3*	This study
6	yMS721 LAC1 LIP1	yMS721 *TDH3pr-LAC1-CYC1term TDH3pr-LIP1-CYC1term* (tandem) *URA3*	This study
7	yMS721 CerS1	yMS721 *TDH3pr-CERS1-CYC1term URA3*	This study
8	yMS721 CerS2	yMS721 *TDH3pr-CERS2-CYC1term URA3*	This study
9	yMS721 CerS3	yMS721 *TDH3pr-CERS3-CYC1term URA3*	This study
10	yMS721 CerS4	yMS721 *TDH3pr-CERS4-CYC1term URA3*	This study
11	yMS721 CerS5	yMS721 *TDH3pr-CERS5-CYC1term URA3*	This study
12	yMS721 CerS6	yMS721 *TDH3pr-CERS6-CYC1term URA3*	This study
13	KO and DAmP library	BY4741 *KanMX4*	Maya Schuldiner
14	WT (BY4741)	MATa *his3Δ1 leu2Δ0 met15Δ0 ura3Δ0*	Riezman lab
15	BY4741 CerS3	BY4741 *TDH3pr-CERS3-CYC1term URA3*	This study
16	BY4741 CerS3 SATAY	BY4741 *TDH3pr-CERS3-CYC1term KanMX6 ade2Δ::HIS3*	This study
17	BY4741 CerS3 *bar1Δ*	BY4741 CerS3 *bar1Δ::HIS3*	This study
18	BY4741 CerS3 *dyn1Δ*	BY4741 CerS3 *dyn1Δ::KanMX6*	This study
19	BY4741 CerS3 *bik1Δ*	BY4741 CerS3 *bik1Δ::KanMX6*	This study
20	BY4741 CerS3 *num1Δ*	BY4741 CerS3 *num1Δ::KanMX6*	This study
21	BY4741 CerS3 *pac1Δ*	BY4741 CerS3 *pac1Δ::KanMX6*	This study
22	BY4741 CerS3 *pac11Δ*	BY4741 CerS3 *pac11Δ::KanMX6*	This study
23	BY4741 CerS3 *kip2Δ*	BY4741 CerS3 *kip2Δ::KanMX6*	This study
24	BY4741 CerS3 *cka2Δ*	BY4741 CerS3 *cka2Δ::KanMX6*	This study
25	BY4741 CerS3 *sap190Δ*	BY4741 CerS3 *sap190Δ::KanMX6*	This study
26	BY4741 CerS3 Mdh1-mCherry	BY4741 CerS3 *MDH1-mCherry KanMX4*	This study
27	*are1Δ are2Δ dga1Δ lro1Δ*	*are1Δ are2Δ dga1Δ lro1Δ*	Riezman lab
28	*are1Δ are2Δ dga1Δ lro1Δ* CerS3	*are1Δ are2Δ dga1Δ lro1Δ TDH3pr-CERS3-CYC1term KanMX6*	This study
29	BY4741 CerS3 *ypc1Δ ydc1Δ pep4Δ*	BY4741 CerS3 *ypc1Δ::KanMX6 ydc1Δ::HphMX4 pep4Δ::LEU2*	This study

All yeast strains were cultured at 30°C.

Yeast media

1. YPD: 1% yeast extract, 2% peptone, 2% glucose (2% agar)
2. SC: 0.67% yeast nitrogen base (without amino acids, with ammonium sulfate), 1.92 g/l drop-out supplements (2% agar)
3. SD: SC, 2% glucose (2% agar)

4. SD MSG: 2% glucose, 0.67% yeast nitrogen base (without amino acids, without ammonium sulfate), 1 mg/ml monosodium glutamate, 1.92 g/l drop-out supplements (2% agar)
5. SPO: 0.05% glucose, 1% potassium acetate, 0.1% yeast extract, 0.1 g/l drop-out supplements (2% agar)
6. YPG: 1% yeast extract, 2% peptone, 3% ($^{w}/_{v}$) glycerol, 10 mM MES (2% agar)
7. Anaerobic YPD: YPD, 10 mM 2-(*N*-morpholino)ethanesulfonic acid (MES), 10 mg/l ergosterol, and 420 mg/l Tween® 80 (2% agar)
8. Anaerobic YPEG: 1% yeast extract, 2% peptone, 2% ($^{w}/_{v}$) glycerol, 2% ethanol (after autoclaving), 10 mM MES, 10 mg/l ergosterol, 420 mg/l Tween® 80 (2% agar)
9. Anaerobic YPL: 1% yeast extract, 2% peptone, 2% sodium lactate, 10 mM MES, 10 mg/l ergosterol, 420 mg/l Tween® 80 (2% agar)

Sphingoid bases

Sphinganine (Avanti 860498), 1-deoxy-sphinganine (Avanti 860493), 1-deoxymethyl-sphinganine (Avanti 860473). The sphingoid bases were dissolved in ethanol and sonicated for 5 min using an ultrasonic bath to make stock solutions. The solutions were stored at -20°C. Before use, the solutions were brought to room temperature and sonicated for 5 min.

Yeast spot assay

YPD agar + 10 mM MES + 0.05% ($^{v}/_{v}$) Tergitol™ NP-40 + a sphingoid base was prepared 2 days in advance. On the spotting day, cells were suspended at a ten-fold serial dilution with OD_{600} of 1.5 at the highest in 200 µl of YPD liquid in a U-bottom 96-well plate. The cells were spotted on the medium using a 48-pin tool. The culture was incubated at 30°C for 2 days.

Yeast growth curve assay

Cells were suspended at OD_{600} of 0.1 in 200 µl of YPD liquid in a flat-bottom 96-well plate. The cover of the plate was replaced with a gas permeable seal (4titude 4ti-0516-96). The culture was incubated at 30°C with agitation for 16 or 24 h in a plate reader (Biotek™ Synergy™ H1) while OD_{600} of the culture was recorded every 10 min.

Yeast lipidomic analysis

Treatment – Exponentially growing cells (OD_{600} of 0.8-0.9) in YPD liquid were treated with 1-deoxy-sphinganine (1-doxSa) at 30°C for 1.5 h. Then, the metabolism of the cells was immediately quenched with 5% of trichloroacetic acid.

Lipid extraction – Lipid extraction was performed as described before [191] with minor modifications. Briefly, a mixture of lipid standards (7.5 nmol of 17:0/14:1 PC, 7.5 nmol of 17:0/14:1 PE, 6.0 nmol of 17:0/14:1 PI, 4.0 nmol of 17:0/14:1 PS, 1.2 nmol of C_{17} ceramide, 1.2 nmol of C_{12} 1-deoxy-dihydroceramide, and 2.0 nmol of C_8 glucosylceramide) was added to 25 OD_{600} units of cells. The cells were subjected to two-round lipid extraction with 1.5 ml of extraction solvent (ethanol, water, diethyl ether, pyridine, 4.2 N ammonium hydroxide 15:15:5:1:0.018) and 250 µl of glass beads by vigorous vortexing for 5 min followed by incubation at 60°C for 20 min. Cell debris was pelleted at 800 ×*g* for 5 min, and the supernatant was collected. The combined supernatant

was divided into two equal aliquots for glycerolipid and sphingolipid analyses. Both aliquots were dried by a stream of nitrogen. The sphingolipid aliquot was then treated with 0.5 ml of monomethylamine reagent (methanol, water, *n*-butanol, methylamine 4:3:1:5) at 53°C for 1 h and dried again. Next, both dried aliquots were subjected to three-round desalting by resuspending them in 300 µl of water-saturated *n*-butanol and 150 µl of water followed by centrifugation at 3,200 ×*g* for 10 min to induce phase separation. The upper phases were collected. To start another round of desalting, the lower phase was mixed again with 300 µl of water-saturated *n*-butanol. The combined upper phases were dried and stored at -80°C.

Mass spectrometry – The dried lipid extracts were dissolved in 500 µl of chloroform:methanol (1:1). Each extract was diluted with chloroform:methanol:water (2:7:1) or chloroform:methanol (1:2) containing 5 mM of ammonium acetate for positive or negative mode mass spectrometry, respectively. Then, the samples were infused using a Nanomate (Advion) with a gas pressure of 30 psi and a spray voltage of 1.2 kV into a TSQ Vantage mass spectrometer (ThermoFisher) for multiple reaction monitoring analyses. The mass spectrometer was operated with a spray voltage of 3.5 kV in positive mode and 3 kV in negative mode. The capillary temperature was set to 190°C. Lipid amounts were normalized by the amounts of inorganic phosphate.

The first genetic screen (KO and DAmP)

Synthetic genetic array – CerS3 was introduced into the collection of knockout and hypomorphic (DAmP) mutants by the synthetic genetic array (SGA) method [192]. Briefly, yMS721 CerS3 cells were pinned onto 1536-format arrays of mutant colonies on YPD agar using a pinning robot (Singer Instruments) and incubated at room temperature for 1 day to induce mating. Then, the cells were pinned onto SD MSG agar – Ura + 200 mg/ml G418 and incubated at 30°C for 1 day to select diploid cells. The selection was repeated once. Next, the cells were pinned onto SPO agar and incubated at room temperature for 5 days to induce sporulation. The plates were wrapped with a moist towel to prevent desiccation. Then, the cells were pinned onto SD MSG agar – His/Lys/Arg/Ura + 50 mg/l canavanine + 50 mg/l thialysine and incubated at 30°C for 2 days to select cells with the same mating type as that of the mutants in the collection. Next, the cells were pinned onto SD MSG agar – His/Lys/Arg/Ura + 50 mg/l canavanine + 50 mg/l thialysine + 200 mg/ml G418 and incubated at 30°C for 1 day to select the mutants in the collection that carry CerS3. The selection was repeated once. The library was maintained on the same medium without G418.

Treatment and colony size measurement – The cells in the library were pinned onto SD MSG agar – His/Lys/Arg/Ura + 50 mg/l canavanine + 50 mg/l thialysine + 0.05% ($^{v}/_{v}$) Tergitol^{TM} NP-40 + 1-doxSa and incubated at 30°C for 1 day. Then, the plates were scanned using a paper scanner (Hewlett Packard). The size of colonies was determined using the "Balony" software [193] by including the row-column correction.

The second genetic screen (SATAY)

Library generation – SAturated Transposon Analysis in Yeast (SATAY) was performed as described before [194] with minor modifications. Briefly, BY4741 CerS3 SATAY cells were transformed with pBK257 plasmid containing the transposon. Freshly transformed cells were inoculated into 1 l of SC liquid + 0.2% glucose + 2% raffinose – Ura at OD_{600} of 0.15 and grown at 30°C until saturation (OD_{600} of 3-4). Then, the culture was

concentrated ten times by centrifugation at 600 ×*g* for 5 min to obtain final OD_{600} of 37. To induce transposition, the cells were plated using glass beads onto 433 8.5-cm Petri dishes of SC agar + 2% galactose – Ade and incubated at 30°C for 3 weeks. Contaminated plates were removed during the incubation time. Next, colonies were scrapped using a glass rod with minimum amounts of SC liquid + 2% glucose – Ade, pooled, inoculated into 1 l of SC liquid + 2% glucose – Ade at OD_{600} of 0.125, and incubated at 30°C until OD_{600} of 0.5. The library was used immediately.

Treatment – The cells in the library were pelleted at 800 ×*g* for 5 min, inoculated into pre-warmed 500 ml of SC liquid + 2% glucose – Ade + 1-doxSa at OD_{600} of 0.1, and incubated at 30°C until saturation. The treatment was repeated once. Next, the cells were harvested by centrifugation at 2,500 ×*g* 4°C for 5 min and stored at -80°C.

DNA preparation – Genomic DNA of about 500 mg of cells was extracted by the phenol/chloroform extraction method. Next, 2 µg of genomic DNA was digested with 50 units of DpnII or NlaIII at 37°C for 24 h. The enzymes were then heat inactivated at 65°C for 20 min. The DNA fragments were circularized with 25 Weiss units of T4 Ligase at 22°C for 6 h. The circularized DNA molecules were precipitated with 0.3 M of sodium acetate pH 5.2, 1 ml of ethanol, and 5 µg linear acrylamide (Ambion AM9520) at -20°C overnight. Then, DNA was pelleted at 16,100 ×*g* 4°C for 20 min, washed with 1 ml of 70% ethanol, and dried at 37°C for 10 min. Next, transposon fragments were amplified with Taq polymerase (New England Biolabs). The PCR products were then purified with the PCR clean-up/gel extraction kit (Macherey-Nagel) according to the manufacturer instruction, with the following modifications. DNA was bound to the column by centrifugation at 3,000 ×*g* for 30 s. Then, 30 µl of elution buffer (10 mM Tris-HCl pH 8.5, 0.1% ($^{v}/_{v}$) Tween® 20) was applied to the column, incubated for 3 min, and eluted by centrifugation at 11,000 ×*g* 20°C for 1 min. The eluate was reapplied to the column and a second elution was performed under the same conditions.

Deep sequencing – Equal amounts of DNA from DpnII- and NlaIII-digested samples were pooled and sequenced using MiSeq v3 chemistry, according to the manufacturer instruction.

Cell cycle analysis

Arresting at G1/S – BY4741 CerS3 *bar1Δ* cells were cultured in YPD liquid at 30°C from OD_{600} of 0.025 to 0.1. Then, the culture was mixed with two-volume of pre-warmed YPD liquid supplemented with 5 µM of α-factor and incubated at 30°C for 3 h.

Arresting at S – BY4741 CerS3 cells were cultured in YPD liquid at 30°C from OD_{600} of 0.025 to 0.1. Then, the culture was supplemented with hydroxyurea powder to a final concentration of 0.2 M and incubated at 30°C for 3 h.

Arresting at G2/M – BY4741 CerS3 cells were cultured in YPD liquid at 30°C from OD_{600} of 0.025 to 0.1. Then, the culture was supplemented with nocodazole to a final concentration of 15 µg/ml and incubated at 30°C for 3 h.

Treatment and microscopy – The cells were pelleted at 800 ×*g* for 5 min, washed four times with 50 ml of pre-warmed YPD liquid, and released into pre-warmed YPD liquid supplemented with 1-doxSa at OD_{600} of 0.05 for 3 h. Next, the cells were fixed with 4% paraformaldehyde, washed with a washing buffer (0.1 M Potassium phosphate pH 7.5, 1.2 M sorbitol), and observed by DIC microscopy. The number of cells was counted using ImageJ.

Fluorescence microscopy

Actin cytoskeleton – Exponentially growing BY4741 CerS3 cells were inoculated into pre-warmed YPD liquid supplemented with 1-doxSa at OD_{600} of 0.05 and incubated at 30°C for 3 h. Next, the cells were fixed by directly adding paraformaldehyde to the culture to a final concentration of 4%. Then, 1 OD_{600} unit of cells were washed with 3 ml of washing buffer (0.1 M Potassium phosphate pH 7.5, 1.2 M sorbitol), stained with 50 µl of 1 µM phalloidin-Atto488 (Sigma-Aldrich) at 4°C for 1 h in the dark, and observed by confocal microscopy.

Mitochondria – Exponentially growing BY4741 CerS3 Mdh1-mCherry cells were inoculated into pre-warmed YPD liquid supplemented with 1-doxSa at OD_{600} of 0.05 and incubated at 30°C for 3 h. Next, the cells were observed by confocal microscopy immediately without fixation.

Hydrophobic bodies – Exponentially growing BY4741 CerS3 cells were inoculated into pre-warmed YPD liquid supplemented with 1-doxSa at OD_{600} of 0.05 and incubated at 30°C for 3 h. Next, the cells were fixed by directly adding paraformaldehyde to the culture to a final concentration of 4%. Then, 1 OD_{600} unit of cells were washed with 3 ml of washing buffer, stained with 100 µl of 1 mg/ml Nile Red at 4°C for 15 min in the dark, and observed by confocal microscopy.

DNA – Exponentially growing BY4741 CerS3 cells were inoculated into pre-warmed YPD liquid supplemented with 1-doxSa at OD_{600} of 0.05 and incubated at 30°C for 3 h. Next, the cells were fixed by directly adding paraformaldehyde to the culture to a final concentration of 4%. Then, 1 OD_{600} unit of cells were washed with 3 ml of washing buffer, stained with 100 µl of 1 µg/ml DAPI at 4°C for 15 min in the dark, and observed by confocal microscopy.

Yeast ROS measurement

Exponentially growing BY4741 CerS3 cells were inoculated into pre-warmed YPD liquid supplemented with H_2O_2 or 1-doxSa at OD_{600} of 0.05 and incubated at 30°C for 3 h. Next, 1 OD_{600} unit of cells were pelleted at 2,300 ×*g* for 1 min, washed twice with 1 ml of 0.1 M potassium phosphate pH 7.5, resuspended in 100 µl of the buffer with 100 µM CM-H_2DCFDA (ThermoFisher), and incubated at room temperature for 30 min in the dark. Then, the cells were washed with 1 ml of the buffer and resuspended in 200 µl of the buffer. The fluorescence intensity of the indicator was measured using a plate reader with Ex/Em 493/522 nm. The OD_{600} of the suspension was also measured using the same plate reader. The fluorescence intensity was normalized by OD_{600}.

Yeast anaerobic culture

Cells were spotted on an anaerobic agar medium as described above. The Petri dish was placed inside an airtight chamber (ThermoFisher) equipped with a pack of oxygen-consuming reagent (ThermoFisher) and oxygen color indicators (ThermoFisher). The chamber was closed immediately and incubated at 30°C for 3 days.

Generating ρ^0 cells

Exponentially growing BY4741 CerS3 cells were cultured into SD liquid supplemented with 25 µg/ml of ethidium bromide from OD_{600} of 0.1 until saturation (24 h). The step was repeated twice.

Yeast transmission electron microscopy

Transmission electron microscopy was performed as described before [195] with minor modifications. Briefly, exponentially growing BY4741 CerS3 cells were inoculated into pre-warmed YPD liquid supplemented with 1-doxSa at OD_{600} of 0.05 and incubated at 30°C for 3 h. Next, 2 OD_{600} units of cells were fixed by directly adding EM-grade glutaraldehyde (0.5% final) and EM-grade paraformaldehyde (4% final) to the culture followed by incubation at room temperature for 5 min. Then, the cells were pelleted at 800 ×*g* for 5 min, resuspended in 1 ml of fixation buffer (0.2 M PIPES pH 6.8, 0.2 M sorbitol, 2 mM $MgCl_2$, 2 mM $CaCl_2$, 0.5% EM-grade glutaraldehyde, 4% EM-grade paraformaldehyde), and incubated 4°C for 30 min. Next, the cells were washed three times with 1 ml of ice-cold washing buffer (0.2 M PIPES pH 6.8, 0.2 M sorbitol, 2 mM $MgCl_2$, and 2 mM $CaCl_2$). To partially digest the cell wall, the cells were resuspended in 1 ml of digestion buffer (50 mM Tris-HCl pH 7.5, 1.4 M sorbitol, 5 mM $MgCl_2$, 0.5% ß-mercaptoethanol, 0.15 mg/ml Zymolyase 20T) at room temperature for 10 min. Then, the cells were washed four times with 1 ml of the washing buffer, subjected to the second fixation with 0.5% of osmium tetroxide and 0.8% of potassium ferrocyanide, followed by *en bloc* staining with 1% uranyl acetate. The specimen was observed using transmission electron microscope (Tecnai G2).

2D-HPTLC

Lipid extract of 25 OD_{600} units of cells was prepared in the same way as preparing glycerolipid extract for lipidomic analysis described above. HPTLC plate was cleaned by dipping one side of the plate into chloroform in a TLC chamber until the whole surface of the plate was completely wet with chloroform. The plate was then air dried. The lipid extract was dissolved in 200 µl of chloroform:methanol (1:1) and spotted on one corner of the plate. The first chromatography was run with petroleum ether:diethyl ether (1:1), and the solvent was air dried. The second chromatography was run with petroleum ether:diethyl ether (49:1), and the solvent was air dried. Next, the spots were visualized by dipping the plate into charring solution (0.63 g $MnCl_2.4H_2O$, 60 ml water, 60 ml methanol, 4 ml H_2SO_4 fuming), followed by incubation at 110°C for 3 min.

Chemical proteomics

Synthesis of pac-lipids – The photocrosslinkable and clickable (pac) lipid analogs were synthesized by Per Haberkant (EMBL-Heidelberg) and Suihan Feng (University of Geneva) by following the synthesis routes described before [196,197]. Briefly, pac-fatty acid (pac-FA) was synthesized and then linked to sphinganine or 1-doxSa to obtain pac-dihydroceramide (pac-DHCer) or pac-1-deoxy-dihydroceramide (pac-1-doxDHCer), respectively.

Preparation of small unilamellar vesicles – Small unilamellar vesicles (SUVs) were used to present pac-lipids to proteins in cell lysates. Five mole% of pac-lipid were mixed with 95 mole% of vesicle lipid in a glass tube and dried under a stream of nitrogen. POPC (Avanti 850457) was used to present pac-FA and pac-DHCer, while egg sphingomyelin (Sigma-Aldrich S0756) was used to present pac-1-doxDHCer. Next, the lipid film was hydrated with MilliQ water and incubated at 60°C for 10 min. Then, the lipid suspension was vortexed vigorously until multilamellar vesicles were formed. To form SUVs, the suspension was sonicated at room temperature for 1 h using an ultrasonic bath. SUVs were always prepared fresh.

Cell fractionation – Cell fractionation was performed at 4°C. All materials and instruments were kept ice-cold. Briefly, 5 OD_{600} units of exponentially growing BY4741 CerS3 *ypc1Δ ydc1Δ pep4Δ* cells were pelleted at 1,200 ×*g* for 5 min, washed with 3 ml of lysis buffer (50 mM HEPES-NaOH pH 7.5, 100 mM NaCl, 1 mM PMSF, protease inhibitor cocktail without EDTA (Roche)), and resuspended in 150 µl of lysis buffer and 150 µl of glass beads. The cells were lysed by vigorous vortexing for 10 min using a cell disruptor (Genie). Then, cell debris and glass beads were pelleted at 300 ×*g* for 5 min, and the supernatant was collected. The pellet was resuspended in 100 µl of lysis buffer, centrifuged at 300 ×*g* for 5 min, and the supernatant was collected. Next, the pooled supernatant was centrifuged at 13,000 ×*g* for 10 min to obtain $P_{13,000}$ and $S_{13,000}$ fractions. The $S_{13,000}$ fraction was centrifuged at 100,000 ×*g* for 1 h to obtain $P_{100,000}$ and $S_{100,000}$ fractions. For pull-down and mass spectrometry analysis, 80 OD_{600} units of cells were collected.

Photocrosslinking – A pac-lipid in SUVs (10 µM final pac-lipid concentration) was mixed with the cell fractions (2 mg/ml final protein concentration) and digitonin (0.5% final). The mixture was incubated at room temperature for 1 h in the dark. Next, the mixture was placed on ice and irradiated with UV (365 nm) light for 5 min using a UV crosslinker (UVP). The mixture might be stored at -20°C.

In-gel fluorescence – The crosslinked mixture was subjected to click chemistry to link TAMRA with the pac-lipid. Briefly, 7 µl of premixed click reagents (50 µM TAMRA-azide, 1 mM TCEP, 100 µM TBTA, 1 mM $CuSO_4$) was added to 50 µl of the crosslinked mixture. The mixture was incubated at room temperature for 1 h in the dark. The reaction was stopped by adding Laemmli's sample buffer. Next, proteins in the sample were resolved by SDS-PAGE with a 12% running gel. The gel was then scanned using a fluorescence scanner (Hitachi FMBIO II).

Pull-down and mass spectrometry – The crosslinked mixture was subjected to click chemistry to link biotin with the pac-lipid. Briefly, 7 µl of premixed click reagents (50 µM biotin-azide, 1 mM TCEP, 100 µM TBTA, 1 mM $CuSO_4$) was added to 50 µl of the crosslinked mixture. The mixture was incubated at room temperature for 1 h. To precipitate proteins, 4 volumes of cold methanol and 1 volume of cold chloroform were mixed with the sample. Then, 3 volumes of cold water were mixed with the sample. The sample was centrifuged at 14,000 ×*g* 4°C for 5 min to induce phase separation. The upper and lower phases were removed, leaving the protein interface. The protein pellet was air dried and resolubilized in 1 ml of 2% SDS in PBS using a needle sonicator. The insolubilized proteins were pelleted at 4,700 ×*g* for 5 min. The supernatant was collected and diluted 10 fold with PBS. To enrich crosslinked proteins, 50 µl of washed streptavidin beads were added to the supernatant. Then, the mixture was incubated at 4°C overnight in the dark on a rotary mixer. The beads were pelleted at 1,000 ×*g* for 1 min and

washed once with 10 ml of 1% SDS in PBS, three times with 10 ml of PBS, and three times with 10 ml of water. Next, the beads were resuspended in 500 µl of 6 M urea in PBS containing TCEP (10 mM final) and incubated at room temperature for 30 min in the dark on a rotary mixer. Then, the suspension was supplemented with iodoacetamide (25 mM final) and incubated again with the same conditions. The suspension was then diluted with 700 µl of PBS and centrifuged at 1,400 ×*g* for 2 min to remove the supernatant. To digest the proteins on the beads, the beads were resuspended in 150 µl of digestion solution (2 M urea in 50 mM NH_4HCO_3 pH 8, 1 mM $CaCl_2$, 3 µg/ml EM-grade trypsin) and incubated at 37°C for 12 h in the dark. Next, the peptides were desalted using a peptide desalting kit (Agilent) according to the manufacturer instruction. The peptides were analyzed by mass spectrometry by Michaël Plank (University of Geneva).

Worm strains

N°	Name	Genotype	Source
1	N2 Bristol	WT	CGC
2	IE4348	ttTi4348 I:2850991..2851093	NEMAGENETAG
3	Si *sptl-1*^{WT}	Si4348 GFPub-*sptl-1*^{WT}-3×c-Myc	This study
4	Si *sptl-1*^{C133W} (HSAN IA)	Si4348 GFPub-*sptl-1*^{C133W}-3×FLAG	This study
5	NL2099	*rrf-3*(pk1426) II	CGC
6	FX02031	*hyl-2*(tm2031) X	Jean-Claude Martinou
7	HSAN IA *rrf-3*	HSAN IA *rrf-3*(pk1426) II	This study
8	HSAN IA *hyl-2*	HSAN IA *hyl-2*(tm2031) X	This study

All worm strains were reared at 20°C.

Establishing worm model of HSAN IA

Single gene insertion was performed by the mos1-mediated Single Copy Insertion (mosSCI) method as described before [198] with minor modifications.

Background strain – The background strain was IE4348 which carries an inserted Mos1 transposon in chromosome I:2850991..2851093. The strain was crossed with N2 for 4 rounds to eliminate secondary transposon insertion. The strain was maintained on NGM plate seeded with *E. coli* HB101.

Injection mix – Targeting plasmid was constructed by replacing *Cb-unc-119* positive selection marker of pCFJ352 with P*eft-3*::GFP::H2B and inserting a *sptl-1* allele (WT or C133W) with its endogenous promoter and terminator. The injection mix consisted of 50 ng/µl of pCFJ601 (P*eft-3*::transposase), 22.5 ng/µl of the targeting plasmid, 10 ng/µl of pMA122 (P*hsp*::*peel-1*), 10 ng/µl of pGH8 (P*rab-3*::mCherry), 2.5 ng/µl of pCFJ90 (P*myo-2*::mCherry), and 5 ng/µl of pCFJ104 (P*myo-3*::mCherry). The injection mix was centrifuged at top speed for 1 min to pellet impurities.

Gene insertion – Young adult hermaphrodites were injected with the injection mix using the standard worm injection setup and placed at room temperature for 1 h to recover. Each injected worm was placed on individual NGM plate seeded with *E. coli* OP50 and incubated at 20°C for 7 days until all adult worms have died off after starvation. Next, the worms were heat treated by placing the plate inside an air incubator at 34°C for 2 h. The worms were visually screened for worms with putative gene insertion at least 6 h after the heat treatment. The

worms were L1 larvae with GFP-labelled nuclei without mCherry signal. Gene insertion was verified by single-worm PCR and sequencing. Next, the worms were crossed with N2 for 4 rounds to eliminate secondary mutations before being used in an experiment.

Worm RNA interference

RNAi was performed as described before [199] with minor modifications. Briefly, standard NGM agar supplemented with carbenicillin (25 μg/ml final) and IPTG (1 mM) was prepared a week in advance. The plate was then seeded with *E. coli* HT115(DE3) carrying L4440 plasmid with an insert corresponding to the targeted gene. The culture was incubated at 37°C overnight. Next, synchronized L1 larvae were placed onto the seeded medium and incubated at 20°C for 3 days to observe the phenotypes of young adults.

Worm lipidomic analysis

Worm lysis – About 8,000 synchronized young adults (without embryos) were collected with water. Bacteria were washed away, and the worms were transferred into a cryolysis tube. Next, worms were lysed with 100 μl of 1.4-mm zirconium oxide beads (Bertin Technologies) in 800 μl of water using a cryolysis machine (Bertin Technologies). Lysate was eluted into a glass tube with lipid standards by centrifugation at 600 ×*g* for 1 min. The beads were rinsed once with 200 μl of water. The eluates were combined.

Lipid extraction and mass spectrometry – Lipids were extracted with 3.6 ml of chloroform:methanol (1:2) by vigorous vortexing. The suspension was centrifuged at 800 ×*g* for 5 min, and the supernatant was transferred into another glass tube. Then, 0.5 ml of water and 0.5 ml of chloroform were added to the supernatant, vortexed, and centrifuged at 800 ×*g* for 5 min to induce phase separation. The lower phase was recovered and divided into two equal aliquots for glycerolipid and sphingolipid analyses. Then, the two aliquots were further processed in the same ways as those for yeast lipid aliquots described above.

Worm thermotaxis assay

Thermotaxis assay was performed by Dominique Glauser (University of Fribourg) as described before [200]. Briefly, synchronized young adults were transferred onto fresh NGM agar seeded with *E. coli* OP50 and incubated at 20°C for 3-4 h prior to the assay to acclimatize the worms. Next, the worms were collected, washed twice with water, and transferred on the center of a custom-made thermotaxis plate. The temperature at the center of the plate was 23°C. The temperature gradient of the plate was 0.67°C/cm. The worms were assayed for 10 min, and the thermotaxis index was calculated as follow: (number of worms above starting temperature - number of worms below starting temperature)/total number of worms.

Worm anoxia assay

Anoxia assay was performed by Thomas Hannich (University of Geneva) as described before [201]. Anoxia environment was created using a 15-liter vacuum desiccator (Fisher Scientific) which was constantly flushed with water-saturated nitrogen gas (N_2 5.0, <0.001 kPa O_2, Pangas) at a rate of 0.5 ml/min. The chamber was placed inside a 489-liter glove box (Plas-Lab) whose oxygen level was maintained at <0.3% and temperature was maintained at 20°C. The assay was performed by placing synchronized young adults on standard NGN agar seeded

with *E. coli* OP50 inside the chamber for a period of time. Then, the worms were transferred into a standard incubator at 20°C for 24 h to recover before their viability was assessed. Viability was evaluated using an inverted microscope.

Results

1. 1-deoxy-sphingolipids are toxic to the budding yeast

1.1. 1-deoxy-ceramides are the main toxic lipids

The detrimental effects of elevated levels of 1-deoxy-sphingolipids (1-doxSphs) on the cell have never been examined in the budding yeast. Therefore, we first asked whether elevated levels of 1-doxSphs are also toxic to the yeast. Since 1-doxSphs comprise two groups of interconvertible metabolites, 1-deoxy-sphingoid bases (1-doxSB) and 1-deoxy-ceramides (1-doxCers), we further asked which group of metabolites contributes more to the toxicity. To this end, we examined the effects of 1-doxSB on the growth of yeast overexpressing yeast ceramide synthase. Yeast ceramide synthase may be composed of Lag1-Lac1 heterodimer or Lag1 or Lac1 homodimer. Each dimer contains at least two essential subunits of ceramide synthase Lip1 that is required for its optimum activity [36]. The ceramide synthase was overexpressed by integrating an additional copy of its gene with the constitutively active strong promoter of glyceraldehyde-3-phosphate dehydrogenase isozyme 3 (Tdh3) into the yeast genome. The growth of yeast was assayed by spotting yeast cells onto rich agar media supplemented with 1-doxSB. In this assay, overexpression of yeast ceramide synthase enhances the conversion of 1-doxSB to 1-doxCers, thereby reducing the contribution of 1-doxSB while increasing the contribution of 1-doxCers to the toxicity of 1-doxSphs.

The assay showed that the typical sphingoid base, sphinganine did not inhibit the growth of yeast regardless of the overexpressed ceramide synthase at up to 200 μM (**Fig. 5a**). At this concentration, the cell was still able to prevent the accumulation of ceramide to toxic levels by degrading it or by converting it to more complex sphingolipids. In contrast, 1-deoxy-sphinganine (1-doxSa) inhibited the growth of yeast overexpressing Lac1 and Lip1 at 20 μM (**Fig. 5b**). Similar to 1-doxSa, 1-deoxymethyl-sphinganine (1-doxmetSa) also inhibited the

growth of the yeast strain at the same concentration, albeit to a lesser degree (**Fig. 5c**). Since the toxicity of both 1-doxSB increased with the increased activity of ceramide synthase, these results suggest that 1-doxSphs are toxic to the yeast and that their toxicity is mainly attributed to the accumulation of 1-doxCers. The latter finding is consistent with the previous findings in mammalian cells [185,187,188]. Their toxicity, however, was not modulated by the overexpression of Lag1 and Lip1. It is possible that Lag1 cannot utilize 1-doxSB as substrates to produce 1-doxCers or that the expression level of Lag1 was lower than that of Lac1 since *LAC1* encodes the more abundantly expressed protein [202].

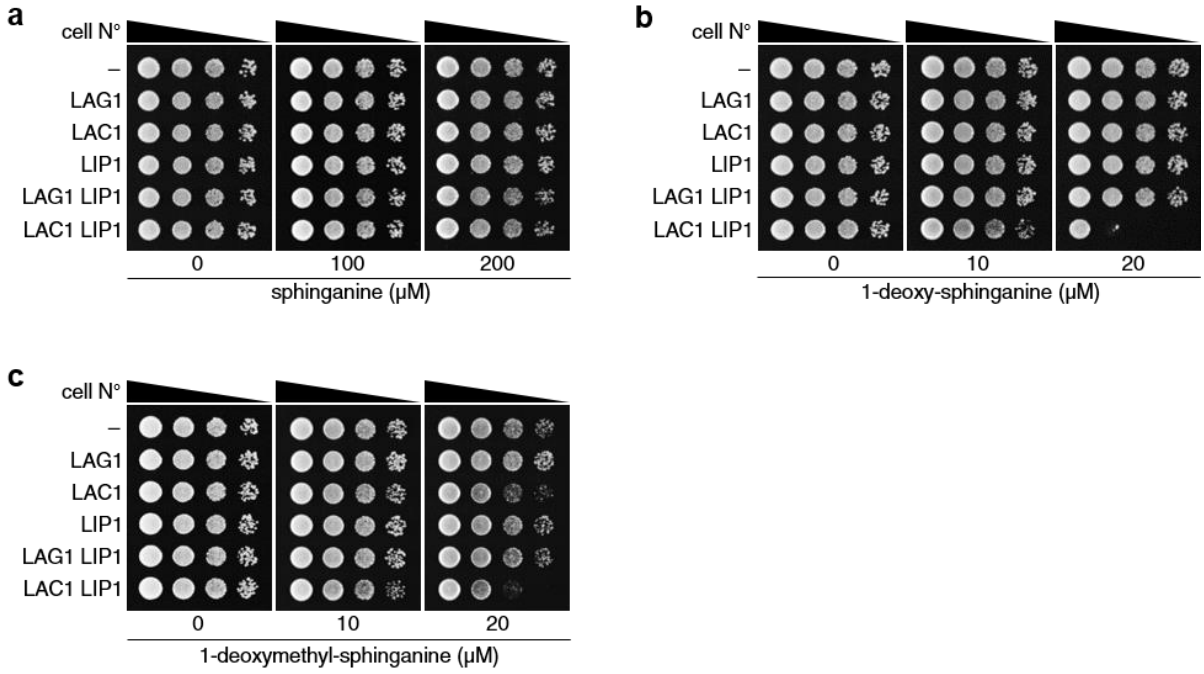

Figure 5. 1-deoxy-ceramides are the main toxic lipids. WT (BY4741) cells overexpressing yeast ceramide synthase were spotted onto rich agar media supplemented with the indicated concentrations of sphinganine (**a**), 1-deoxy-sphinganine (**b**), or 1-deoxymethyl-sphinganine (**c**). The cells were spotted at a ten-fold serial dilution.

1.2. Toxicity of 1-deoxy-ceramide depends on the length of its acyl chain

To evaluate the toxicity of 1-doxCers bearing different lengths of acyl chain, we made use of the fatty acid specificity of mammalian ceramide synthases [10] (**Fig. 6a**). Expression of each mammalian ceramide synthase by integrating the gene with the promoter of Tdh3 into

the yeast genome is able to rescue the lethality of yeast ceramide synthase depletion. This indicates that each of them is functional in yeast cells. More importantly, they retain their fatty acid specificity, allowing us to selectively increase the levels 1-doxCers bearing particular lengths of acyl chain in the cell by treating the cell expressing a corresponding mammalian ceramide synthase with 1-doxSB [Thomas Hannich, unpublished data] (**Fig. 6b**). We tested the toxicity of 1-doxCers bearing different lengths of acyl chain with the spot assay.

The assay showed that sphinganine started to inhibit the growth of yeast expressing CerS5 or CerS6 at 200 μM (**Fig. 6c**). This suggests that high levels of C_{16} ceramide can be toxic to yeast that normally produces C_{26} ceramide. Compared to sphinganine, 1-doxSa already showed more apparent inhibition of the growth of yeast expressing CerS3 at 5 μM and CerS5 or CerS6 at 10 μM (**Fig. 6d**). The amount of C_{26} 1-deoxy-ceramide (1-doxCer) which is mostly 1-deoxy-dihydroceramide (1-doxDHCer) that accumulated in the CerS3 strain following 1-doxSa treatment was about a half of those of C_{16} 1-doxCer that accumulated in the CerS5 or CerS6 strain (**Fig. 6b**). Nevertheless, the CerS3 strain was more sensitive to 1-doxSa than the CerS5 or CerS6 strain. These data strongly suggest that the toxicity of 1-doxCer to yeast depends on the length of its acyl chain, e.g. C_{26} 1-doxCer is more toxic than C_{16} 1-doxCer. In contrast to 1-doxSa, 1-doxmetSa inhibited the growth of yeast regardless of the expressed mammalian ceramide synthase at 40 μM (**Fig. 6e**). This suggests that mammalian ceramide synthase expressed in yeast cannot convert 1-doxmetSa to 1-deoxymethyl-ceramide (1-doxmetCer). Therefore, we cannot evaluate the toxicity of 1-doxmetCer bearing different lengths of acyl chain. Consequently, we decided to study further the toxicity of 1-doxCer by employing the CerS3 strain (further referred to as "CerS3 cells").

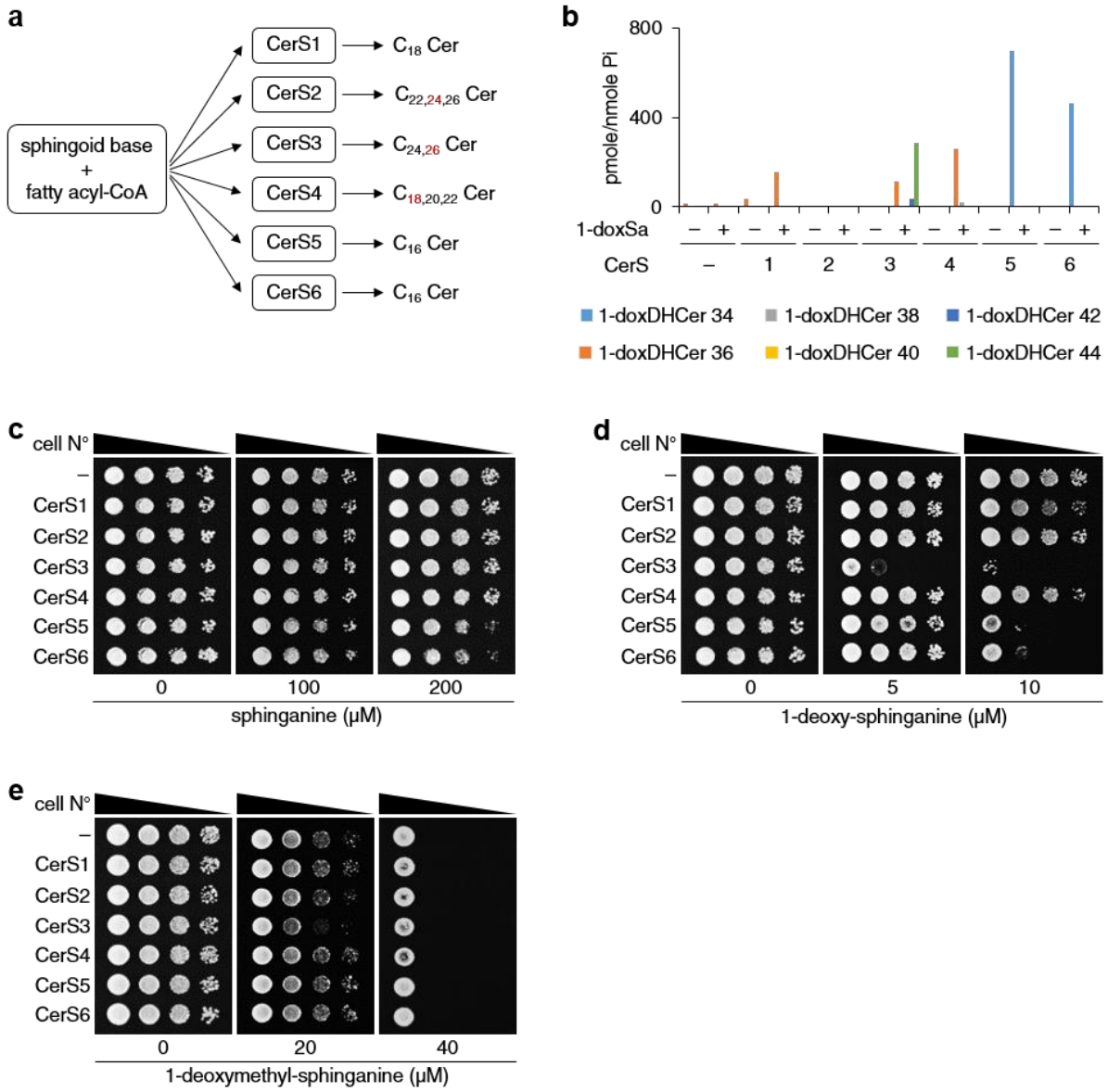

Figure 6. Toxicity of 1-deoxy-ceramide depends on the length of its acyl chain. (**a**) Fatty acid specificity of mammalian ceramide synthases. Red numbers indicate the major ceramide species produced by the enzymes. (**b**) Mammalian ceramide synthases expressed in yeast retain their fatty acid specificity. Exponentially growing WT cells expressing mammalian ceramide synthase were treated with 2.5 μM of 1-deoxy-sphinganine (1-doxSa) for 1.5 h. The amounts of lipids were determined by mass spectrometry. (**c-e**) WT cells expressing mammalian ceramide synthase were spotted onto rich agar media supplemented with the indicated concentrations of sphinganine (**c**), 1-deoxy-sphinganine (**d**), or 1-deoxymethyl-sphinganine (**e**). The cells were spotted at a ten-fold serial dilution.

1.3. 1-deoxy-ceramide has distinct biological properties

To examine the biological properties of 1-doxCer, we measured changes in the lipidomic profile of the cell following its accumulation. We reasoned that the changes must

reflect the detrimental effects of 1-doxCer or the adaptation of the cell to minimize them. Therefore, the changes in lipidomic profile might indicate the biological properties and the mode of action of 1-doxCer. The lipidomic analysis revealed that the level of 1-doxCer (mostly C_{26} 1-doxCer) in CerS3 cells increased 43.6 or 98.2 fold following a treatment of 2.5 or 5 μM of 1-doxSa, respectively. The increase was not accompanied by marked changes (min. 0.7 fold and max. 2 fold) in the levels of other lipid classes (**Fig. 7a,b**). In addition, lipid species whose levels changed significantly accompanying the accumulation of 1-doxCer are minor lipids with minor changes without unifying features (**Fig. 7c**). Since 1-doxCer could accumulate up to 13.9% of the amount of phosphatidylcholine (the major yeast glycerolipid) (**Fig. 7b**), the changes in the levels of other lipids are too small and too random to reflect the detrimental effects of 1-doxCer or the adaptation of the cell.

To further examine the biological roles of 1-doxSa and 1-doxCer in comparison with yeast sphingoid bases and ceramides, we inhibited the synthesis of the normal sphingolipids with myriocin and determined the effect on the toxicity of 1-doxCer. The idea is that if myriocin and 1-doxCer work independently, then their toxic effects should not show interaction. To this end, we monitored the growth of CerS3 cells treated with myriocin in combination with 1-doxSa by a plate reader. We found that the combined inhibitory effects of myriocin and 1-doxCer could be explained by the sum of their inhibitory effects, indicating that myriocin and 1-doxCer act independently (**Fig. 7d**). These results suggest that 1-doxSa and 1-doxCer do not mimic yeast sphingoid bases and ceramides, respectively. Moreover, the toxicity of 1-doxCer is not due to intervention of the normal functions of ceramides. Together, these data show that 1-doxCer has distinct biological properties.

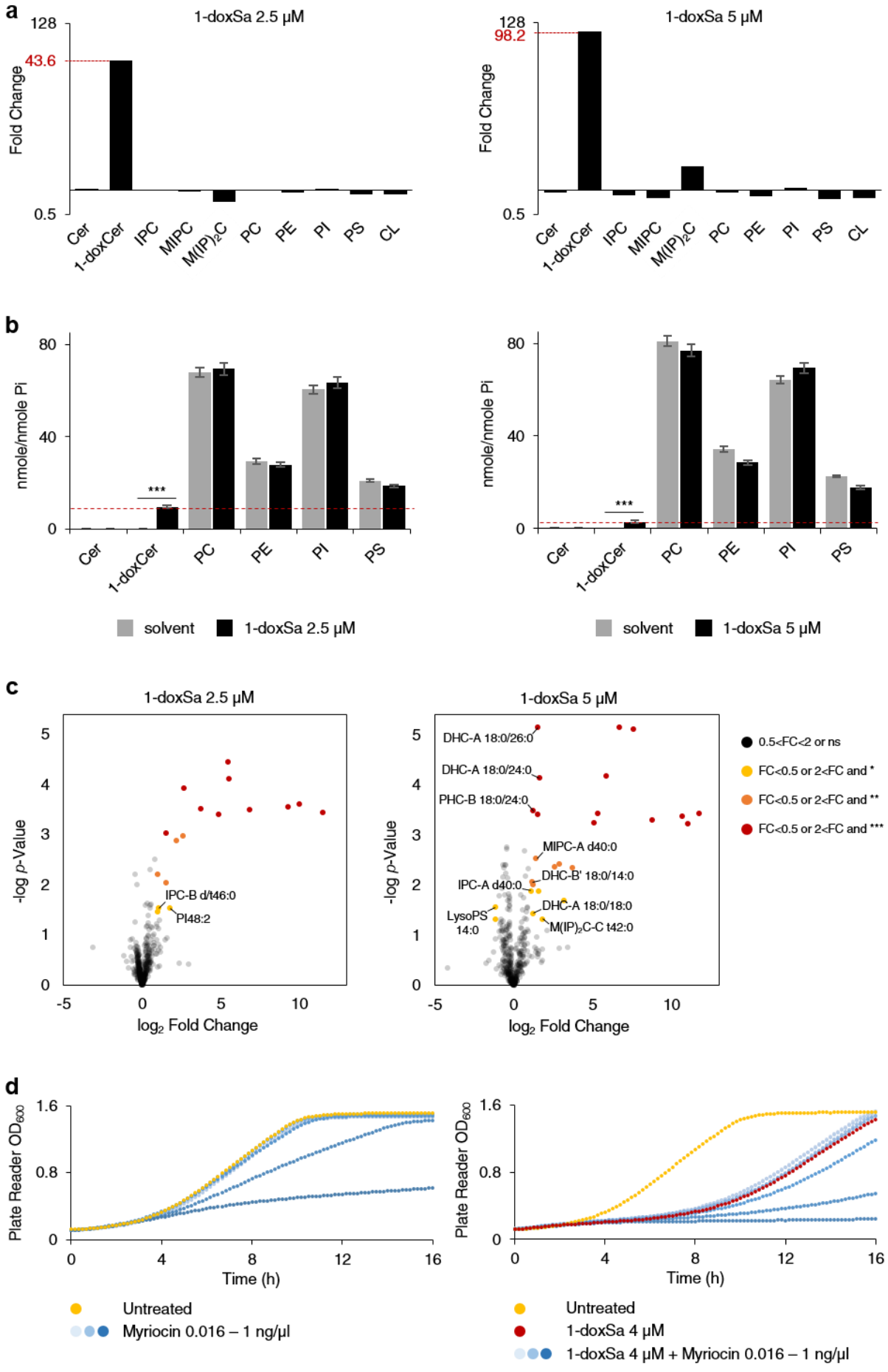
a
1-doxSa 2.5 µM
1-doxSa 5 µM
Fold Change
128
43.6
98.2
0.5
Cer
1-doxCer
IPC
MIPC
M(IP)2C
PC
PE
PI
PS
CL
b
nmole/nmole Pi
80
40
0
***
solvent
1-doxSa 2.5 µM
1-doxSa 5 µM
c
-log p-Value
log2 Fold Change
IPC-B d/t46:0
PI48:2
DHC-A 18:0/26:0
DHC-A 18:0/24:0
PHC-B 18:0/24:0
MIPC-A d40:0
DHC-B' 18:0/14:0
IPC-A d40:0
DHC-A 18:0/18:0
LysoPS 14:0
M(IP)2C-C t42:0
0.5<FC<2 or ns
FC<0.5 or 2<FC and *
FC<0.5 or 2<FC and **
FC<0.5 or 2<FC and ***
d
Plate Reader OD600
Time (h)
Untreated
Myriocin 0.016 – 1 ng/µl
1-doxSa 4 µM
1-doxSa 4 µM + Myriocin 0.016 – 1 ng/µl

Figure 7. 1-deoxy-ceramide has distinct biological properties. Changes in the levels of lipid classes (**a,b**) or lipid species (**c**) accompanying the accumulation of 1-deoxy-ceramide (1-doxCer). Lipid species whose levels change significantly are 1-doxCer species unless indicated otherwise. Exponentially growing Cers3 cells were treated with 2.5 or 5 μM of 1-deoxy-sphinganine (1-doxSa) for 1.5 h. The amounts of lipids were determined by mass spectrometry. PC: phosphatidylcholine, PE: phosphatidylethanolamine, PI: phosphatidylinositol, PS: phosphatidylserine, CL: cardiolipin. (**d**) Myriocin and 1-doxCer act independently on the cell. CerS3 cells were treated without or with 4 μM of 1-doxSa in combination with various concentrations of myriocin. The growth of yeast was followed with a plate reader.

2. Genetic screens reveal the natures of the toxicity of 1-deoxy-sphingolipids

2.1. 1-deoxy-sphingolipids disrupt multiple cellular processes

To determine the mode of action of 1-doxSphs, we performed a genome-wide genetic screen for gene products whose depletion or reduced amounts confer hypersensitivity or resistance to 1-doxSphs. To this end, we expressed mammalian CerS3 in a collection of knockout and hypomorphic (DAmP) strains by the synthetic genetic array (SGA) method [192]. In this method, a series of colony pinning onto different agar media was performed to cross the CerS3 strain with the strains in the collection, select diploid cells, sporulate diploid cells, select cells with the same mating type as that of the strains in the collection, and finally select the strains in the collection that carry CerS3. Then, we replica plated the strains onto agar media supplemented with different concentrations of 1-doxSa. Two levels of concentration were chosen, so that hypersensitive or resistant strains were revealed prominently at the lower or higher concentration, respectively. Colony size was scored as a measure of fitness of the strains (**Fig. 8a**). The screen covered 79.5% of non-essential genes and 68.8% of essential genes (**Fig. 8b**).

The screen revealed that depletion of genes that are required for efficient synthesis of very long-chain fatty acyl-CoA or import of sphingoid bases confers strong resistance to 1-doxSphs on the cell. Since the conversion of 1-doxSa to the main toxic lipid C_{26} 1-doxCer

requires very long-chain fatty acyl-CoA, this finding validates that changes in the fitness of the strains reflect the extent of the toxicity of 1-doxSphs especially of C_{26} 1-doxCer (**Fig. 8c**).

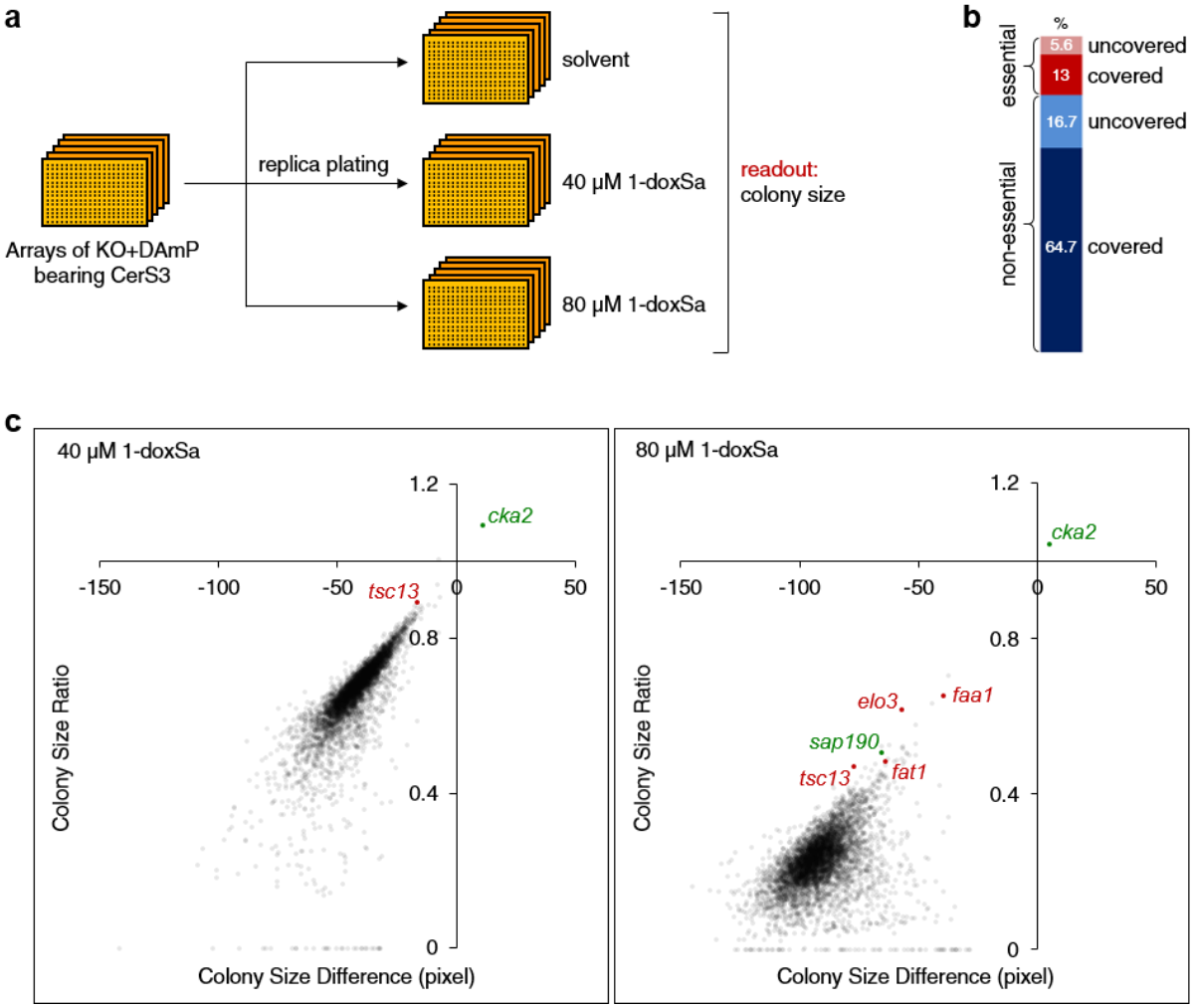

Figure 8. Genetic screen of knockout and hypomorphic (DAmP) strains for gene products involved in the toxicity of 1-deoxy-sphingolipids. (**a**) Schematic workflow of the genetic screen. (**b**) Coverage of the genetic screen. (**c**) Changes in colony size following treatments of the indicated concentrations of 1-deoxy-sphinganine. Genes indicated in red are known genes required for efficient synthesis of very long-chain fatty acyl-CoA or import of sphingoid bases.

Gene ontology (GO) enrichment analysis of resistant genes showed that there is no enrichment of particular molecular functions, cellular components, or biological processes. Furthermore, the same analysis of hypersensitive genes and examination of individual resistant or hypersensitive genes failed to reveal a clear hypothesis for the mode of action of 1-doxSphs.

Therefore, we suspected that 1-doxSphs might perturb more than one cellular processes. In this case, a single gene perturbation is not sufficient to strongly modulate the toxicity of 1-doxSphs. An alternative explanation is that 1-doxSphs negatively affect an essential cellular function that cannot be suppressed by disrupting its upstream or downstream components. During the examination of individual genes, we found that the identities of about 10% of the strains in the collection could not be confirmed by colony PCR. In addition, several newly generated strains with relevant genotypes failed to show the same responses to 1-doxSphs as those initially found by the results of the screen. These raised concern that the mutants in the collection had accumulated too many suppressors.

To evaluate whether we missed important components of the toxicity of 1-doxSphs due to the screening method, we decided to perform another genome-wide genetic screen of a freshly-generated mutant library with a recently developed independent technology. The screen is termed SAturated Transposon Analysis in Yeast (SATAY) [194]. In this analysis, we induced random insertion of a transposon from a plasmid into the genome of CerS3 cells to generate a mutant library. The library was then divided and subjected to two-round treatments of different concentrations of 1-doxSa. Two levels of concentration were chosen for the same purpose as that in the previous screen. Transposon number and sequencing read per gene were recorded as measures for determining hypersensitive and resistant genes, respectively (**Fig. 9a**). The screen covered 91.5% of non-essential genes and 52.5% of essential genes (**Fig. 9b**).

Following the treatment with the lower concentration of 1-doxSa, the transposon numbers of most mutants remained unchanged, suggesting that the library maintained its complexity and that technical variability had minimum effects on the readout (**Fig. 9c**). Moreover, changes in sequencing reads revealed a set of resistant genes that are required for efficient synthesis of very long-chain fatty acyl-CoA or import of sphingoid bases and therefore also required for the production of C_{26} 1-doxCer similar to those found in the previous screen.

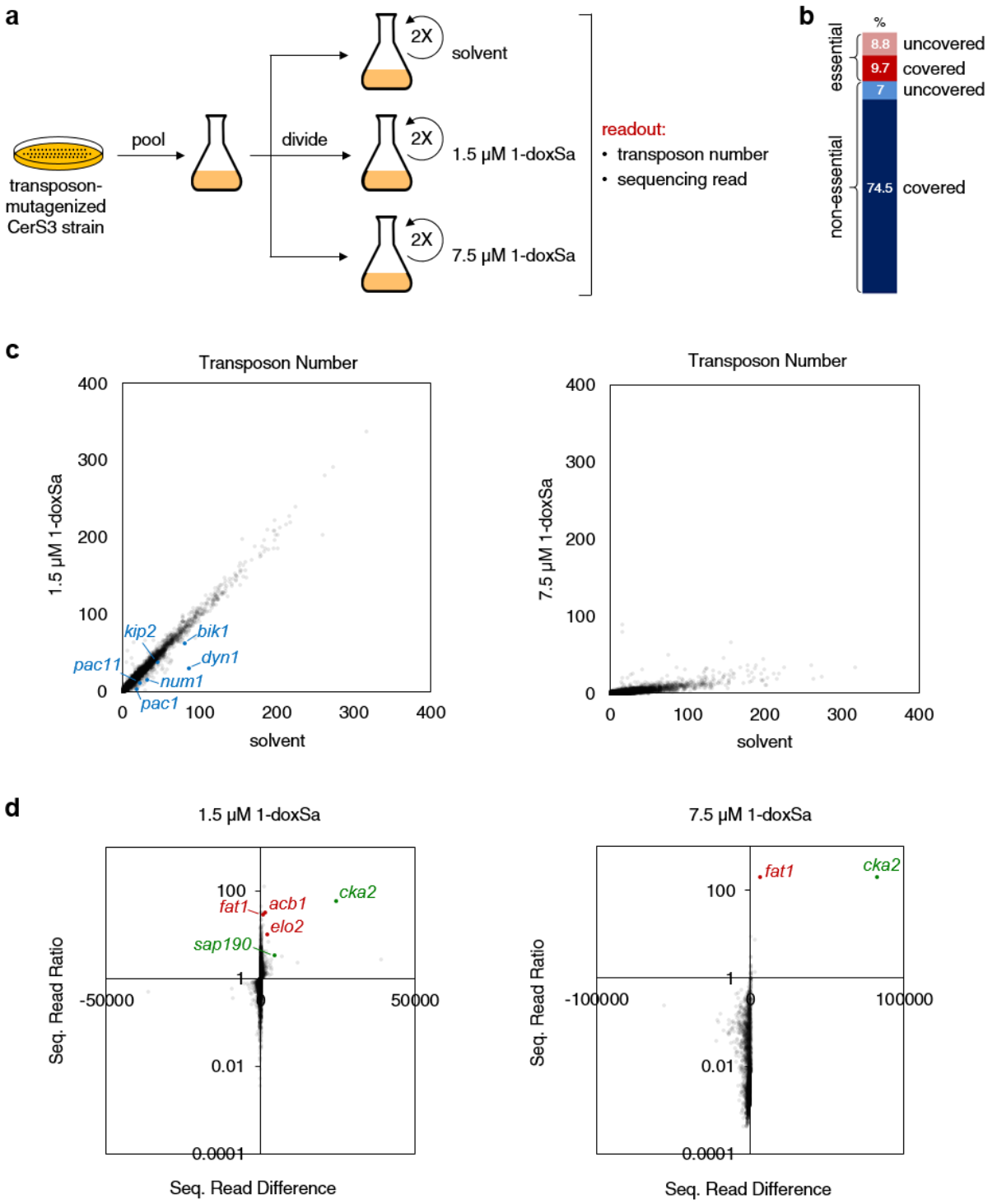

Figure 9. Genetic screen of strains generated by transposon mutagenesis for gene products involved in the toxicity of 1-deoxy-sphingolipids. (**a**) Schematic workflow of the genetic screen. (**b**) Coverage of the genetic screen. Changes in transposon number per gene (**c**) or sequencing read per gene (**d**) following treatments of the indicated concentrations of 1-deoxy-sphinganine. Genes indicated in blue are required for the late pathway of nuclear migration, whereas those indicated in red are known genes required for efficient synthesis of very long-chain fatty acyl-CoA or import of sphingoid bases.

This finding validates that the screen also charted the responses of mutants in the library to the toxicity of 1-doxSphs particularly of C_{26} 1-doxCer (**Fig. 9d**).

The treatment of the higher concentration of 1-doxSa, however, caused marked reduction in transposon number and sequencing read of virtually all mutants, suggesting that the library lost its complexity leaving only two mutants (*cka2Δ* and *fat1Δ*) with reduced levels of C_{26} 1-doxCer in the population (**Fig. 9c and d**). It also suggests that none of the screened genes, except for *cka2* and *fat1*, is the key factor in the toxicity of 1-doxSphs. Therefore, the results of the screen support our previous hypothesis that 1-doxSphs perturb multiple cellular processes or inhibit an essential function that cannot be suppressed by upstream or downstream mutations. As stated before, this mode of action might be achieved via direct inhibition of an essential protein with multiple functions, direct inhibition of multiple essential proteins, or perturbations of the structure of cellular membranes.

2.2. Toxicity of 1-deoxy-sphingolipids involves inhibition of nuclear migration

GO enrichment analysis of hypersensitive genes revealed by SATAY showed that (1) there is no enrichment of a particular molecular function, (2) dynein complex is the most enriched (21.2 fold) cellular component, and (3) nuclear migration along microtubules is the most enriched (17 fold) cellular process (**Fig. 10a**). In the budding yeast, nuclear migration is achieved by two sequential and partially overlapping pathways called the early and late pathways [203]. In the early pathway, the spindle is positioned along the mother-bud axis by the movement of myosin V attached to the plus ends of cytosolic microtubules along actin cables towards the bud tip.

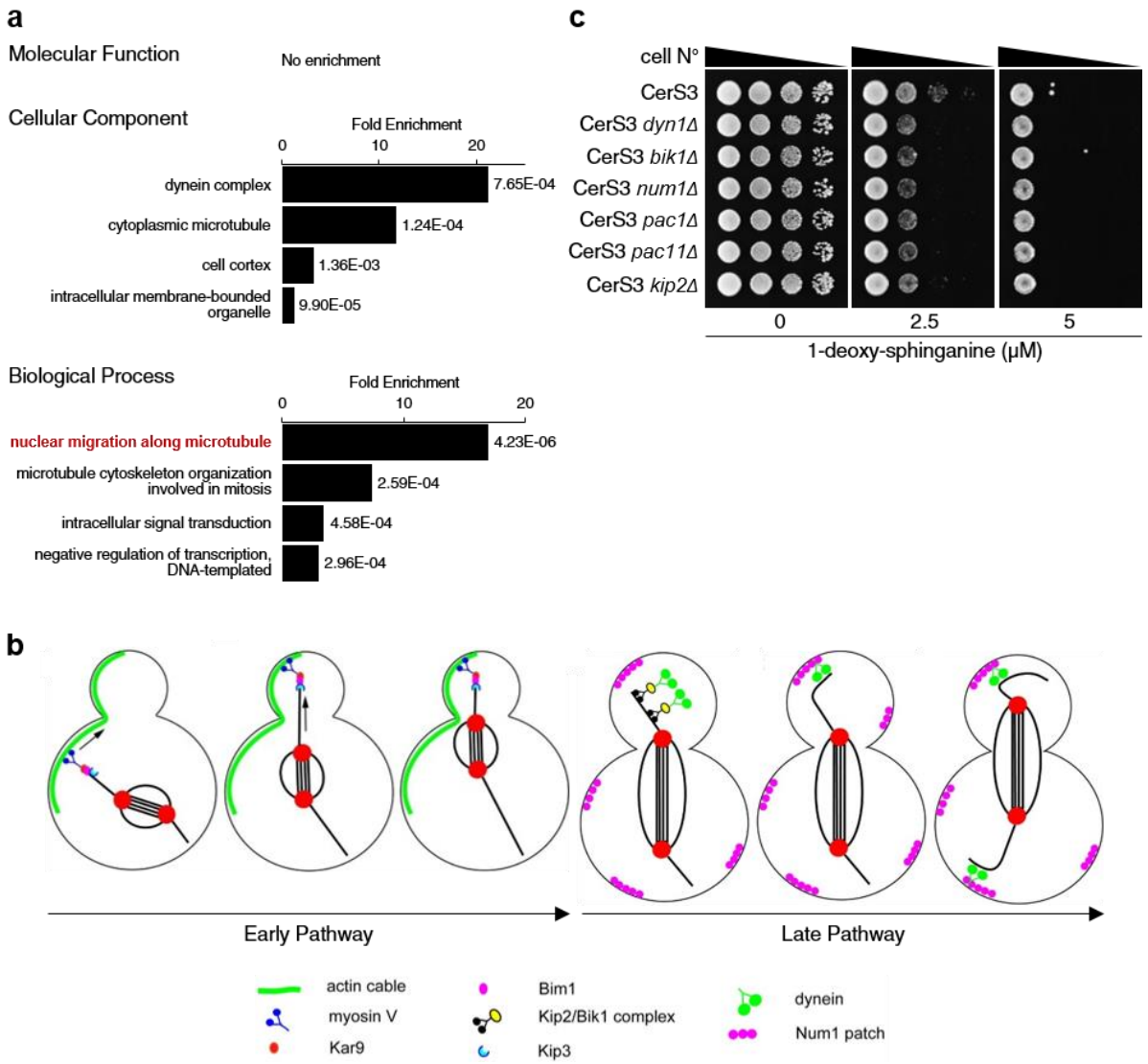

Figure 10. Gene ontology enrichment analysis reveals inhibition of nuclear migration by 1-deoxy-sphingolipids. (**a**) Gene ontology enrichment analysis of hypersensitive genes revealed by SATAY. Numbers in the histogram are *p*-values. (**b**) Schematic diagram of nuclear migration in the budding yeast. Modified from [203]. (**c**) CerS3 cells lacking the hypersensitive genes required for the late pathway of nuclear migration were spotted onto rich agar media supplemented with the indicated concentrations of 1-deoxy-sphinganine. The cells were spotted at a ten-fold serial dilution.

Once the plus ends have reached the bud tip, they are depolymerized thereby pulling the spindle towards the bud neck. In the late pathway, dynein molecules are transported towards the plus ends of cytosolic microtubules. Once they have arrived, dynein molecules are transferred onto the bud tip where they can slide the microtubules thereby pulling the spindle towards the bud. An analogous series of events to that in the bud in the late pathway also occurs in the mother

cell at late anaphase to prevent movement of the spindle all the way into the bud (**Fig. 10b**). The GO enrichment analysis found six hypersensitive genes that are involved in nuclear migration (*dyn1*, *bik1*, *num1*, *pac1*, *pac11*, and *kip2*). The spot assay showed that deletion of each of these genes mildly reduced the growth of CerS3 cells when 1-doxSa is presence in the medium (**Fig. 10c**). This result is consistent with that of SATAY, which is the sensitivity of most mutants of the six genes to 1-doxSphs was not strikingly higher than that of the other mutants in the library (**Fig. 9c**). In addition, it supports our hypothesis that 1-doxSphs perturb multiple cellular processes, among them nuclear migration.

To further confirm that the toxicity of 1-doxSphs involves inhibition of the cellular process, we conducted a cell cycle analysis. In this analysis, exponentially growing CerS3 cells were synchronized at different points in the cell cycle with different agents for 3 hours and then released in rich liquid media supplemented with different concentrations of 1-doxSa for 3 hours. Since cell shape changes through the cell cycle, we followed cell cycle progression of the populations by examining the proportion of cells with different cell shapes (**Fig. 11a**). The fact that nuclear migration is one of multiple cellular processes that are inhibited by 1-doxSphs poses two restrictions. First, a correct dose of 1-doxSa is required to observe the inhibition. It is because too much 1-doxSphs would strongly block cell cycle progression at all points, while too little 1-doxSphs would not affect cell cycle progression at all. Second, a large number of cells must be examined in each population to confidently detect the inhibition as it is expected to be subtle at the correct dose of 1-doxSa.

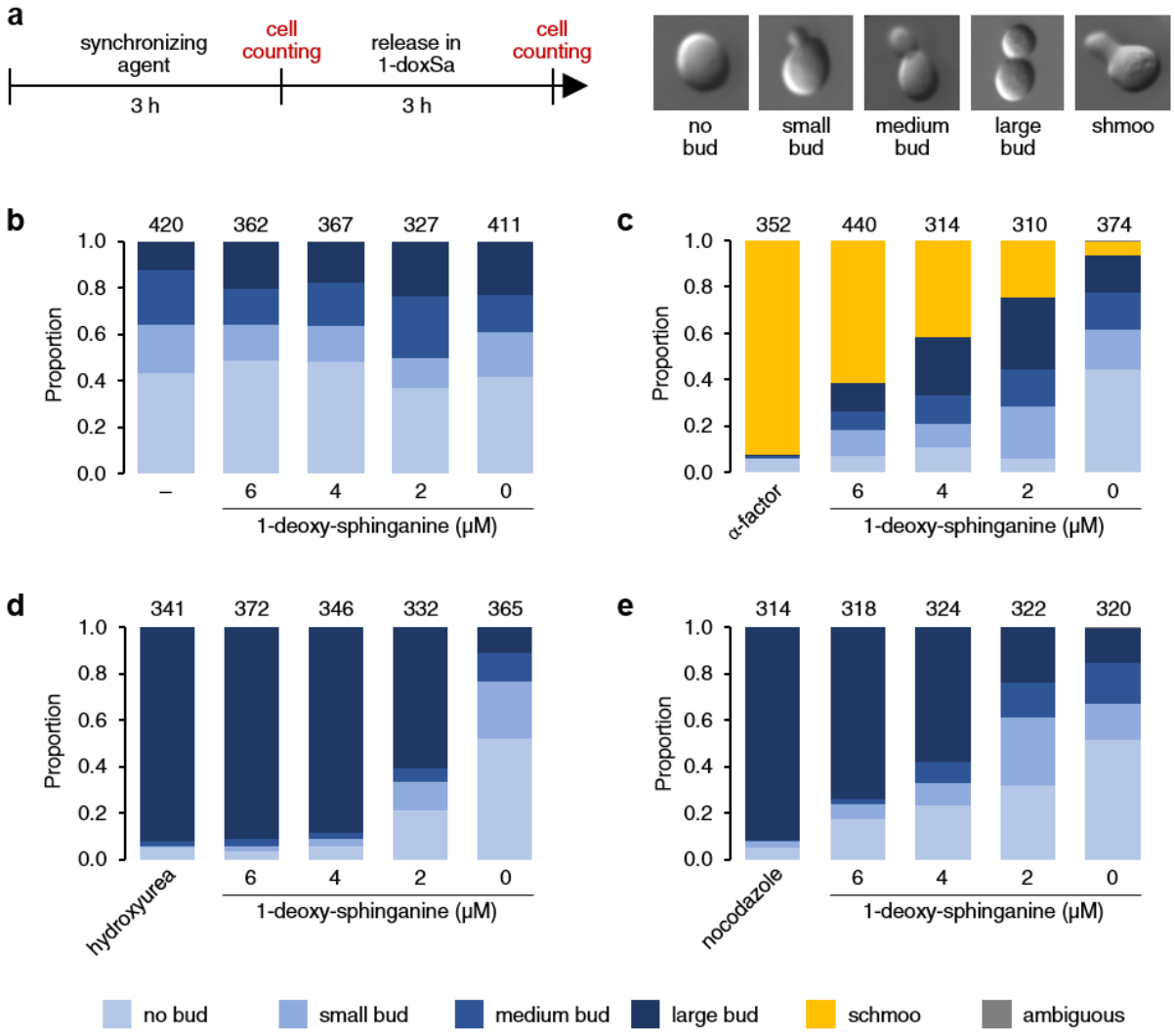

Figure 11. Cell cycle analysis reveals inhibition of nuclear migration by 1-deoxy-sphingolipids. (**a**) Schematic workflow of the cell cycle analysis showing representative cell shapes that were scored. (**b-e**) Changes in the proportion of CerS3 cells with different shapes following cell cycle synchronization and release in rich liquid media supplemented with the indicated concentrations of 1-deoxy-sphinganine (1-doxSa). Exponentially growing CerS3 cells were not synchronized (**b**) or synchronized with α-factor (**c**), hydroxyurea (**d**), or nocodazole (**e**).

The six hypersensitive genes are not essential and are exclusively required for the late pathway of nuclear migration. Since the early and late pathways are partially redundant, these indicate that the proteins encoded by the genes are not the direct targets of 1-doxSphs and that 1-doxSphs inhibit the early pathway. This inhibition would result in the accumulation of cells with medium buds in the population. The cell cycle analysis showed that asynchronous population had increased proportion of cells with medium buds following a treatment with 2

μM of 1-doxSa (**Fig. 11b**). It suggests that indeed 1-doxSphs inhibit the early pathway of nuclear migration. This inhibition, however, was not observed in populations treated with 4 or 6 μM of 1-doxSa. It is possible because 1-doxSphs might perturb multiple cellular processes, therefore higher levels of 1-doxSphs could also enhance perturbations of other cellular processes. These enhanced broad perturbations lead to inhibition of cell cycle progression at all points, obscuring the inhibition of nuclear migration. This inhibition, therefore, was best observed following a treatment with 2 μM of 1-doxSa in the analysis.

Nuclear migration begins in the G2 phase of the cell cycle. Its inhibition was also observed in the population synchronized at G1/S with α-factor after being released in a medium containing 2 μM of 1-doxSa (**Fig. 11c**). The population had increased proportion of cells with large buds, probably because these cells were shmoo cells that acquired slight increase in bud size as they progressed through the S phase. Inhibition of nuclear migration was most obvious in the population synchronized at the S phase with hydroxyurea after being released in a medium containing 2 μM of 1-doxSa (**Fig. 11d**). The population had difficulties in progressing through the cell cycle as nuclear migration takes place right after the S phase. Inhibition of nuclear migration was not observed in the population synchronized at G2/M with nocodazole after being released in a medium containing 2 μM of 1-doxSa (**Fig. 11e**). It was because the population had to go through a complete cell cycle to experience inhibition of nuclear migration in the G2 phase. This long time gap combined with the subtle inhibition of nuclear migration obscured the impacts of 1-doxSphs on the cell cycle. Taken together, 1-doxSphs inhibit the early pathway of nuclear migration among other cellular processes.

2.3. Sap190 ensures the normal proportion of C_{24} to C_{26} fatty acyl-CoA

Growth inhibition of CerS3 cells following 1-doxSa treatment involves several processes including the uptake of 1-doxSa from the medium, the production of C_{26} fatty acyl-

CoA, and the acylation of 1-doxSa by CerS3 using the fatty acyl-CoA to form C_{26} 1-doxDHCer. The lipid is much more toxic than 1-doxSa and is the major 1-doxCer produced by CerS3 cells. Therefore, genetic perturbations that lead to the reduction of the efficiency of the processes confer resistance to 1-doxSphs on the cell. Indeed, resistant mutants found by the genetic screens are defective in various known steps for efficient synthesis of very long-chain ($C_{24\text{-}26}$) fatty acyl-CoA or import of sphingoid bases in yeast (**Fig. 12**). This provides a strong indication that the screens might also reveal novel proteins that have not been assigned to the processes.

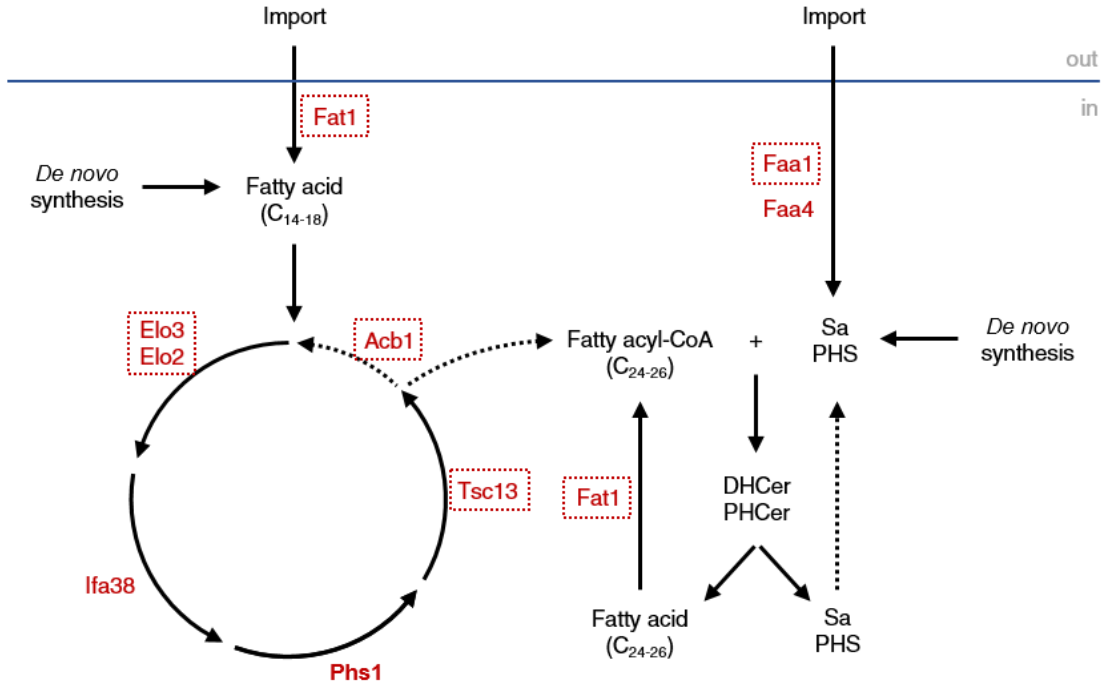

Figure 12. The genetic screens capture most known proteins required for efficient synthesis of very long-chain fatty acyl-CoA or import of sphingoid bases in yeast. Proteins are indicated in red. Essential protein is indicated in bold type. Proteins captured by the screens are indicated by dashed red rectangles.

Among the resistant genes that were consistently revealed in the two screens, *CKA2* and *SAP190* were not known to be required for efficient synthesis of very long-chain fatty acyl-CoA in yeast. To test whether they are required for the process, first we generated knockout mutants of the genes in CerS3 background and tested their resistance to 1-doxSphs with the spot assay. The assay showed that the *cka2Δ* mutant is extremely resistant, whereas the

sap190Δ mutant is mildly resistant to 1-doxSphs (**Fig. 13a**). This result confirms the results of the screens. Second, we treated exponentially growing cells of the mutants with 2.5 μM of 1-doxSa for 1.5 hours and measured the levels of their 1-doxCer and ceramides (dihydroceramide and phytoceramide) by mass spectrometry. Mass spectrometry analysis showed that the *cka2Δ* mutant has a significantly lower level of 1-doxCer than that of control, whereas the *sap190Δ* mutant has a similar level of 1-doxCer to that of control (**Fig. 13b**).

Next, we quantified the individual 1-doxCer species. The *cka2Δ* mutant produced most of 1-doxCer species at much lower levels than those in control (**Fig. 13c**). Its 1-doxCer species profile, however, did not reflect its ceramide species profile since it produced significantly higher levels of ceramide 36 and 38 than those in control (**Fig. 13e**). These results suggest that Cka2 might be required for the synthesis of C_{26} 1-doxCer rather than for providing the C_{26} fatty acyl-CoA substrate. Phosphorylation of the C-terminal regions of yeast ceramide synthase by Cka2 is required for its maximum activity [37,38]. If this hypothesis is correct, then it is likely that most of the ceramide 36 and 38 are produced via the reverse reaction of yeast ceramidase [204,205]. Phosphorylation also enhances the activity of mammalian CerS3, although the kinase responsible for it is unknown [43]. Therefore, phosphorylation of CerS3 by Cka2 might be required for efficient synthesis of C_{26} 1-doxCer.

In contrast to the *cka2Δ* mutant, the *sap190Δ* mutant produced a significantly higher level of 1-doxCer 42 and a lower level of 1-doxCer 44 than those in control (**Fig. 13d**). The modest reduction in the level of 1-doxCer 44 corresponds to the mild resistance of the mutant to 1-doxSphs. Moreover, the level of 1-doxCer 42 is slightly higher than that of 1-doxCer 44 in the mutant. These results suggest that C_{24} 1-doxCer is much less toxic than C_{26} 1-doxCer. The 1-doxCer species profile of the mutant reflected its ceramide species profile as it also produced a significantly higher level of ceramide 42 and a lower level of ceramide 44 than those in control (**Fig. 13e**). These results suggest that Sap190 affects the proportion of C_{24} to

C_{26} fatty acyl-CoA and therefore affects the ratio of the two 1-doxCer species. The role of Sap190 in maintaining the proportion of C_{24} to C_{26} fatty acyl-CoA was previously unknown. How Sap190 achieves this function remains to be investigated.

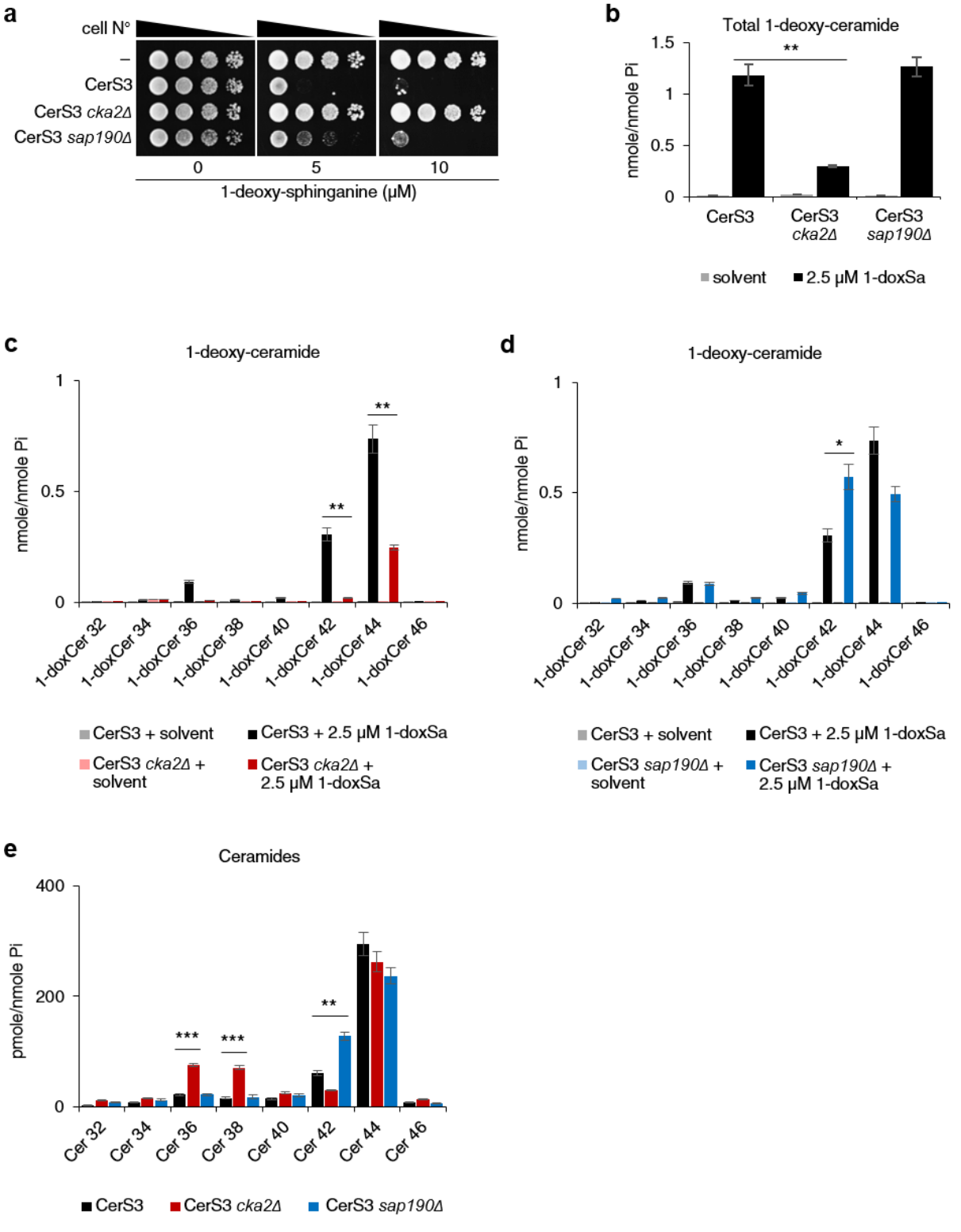

Figure 13. Cka2 and Sap190 are required for efficient synthesis of C_{26} 1-deoxy-ceramide. (**a**) Depletion of Cka2 or Sap190 confers resistance to 1-deoxy-sphingolipids. Cells were spotted onto rich agar media supplemented with the indicated concentrations of 1-deoxy-sphinganine (1-doxSa). The cells were spotted at a ten-fold serial dilution. Impacts of Cka2 or Sap190 depletion on the levels of 1-deoxy-ceramide (1-doxCer) following 1-doxSa treatment (2.5 μM, 1.5 h) (**b-d**) and the levels of ceramides (**e**) in CerS3 cells. The amounts of lipids were determined by mass spectrometry.

3. Features of the toxicity of 1-deoxy-sphingolipids

3.1. 1-deoxy-sphinganine disrupts the organization of actin

Supplementation of 1-doxSa into the growth medium has been shown to markedly reduce the presence of actin stress fibers in a mammalian cell line [184], indicating that the toxicity of 1-doxSphs in mammalian cells involves disruption of actin organization. The second genetic screen (SATAY) revealed that 1-doxSphs inhibit the early pathway of nuclear migration which requires intact actin cables. Therefore, it is possible that 1-doxSphs also disrupt actin organization in yeast cells. To test this hypothesis, we monitored the impact of 1-doxSa treatment on actin organization. Briefly, exponentially growing cells were treated with 1-doxSa for 3 hours and immediately fixed with 4% formaldehyde for 20 min. F-actin was stained with phalloidin-Atto488 for 1 hour and visualized by confocal microscopy.

The microscopy showed that the presence of actin cables and actin patches was greatly reduced. Moreover, multiple micron-sized round bodies stained by phalloidin-Atto488 appeared in the cells. These effects were independent of the expression of mammalian CerS3 (**Fig. 14 upper panel**). This result suggests that 1-doxSa is sufficient to induce the changes in actin organization. This finding was corroborated by the same result in CerS3 *cka2Δ* and CerS3 *sap190Δ* cells that have reduced levels of C_{26} 1-doxCer (**Fig. 14 lower panel**). Disruption of actin organization including the loss of actin cables by 1-doxSa might contribute to the inhibition of nuclear migration. Since 1-doxCer is synthesized later than 1-doxSa, inhibition of nuclear migration could be one of the first events in the toxicity of 1-doxSphs in yeast cells.

However, the disruption of actin organization and the inhibition of nuclear migration are not the main factors that kills the cell because 1-doxSa is much less toxic than 1-doxCer.

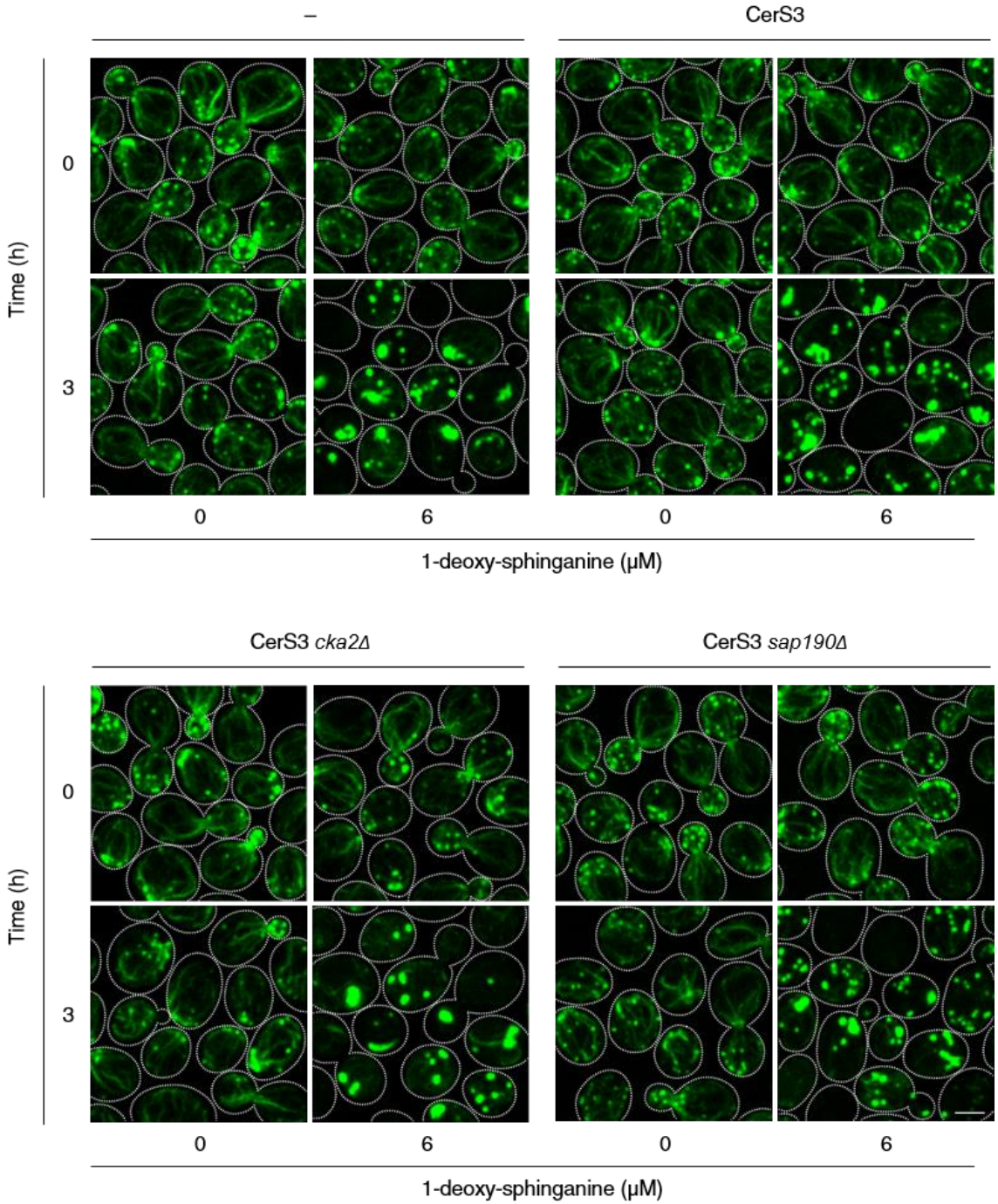

Figure 14. 1-deoxy-sphinganine disrupts the organization of actin. Exponentially growing cells were treated with the indicated concentrations of 1-deoxy-sphinganine for 3 h. Then, the cells were fixed with 4% formaldehyde for 20 min. F-actin was stained with phalloidin-Atto488 for 1 h and visualized by confocal microscopy. Scale bar is 2 μm.

3.2. Toxicity of 1-deoxy-sphingolipids does not involve oxygen-dependent functions of mitochondria

Treatment of 1-doxSa has been shown to induce mitochondrial fragmentation, induce the loss of mitochondrial cristae, reduce respiration, and reduce ATP production in a mammalian cell line [185]. These results indicate that 1-doxSphs perturb mitochondrial functions in mammalian cells. To examine whether 1-doxSphs also perturb mitochondrial functions in yeast cells, we first monitored changes in the shape and distribution of mitochondria following 1-doxSa treatment. Briefly, exponentially growing cells expressing mCherry tagged-mitochondrial malate dehydrogenase (Mdh1-mCherry) were treated with 1-doxSa for 3 hours. Mitochondria were immediately visualized by confocal microscopy without cell fixation.

The microscopy showed that the treatment altered the shape of mitochondria from tubular to spherical. Moreover, the spherical mitochondria could still be found in the buds, indicating that 1-doxSphs do not inhibit the inheritance of mitochondria from the mother to the bud. These effects were independent of the expression of mammalian CerS3 (**Fig. 15 upper panel**), suggesting that 1-doxSa is sufficient to induce the alteration. This finding is confirmed by the same result in CerS3 *cka2Δ* and CerS3 *sap190Δ* cells that have reduced levels of C_{26} 1-doxCer (**Fig. 15 lower panel**). The alteration in the shape of mitochondria might be an indication of inhibition of mitochondrial fission, or mitochondrial tethering to the cell cortex [206,207] or to the ER [208].

Next, we asked if the alteration in the shape of mitochondria is accompanied by inhibition of key functions of mitochondria. The essential function of mitochondria in yeast is to assemble iron-sulfur clusters (ISCs) which are ancient cofactors of proteins implicated in electron transport, enzyme catalysis, and regulation of gene expression [209,210].

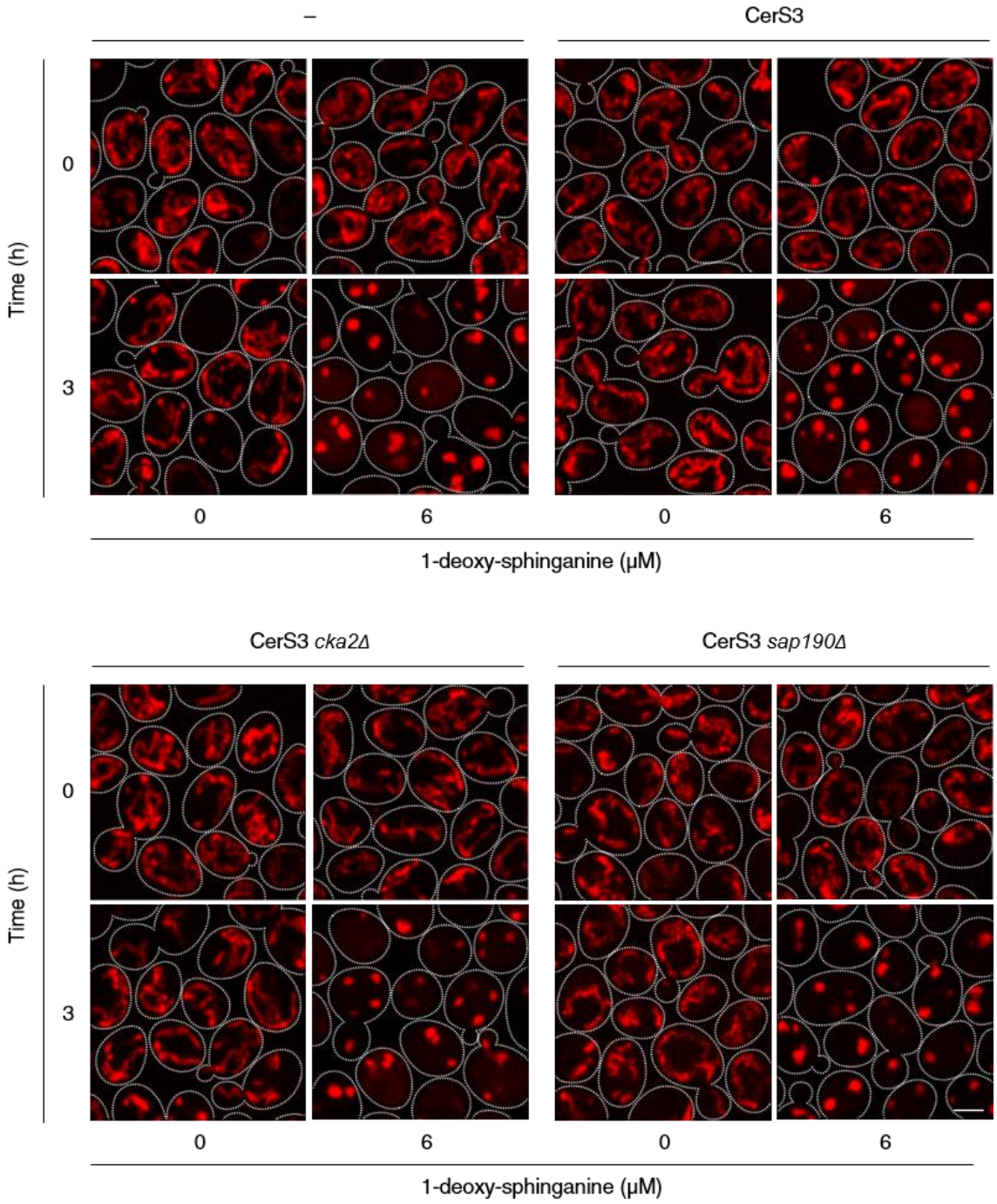

Figure 15. 1-deoxy-sphinganine alters the shape of mitochondria. Exponentially growing cells expressing Mdh1-mCherry were treated with the indicated concentrations of 1-deoxy-sphinganine for 3 h. Mitochondria were visualized by confocal microscopy without cell fixation. Scale bar is 2 μm.

The first genetic screen showed that hypomorphic (DAmP) strains of the essential genes involved in the process were not hypersensitive to 1-doxSphs. In addition, the second genetic screen (SATAY) showed that mutants with disrupted non-essential genes involved in the

process were neither resistant nor hypersensitive to 1-doxSphs. Therefore, we argue that 1-doxSphs do not inhibit the assembly of ISCs in mitochondria.

Another function of mitochondria in yeast is to perform molecular respiration in the presence of oxygen. Perturbations of this process very often lead to the production of excess reactive oxygen species (ROS) which is toxic to the cell at high levels. Therefore, we tested if the accumulation of 1-doxSphs is accompanied by the accumulation of ROS. Briefly, CerS3 cells were cultured in rich media without or with a precursor of the antioxidant glutathione, *N*-acetyl-L-cysteine (NAC) for two generations and then transferred into the same medium supplemented with H_2O_2 for 3 hours. The levels of ROS in the cells were measured using a general ROS fluorescence indicator CM-H_2DCFDA with a microplate reader at Ex/Em 493/522 nm. The measurement showed that H_2O_2 treatment increased the fluorescence intensity of the indicator and that this effect was suppressed by NAC treatment. This result suggests that the method could be used to measure the levels of ROS in the cells. Next, we used the method to measure the levels of ROS in the cells following 1-doxSa treatment. The measurement showed that indeed the accumulation of 1-doxSphs is accompanied by the accumulation of ROS. This result might indicate that 1-doxSphs perturb mitochondrial respiration, leading to the production of excess ROS (**Fig. 16a**).

To further examine the role of ROS in the toxicity of 1-doxSphs, we tested the impact of H_2O_2 on actin and mitochondria by microscopy. The microscopy showed that H_2O_2 perturbed the organization of actin in a dose-dependent manner in a similar way to 1-doxSa. However, H_2O_2 at the same concentrations did not affect the shape and distribution of mitochondria (**Fig. 16b**). These results suggest that elevated levels of H_2O_2 cannot fully account for the toxicity of 1-doxSphs. Next, we tested if NAC can alleviate the impacts of 1-doxSa on actin and mitochondria by microscopy.

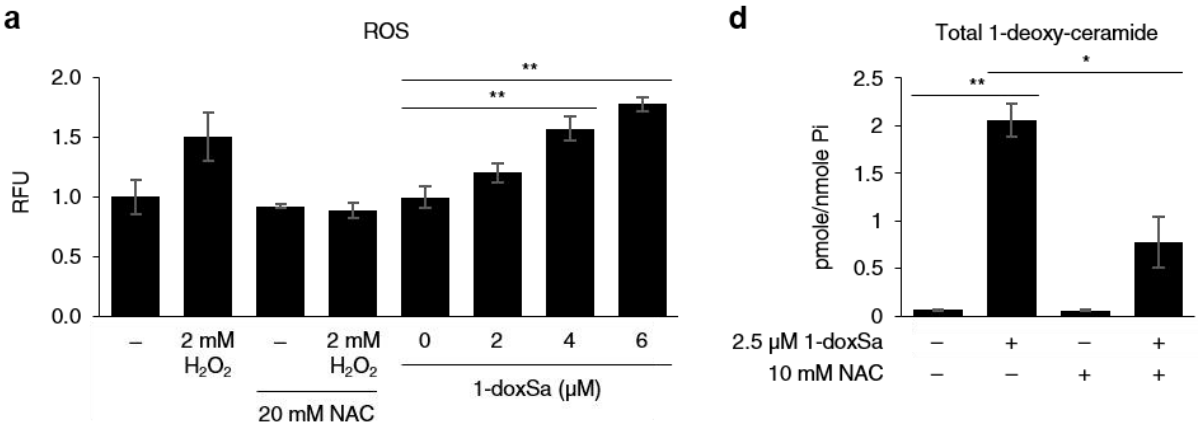
a
ROS
RFU
2.0
1.5
1.0
0.5
0.0
**
**
–
2 mM H2O2
–
2 mM H2O2
0
2
4
6
20 mM NAC
1-doxSa (μM)
d
Total 1-deoxy-ceramide
pmole/nmole Pi
2.5
2
1.5
1
0.5
0
**
*
2.5 μM 1-doxSa
10 mM NAC

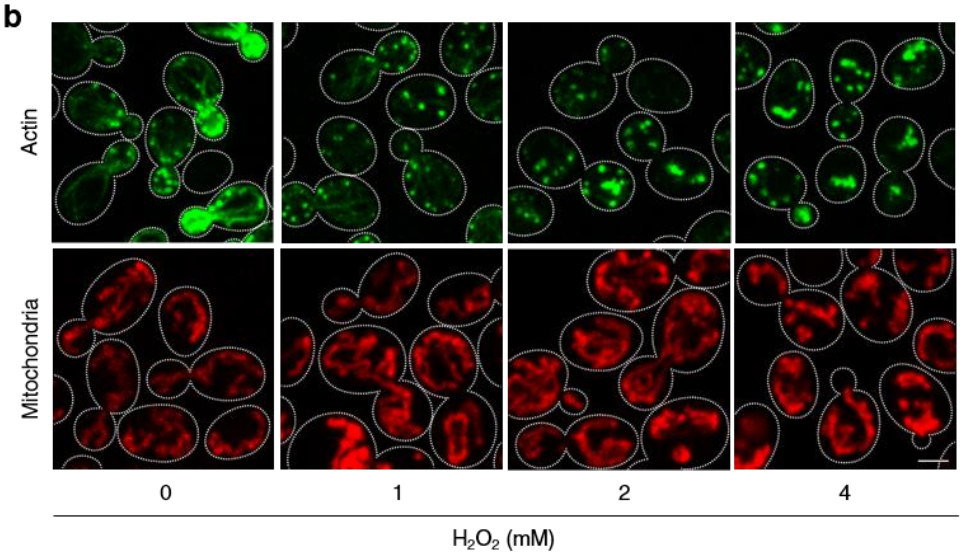
b
Actin
Mitochondria
0
1
2
4
H2O2 (mM)

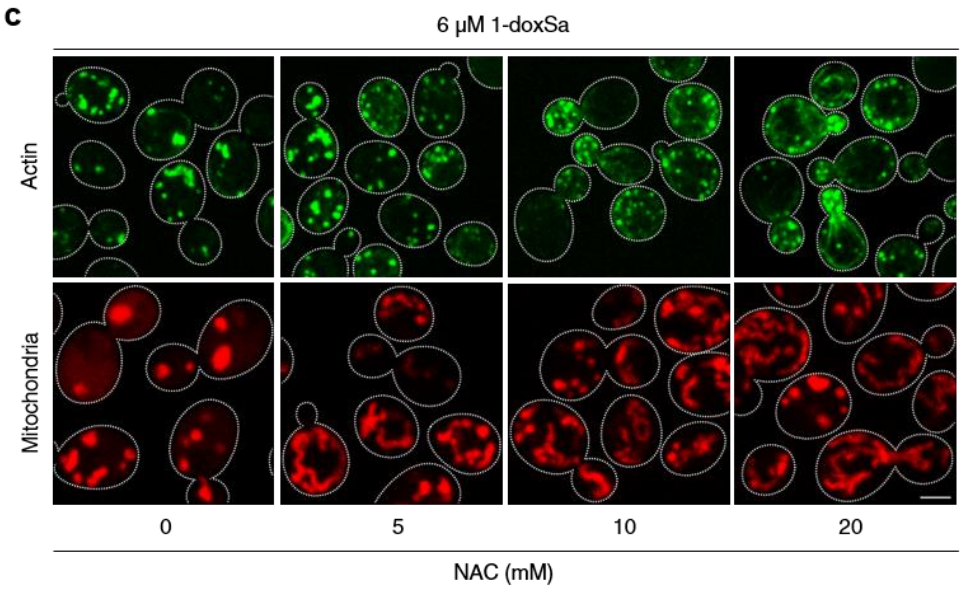
c
6 μM 1-doxSa
Actin
Mitochondria
0
5
10
20
NAC (mM)

Figure 16. *N*-acetyl-L-cysteine alleviates the toxicity of 1-deoxy-sphingolipids. (**a**) Accumulation of 1-deoxy-sphingolipids is accompanied by the accumulation of reactive oxygen species (ROS). (**b**) Impacts of H_2O_2 on actin, but not on mitochondria, mimic those of 1-deoxy-sphinganine (1-doxSa). *N*-acetyl-L-cysteine (NAC) suppresses the impacts of 1-doxSa on actin and mitochondria (**c**) as well as the synthesis of 1-deoxy-ceramide (**d**). Exponentially growing CerS3 cells were treated with the indicated concentrations of H_2O_2 or 1-doxSa for 3 h (1.5 h for lipid analysis). NAC was introduced at two generation times prior to and at the start of the H_2O_2 or 1-doxSa treatment. ROS was measured with CM-H_2DCFDA. Visualization of F-actin and mitochondria as well as measurement of lipid levels were the same as described before.

The microscopy showed that NAC suppressed the perturbations of both actin and mitochondria by 1-doxSa in a dose-dependent manner (**Fig. 16c**), indicating that NAC inhibits the uptake or the action of 1-doxSa. To test these hypotheses, we measured the levels of 1-doxCer following NAC and 1-doxSa treatments by mass spectrometry. The measurement showed that NAC significantly suppressed the accumulation of 1-doxCer (**Fig. 16d**). Since synthesis of 1-doxCer is not required for the effects on the actin cytoskeleton, this suggests that NAC alleviates the toxicity of 1-doxSphs by blocking the accumulation of ROS or by inhibiting the uptake of 1-doxSa from the medium. Further proof of the latter would require the direct measurement of 1-doxSa uptake with and without NAC.

The ROS fluorescence indicators DCFH and its derivatives (incl. CM-H_2DCFDA) are commonly used to measure the levels of ROS in cells. However, they have serious caveats such as (1) they do not directly react to H_2O_2, (2) they can be oxidized by several one-electron oxidizing species, (3) they can actually produce O_2 and H_2O_2, thereby artificially elevating the levels of ROS, and (4) transition metals, cytochrome *c*, and heme peroxidases can catalyze their oxidation [211]. These caveats make them unreliable for measuring the levels of ROS in cells. To evaluate the roles of ROS and oxygen-dependent functions of mitochondria in the toxicity of 1-doxSphs, we tested the effect of oxygen depletion on their toxicity by the spot assay. We established an anaerobic culture condition by absorbing oxygen while simultaneously generating carbon dioxide with a proprietary reagent (Oxoid™ AnaeroGen™)

inside an airtight chamber. The reagent reduces the oxygen level in the chamber to below 1% within 30 minutes. The presence of oxygen inside the chamber was monitored with color indicators. The indicators turned from turquoise to white in the absence of oxygen (**Fig. 17a**).

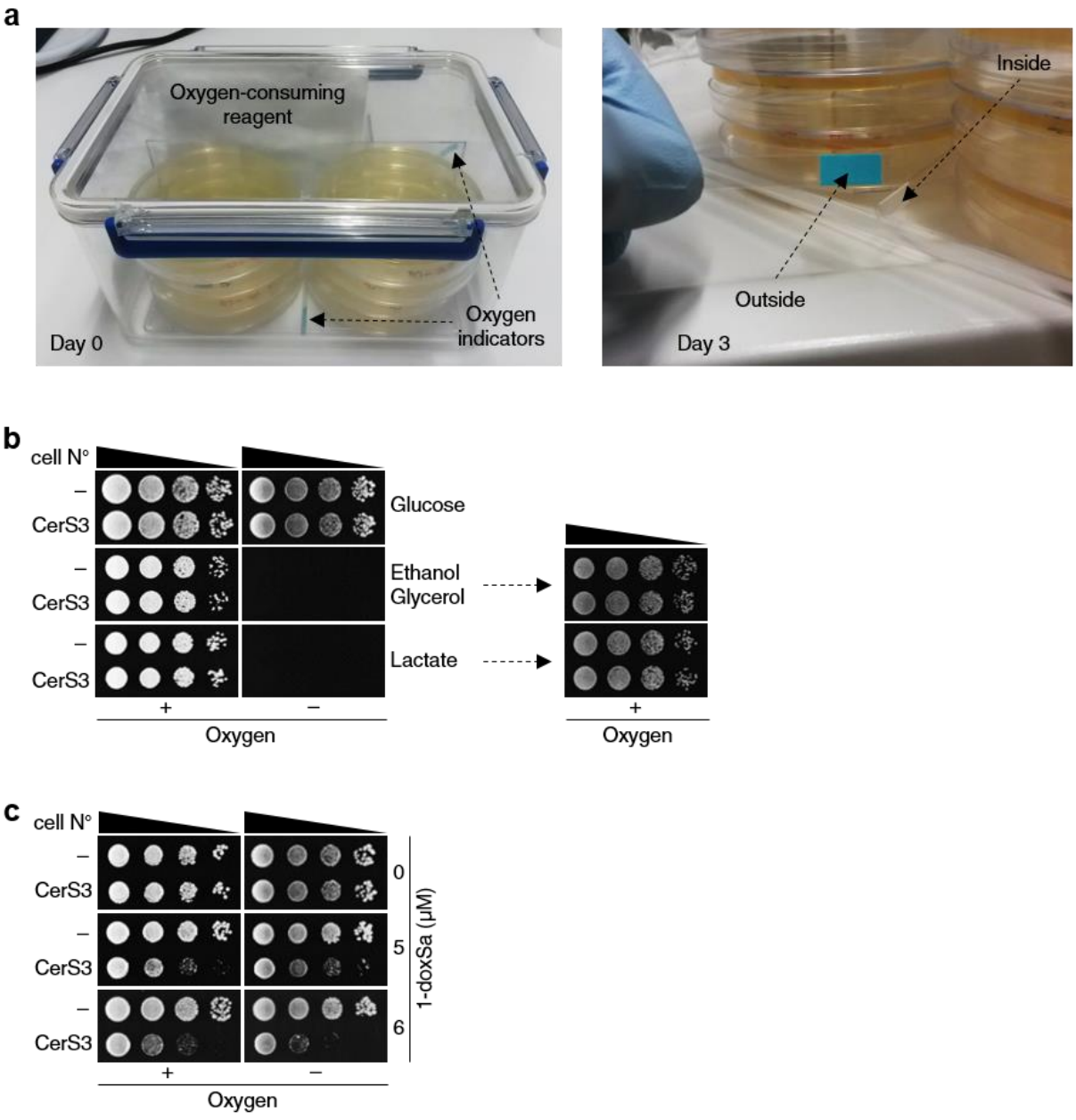

Figure 17. Toxicity of 1-deoxy-sphingolipids does not involve oxygen-dependent functions of mitochondria. (**a**) Overview of the setup of anaerobic cultures. (**b**) Cells cultured on non-fermentable carbon sources could not grow inside the chamber. They resumed their growth once re-oxygenated. The color indicators and the growth of cells indicate that the chamber was oxygen-free. (**c**) Oxygen-dependent functions of mitochondria are not inhibited by 1-deoxy-sphingolipids. Cells were spotted at a ten-fold serial dilution onto rich agar media with the indicated concentrations of 1-deoxy-sphinganine and cultured with or without oxygen in the chamber.

Since the budding yeast requires oxygen to synthesize sterols and unsaturated fatty acids which are essential for growth, the media for the anaerobic cultures were supplemented with ergosterol and Tween® 80. The spot assay showed that cells cultured on agar media with non-fermentable carbon sources (ethanol-glycerol or lactate) were not able to grow inside the chamber after 3 days of incubation. However, they resumed their growth once they were taken out of the chamber (**Fig. 17b**). This result together with the color indicators that turned white demonstrate that oxygen inside the chamber was depleted to a level that cannot support the mitochondrial respiration of yeast. The spot assay also showed that CerS3 cells cultured on rich agar media supplemented with 1-doxSa outside or inside the chamber had comparable growth rates (**Fig. 17c**). This result suggests that ROS and oxygen-dependent functions of mitochondria are not implicated in the toxicity of 1-doxSphs.

The collection of knockout and hypomorphic (DAmP) strains in the first genetic screen did not include strains with mutated genes in the mitochondrial genome. In addition, the transposon mutagenesis in the second genetic screen did not target the mitochondrial genome. Therefore, we could not evaluate the roles of gene products encoded by the mitochondrial genome in the toxicity of 1-doxSphs by the two screens. To fill this gap of information, we generated CerS3 cells lacking the mitochondrial genome (CerS3 ρ^0 cells) by inhibiting the replication of their mitochondrial genome with ethidium bromide for multiple generations. Microscopy of DAPI-stained cells showed that CerS3 ρ^0 cells did not have DNA outside the nucleus (**Fig. 18a**). Moreover, the cells were not able to grow on a medium with a non-fermentable carbon source (glycerol) since its utilization requires functional mitochondrial respiration and intact mitochondrial genome (**Fig. 18b**). These results demonstrate that the cells truly lacked the mitochondrial genome.

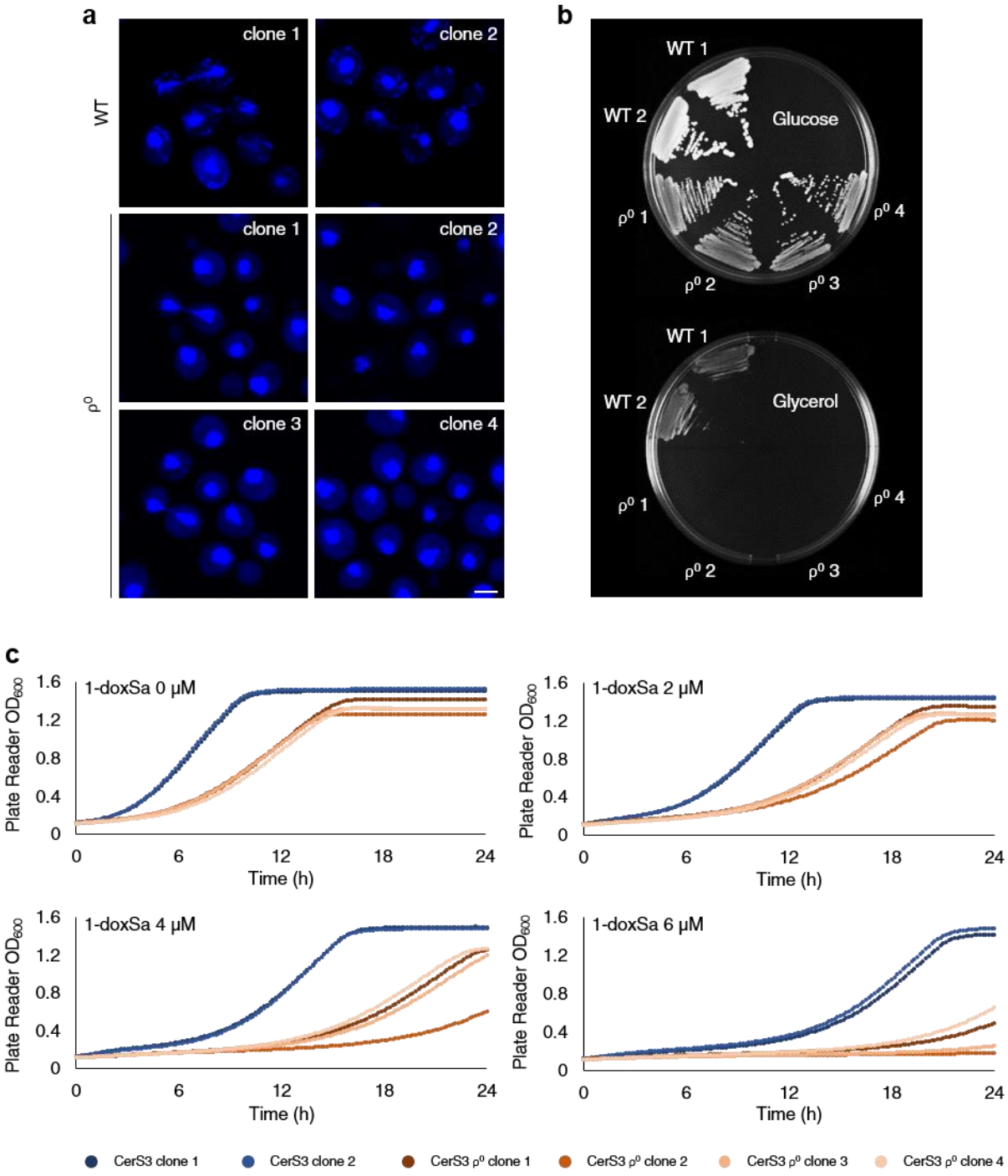

Figure 18. Toxicity of 1-deoxy-sphingolipids does not involve the mitochondrial genome. (**a**) CerS3 ρ^0 cells lack the mitochondrial genome. Cells were fixed with 4% formaldehyde for 20 min. Then, DNA was stained with DAPI for 15 min and visualized by confocal microscopy. Scale bar is 2 µm. (**b**) CerS3 ρ^0 cells cannot utilize glycerol as a carbon source. The microscopy and the growth assay demonstrate that the cells lack the mitochondrial genome. (**c**) Depletion of the mitochondrial genome does not modulate the sensitivity of the cell to 1-deoxy-sphingolipids. CerS3 cells with or without the mitochondrial genome were treated with the indicated concentrations of 1-deoxy-sphinganine. The growth of yeast was followed with a plate reader.

The growth curves of CerS3 and CerS3 ρ^0 cells treated with different concentrations of 1-doxSa collapsed to similar extent, indicating that gene products encoded by the mitochondrial genome are not required for the toxicity of 1-doxSphs (**Fig. 18c**). Since the mitochondrial genome encodes for several proteins required for mitochondrial respiration [212], this result corroborates our finding that the toxicity of 1-doxSphs does not involve oxygen-dependent functions of mitochondria. Taken together, the effects of 1-doxSphs on mitochondria, including alteration of the shape of mitochondria, are not the main contributors to the toxicity of 1-doxSphs to yeast cells.

3.3. 1-deoxy-sphinganine induces the formation of hydrophobic bodies

To obtain more information about the mode of action of 1-doxSphs, we observed the ultrastructure of CerS3 cells following 1-doxSa treatment by transmission electron microscopy according to [195]. Briefly, exponentially growing CerS3 cells were treated with 1-doxSa for 3 hours. The cells were immediately fixed with a mixture of 0.5% glutaraldehyde and 4% formaldehyde for 30 minutes. Next, the cell wall was partially digested with zymolyase to allow better penetration of osmium tetroxide that enhances the contrast of cellular membranes. The cells were then subjected to the second fixation with a mixture of 0.5% osmium tetroxide and 0.8% potassium ferrocyanide, followed by *en bloc* staining with 1% uranyl acetate.

The transmission electron micrographs revealed that 1-doxSa treatment induced the formation of micron-sized cavities in the cytoplasm. The cavities were partially filled with membranous structures. Since lipids were mostly extracted during the preparation of specimens, it is likely that the cavities represent hydrophobic bodies (**Fig. 19a**). Similar structures have also been observed in HSAN IA patient-derived lymphoblasts [213] and a mammalian cell line that accumulates 1-doxSphs due to disruption of the *de novo* biosynthesis of L-serine [214].

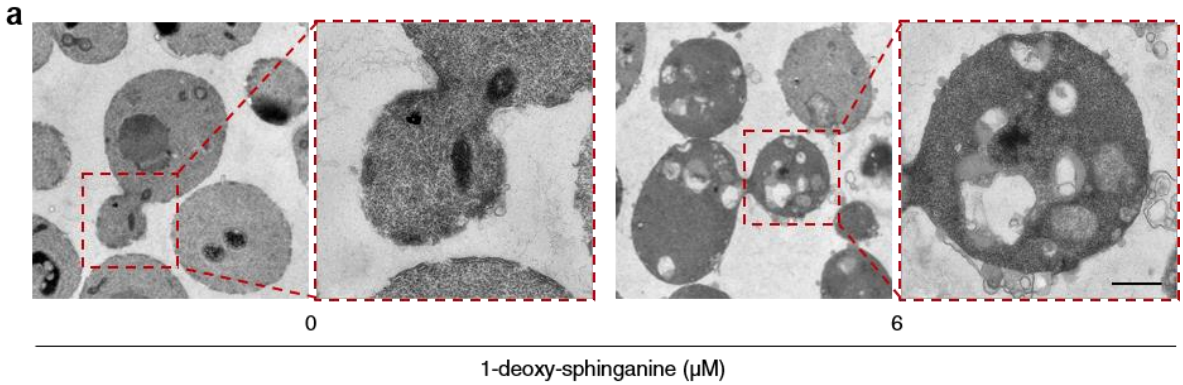
a
0
6
1-deoxy-sphinganine (μM)

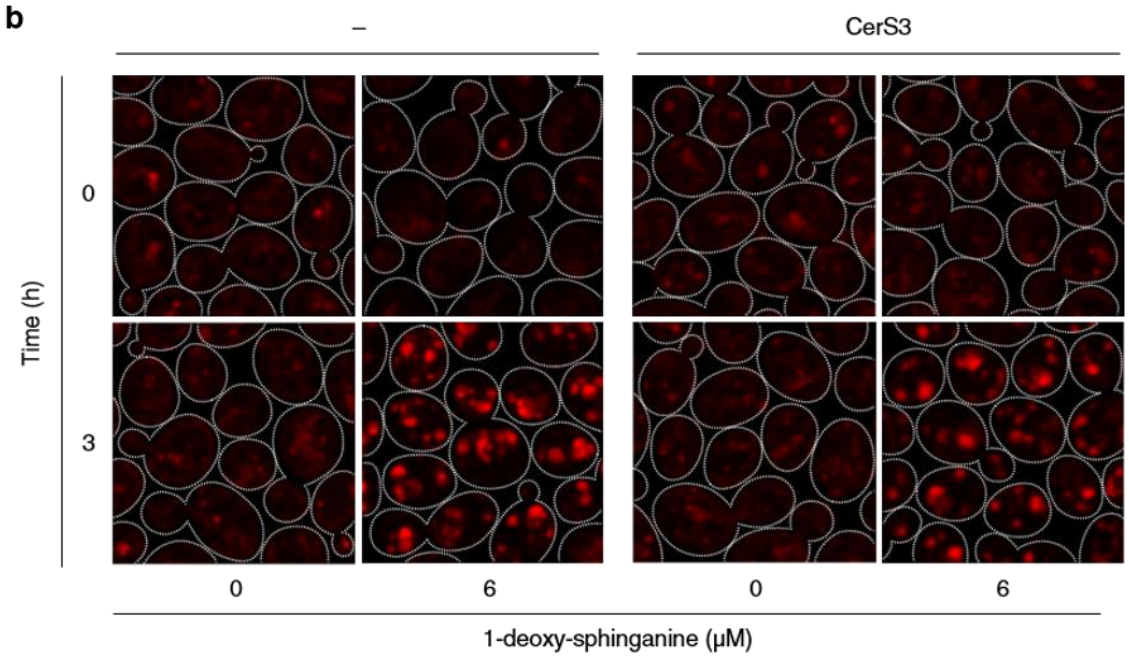
b
–
CerS3
Time (h)
0
3
0
6
0
6
1-deoxy-sphinganine (μM)

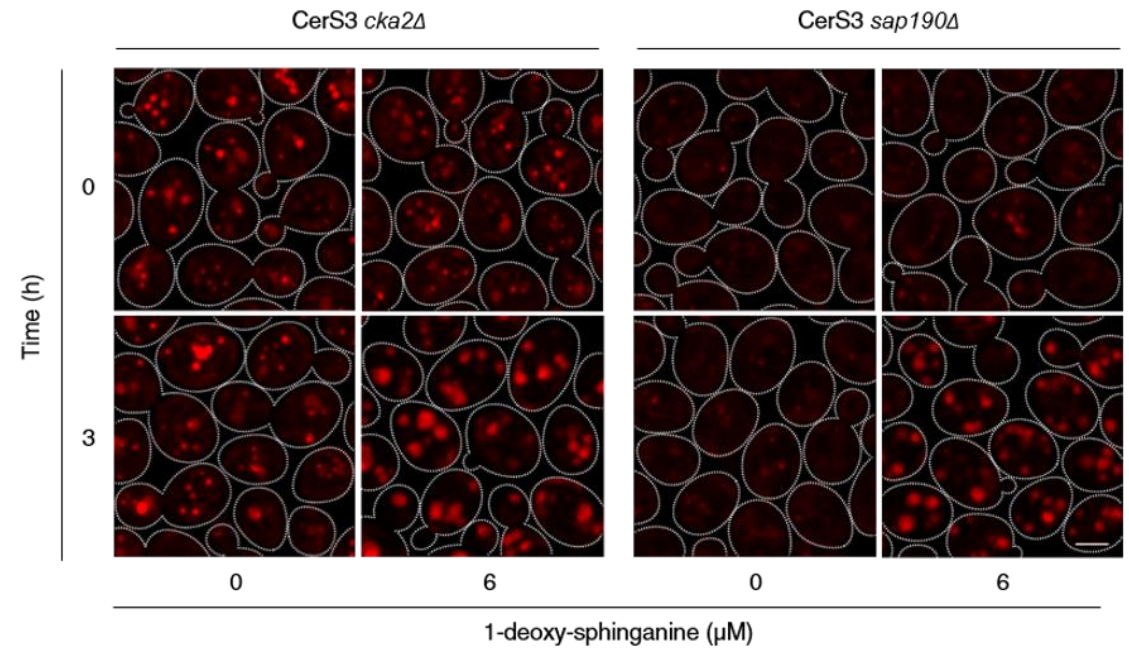
CerS3 cka2Δ
CerS3 sap190Δ
Time (h)
0
3
0
6
0
6
1-deoxy-sphinganine (μM)

Figure 19. 1-deoxy-sphinganine induces the formation of hydrophobic bodies. (**a**) Transmission electron micrographs of CerS3 cells following 1-deoxy-sphinganine (1-doxSa) treatment for 3 h. Scale bar is 0.5 μm. (**b**) Hydrophobic bodies in cells treated with 1-doxSa. Exponentially growing cells were treated with the indicated concentrations of 1-doxSa for 3 h. Next, the cells were fixed with 4% formaldehyde while hydrophobic bodies were simultaneously stained with Nile Red for 20 min. The hydrophobic bodies were then visualized by confocal microscopy. Scale bar is 2 μm.

In addition to the formation of the hydrophobic bodies, the treatment also induced plasma membrane blebs through the partially digested cell wall (**Fig. 19a**). This observation indicates that the cell accumulates non-negligible amounts of lipids following 1-doxSa treatment.

To study the hydrophobic bodies further, we observed their formation by Nile Red staining and confocal microscopy. Nile Red is a solvatochromic fluorophore that only fluoresces in an hydrophobic environment. The microscopy showed that the hydrophobic bodies were formed in cells after 1-doxSa treatment regardless of the expression of mammalian CerS3 (**Fig. 19b upper panel**). They were also formed in CerS3 *cka2Δ* and CerS3 *sap190Δ* cells that have reduced levels of C_{26} 1-doxCer following the same treatment (**Fig. 19b lower panel**). These results suggest that 1-doxSa is sufficient to induce the formation of the hydrophobic bodies. Therefore, their formations are not enough to explain the toxicity of 1-doxSphs in yeast cells.

Next, we examined whether the hydrophobic bodies are distinct from the canonical lipid droplets. First, we compared their appearance by Nile Red staining and confocal microscopy. The microscopy showed that the hydrophobic bodies appear to be different from the canonical lipid droplets in term of size, shape, subcellular localization, and sharpness of the edge (**Fig. 20a**). Second, we examined the levels of neutral lipids which are the main constituents of the canonical lipid droplets in CerS3 cells following 1-doxSa treatment by two-dimensional high performance thin-layer chromatography (2D-HPTLC). The analysis showed that the levels of neutral lipids in the cells remained unchanged after the treatment (**Fig. 20b**). Third, we observed the formation of the hydrophobic bodies in cells lacking the neutral lipid

biosynthesis enzymes (Are1, Are2, Dga1, and Lro1) by Nile Red staining and confocal microscopy. The microscopy showed that the cells were not able to form the canonical lipid droplets even after the population reached the stationary phase. However, the cells were able to form the hydrophobic bodies after 1-doxSa treatment (**Fig. 20c**). Together, these results demonstrate that the hydrophobic bodies are not the canonical lipid droplets. The hydrophobic bodies isolated from mammalian cells that accumulate 1-doxSphs due to non-functioning *de novo* biosynthesis of L-serine are enriched in 1-doxCer [214]. Therefore, it is possible that the main lipid components of the hydrophobic bodies in yeast cells are also 1-doxSphs.

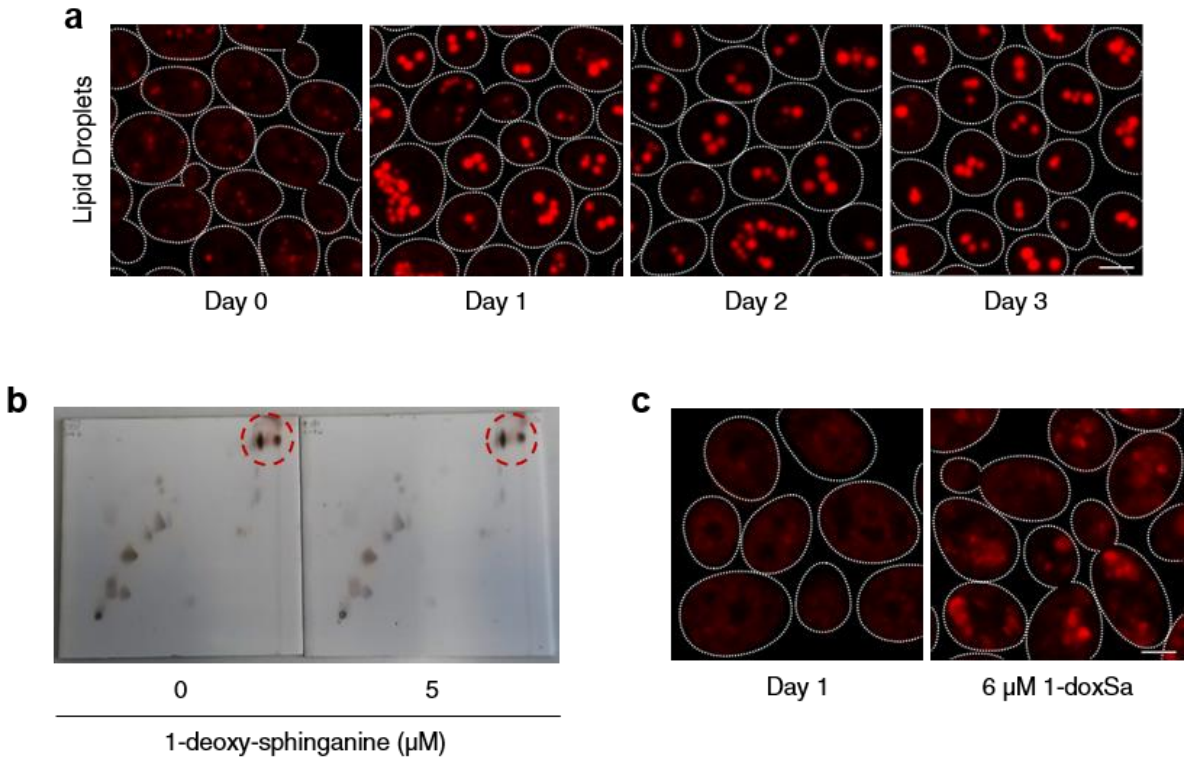

Figure 20. Hydrophobic bodies induced by 1-deoxy-sphinganine are not the canonical lipid droplets. (**a**) The canonical lipid droplets in CerS3 cells. The cells were cultured in a rich liquid medium for up to 3 days. Lipid droplets were visualized using the same method for hydrophobic bodies. Scale bar is 2 μm. (**b**) The levels of neutral lipids in CerS3 cells remain unchanged following 1-deoxy-sphinganine (1-doxSa) treatment for 3 h. Total lipid extracts were spotted on HPTLC plates for 2-D TLC, eluted with petroleum ether/diethyl ether (1:1 $^{v}/_{v}$) then with petroleum ether/diethyl ether (49:1 $^{v}/_{v}$), and developed with a solution of $MnCl_2$, methanol, and H_2SO_4. The dashed circles indicate neutral lipids. (**c**) CerS3 cells bearing *are1Δ are2Δ dga1Δ lro1Δ* are still capable to form hydrophobic bodies following 1-doxSa treatment for 1.5 h. Visualization of hydrophobic bodies was the same as described before. Scale bar is 2 μm.

4. Chemical proteomics captures potential targets of 1-deoxy-ceramide

The datasets of the two genome-wide genetic screens suggest that the main toxic lipid, C_{26} 1-doxCer might directly inhibit an essential protein with multiple functions, directly inhibit multiple essential proteins, or perturb the structure of cellular membranes. Given that there is no positive correlation between the length of the acyl chain and the toxicity of 1-doxCer (e.g. from the most toxic: C_{26} – C_{16} – C_{18} or C_{24} 1-doxCer), different 1-doxCer species might have different modes of action. Therefore, we argue that 1-doxCer perturbs the structure of cellular membranes as the least probable hypothesis.

To narrow down the number of possible candidates for the targets of 1-doxCer, we performed a multicopy suppressor screen for genes whose overexpression alleviates the toxicity of 1-doxCer. In this screen, CerS3 cells were transformed with a pool of plasmids carrying different fragments of the yeast genome. Each plasmid carries 4-5 genes as an insert and a 2-micron sequence that is required for maintenance of a high copy number in yeast cells. Therefore, each transformed cell overproduced the gene products encoded by the genes in the plasmid. The transformed cells were then subjected to three-round treatments of different concentrations (0, 2, 6, and 10 μM) of 1-doxSa in a similar manner to that in the second genetic screen (SATAY).

We found that the cultures treated with 6 or 10 μM of 1-doxSa did not gain noticeable density following the last round of treatments (data not shown). This suggests that there was no gene whose individual overexpression is capable to alleviate the toxicity of 1-doxCer. Considering that the plasmid library covers 97.2% of the yeast genome with 5.4-fold depth of coverage [215] and that the transformed colonies covered the plasmid library with 15.9-fold depth of coverage, it was unlikely that the essential genes encoding for the targets of 1-doxCer were not covered in the screen, unless their overexpression is toxic to the cell. Given the findings of the three genetic screens, we hypothesize that the targets of 1-doxCer might be a

multisubunit essential protein whose inhibition leads to failures in multiple cellular processes or multiple essential proteins implicated in diverse cellular processes.

To identify the targets of 1-doxCer, we used a chemical proteomics approach that employs photocrosslinkable and clickable (pac) 1-doxDHCer, DHCer, and fatty acid analogs as probes (**Fig. 21a**). The lipid analogs were synthesized by Per Haberkant (EMBL-HD) and Suihan Feng (University of Geneva) by following the synthesis routes described before [196,197]. To visualize crosslinked proteins, exponentially growing cells lacking ceramidase (*ypc1Δ ydc1Δ*) and the major vacuolar protease (*pep4Δ*) were fractionated into three fractions (pellet of 13,000 x*g*; pellet of 100,000 x*g*; and supernatant of 100,000 x*g*). The fractions were incubated with one of the analogs delivered in small unilamellar vesicles for 1 hour and then illuminated with 365 nm (UV) light for 5 minutes. Next, protein-analog complexes were linked with a fluorophore TAMRA by click chemistry for 1 hour [216], resolved by SDS-PAGE, and visualized with a fluorescence scanner.

Visualization of crosslinked proteins performed by Janathan Altuzar (University of Geneva) showed that the efficiency of the crosslinking of pac-1-doxDHCer with proteins was significantly enhanced by UV light (**Fig. 21b**), indicating that the crosslinking was UV-dependent and that pac-1-doxDHCer was able to capture transiently-interacting proteins. This ability is required for identifying the targets of 1-doxCer since we found that the growth inhibition effect of 1-doxSa treatment on CerS3 cells can be reversed by removing 1-doxSa from the medium (data not shown). This result indicates that the physical interactions between 1-doxCer and its targets are not mediated by covalent bonds. Visualization of crosslinked proteins also showed that the SDS-PAGE profiles of proteins crosslinked with pac-DHCer or pac-FA were very similar (**Fig. 21c**), suggesting that they might have similar sets of interacting proteins. The profile of proteins that were crosslinked with pac-1-doxDHCer in the $S_{100,000}$

fraction was markedly different from those with pac-DHCer or pac-FA, indicating that the proteins might interact specifically with 1-doxDHCer.

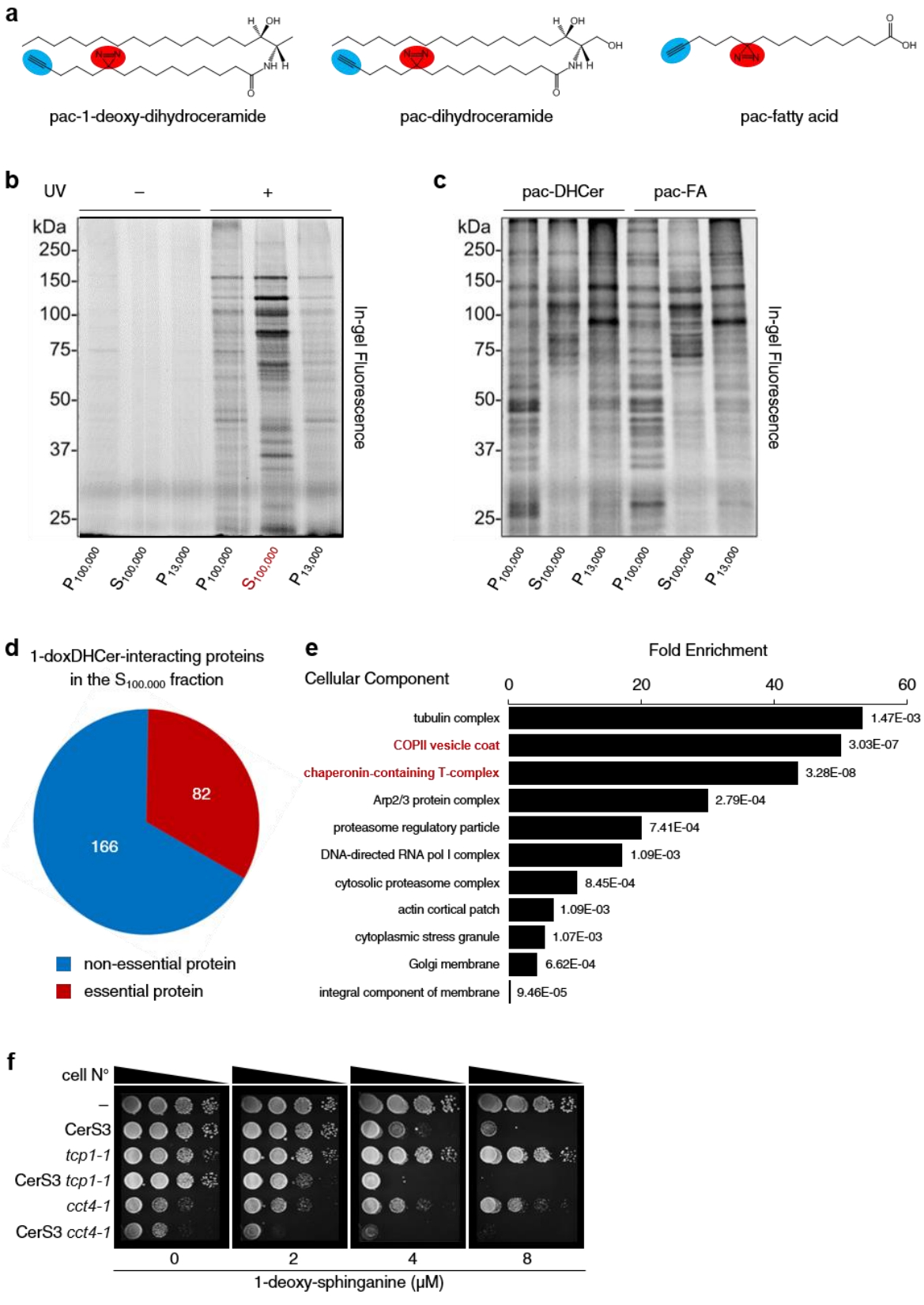

Figure 21. Chemical proteomics captures potential targets of 1-deoxy-ceramide. (**a**) Chemical structures of photocrosslinkable and clickable (pac) lipid analogs. The red and blue circles highlight the photocrosslinkable diazirine ring and the clickable terminal alkyne moiety, respectively. (**b**) UV-dependent crosslinking of pac-1-doxDHCer with proteins in different cellular fractions. (**c**) Profiles of pac-DHCer or pac-FA-crosslinked proteins in different cellular fractions. (**b,c**) Cellular fractions were incubated with pac-1-doxDHCer, pac-DHCer, or pac-FA and then illuminated with UV light. Next, protein-analog complexes were linked with TAMRA by click chemistry, resolved by SDS-PAGE, and visualized with a fluorescence scanner. (**d**) Identified pac-1-doxDHCer-crosslinked proteins in the $S_{100,000}$ fraction. Protein-pac-1-doxDHCer complexes were linked with biotin by click chemistry, subjected to chloroform/methanol precipitation and resolubilization, bound to streptavidin beads, digested with trypsin, and subjected to mass spectrometry. (**e**) GO enrichment analysis of the essential proteins among the identified proteins. Numbers in the histogram are *p*-values. (**f**) Temperature sensitive mutants of subunit 1 or 4 of the CCT complex are hypersensitive to 1-doxSphs at permissive temperature. The spot assay was performed as described above.

To identify the proteins, protein-pac-1-doxDHCer complexes were linked with biotin by click chemistry for 1 hour and then subjected to chloroform/methanol precipitation and resolubilization with a needle sonicator to remove probes that were not crosslinked to proteins and to fully denature the crosslinked proteins. Next, the proteins were enriched with streptavidin beads overnight, digested with trypsin for 12 hours, and subjected to mass spectrometry. Mass spectrometry analysis performed by Michaël Plank (University of Geneva) showed that one third of proteins crosslinked with pac-1-doxDHCer in the $S_{100,000}$ fraction were essential proteins (**Fig. 21d**). GO enrichment analysis showed that the essential proteins were highly enriched with multiprotein complexes that fulfill the criteria as the targets of 1-doxCer. We focus on COPII vesicle coat and chaperonin-containing T-complex (CCT) since they have the smallest *p*-values from the analysis (**Fig. 21e**). A spot assay performed by Thomas Hannich (University of Geneva) showed that a temperature sensitive allele of the subunit 1 (*tcp1-1*) or 4 (*cct4-1*) of CCT conferred hypersensitivity to 1-doxCer on CerS3 cells at permissive temperature (**Fig. 21f**). This result is consistent with the hypothesis that CCT is one of potential targets of 1-doxCer. The chemical proteomics approach complements the genetic approaches to identify the potential targets of 1-doxCer.

5. *C. elegans* model of hereditary sensory and autonomic neuropathy type IA

To study important factors in HSAN IA, the impacts of elevated levels of 1-doxSphs on the nervous system, and the possible roles of 1-doxSphs in resistance to anoxia, I established a *C. elegans* model of HSAN IA. We chose the C133W mutation because it is the most common mutation found in humans and it affects an amino acid residue that is conserved from the budding yeast to human (**Fig. 22a**). The worm model was created by integrating a copy of the worm gene encoding for the subunit 1 of SPT with the C133W mutation (*sptl-1*^{C133W}) into a non-intrusive site in the worm genome by the MosSCI technique [198]. Therefore, the worm model is homozygous with an equal copy number of WT and mutant alleles. This genotype is analogous to that of humans with HSAN IA (**Fig. 22b**).

The integrated HSAN IA (*sptl-1*^{C133W}) or control (*sptl-1*^{WT}) allele was designed to have a significantly different nucleotide sequence from the endogenous *sptl-1* allele, so that each allele can be selectively silenced by RNA interference. The purpose of the design is to be able to tune the relative expression level of the two alleles with siRNA. Gene silencing with siRNA was achieved by seeding stage-one (L1) larvae on lawns of *E. coli* expressing different dsRNAs targeting different alleles of *sptl-1*. The effects of the siRNA treatments on worm development were recorded 3 days later. The gene silencing showed that worms carrying *sptl-1*^{WT} allele treated with siRNA targeting the endogenous allele were bigger than WT worms after the same treatment. Moreover, those treated with siRNA targeting the integrated allele had similar normal body sizes to WT worms treated with the same siRNA. This result suggests that the *sptl-1*^{WT} allele was functional and that the two alleles could be silenced independently as designed (**Fig. 22c**).

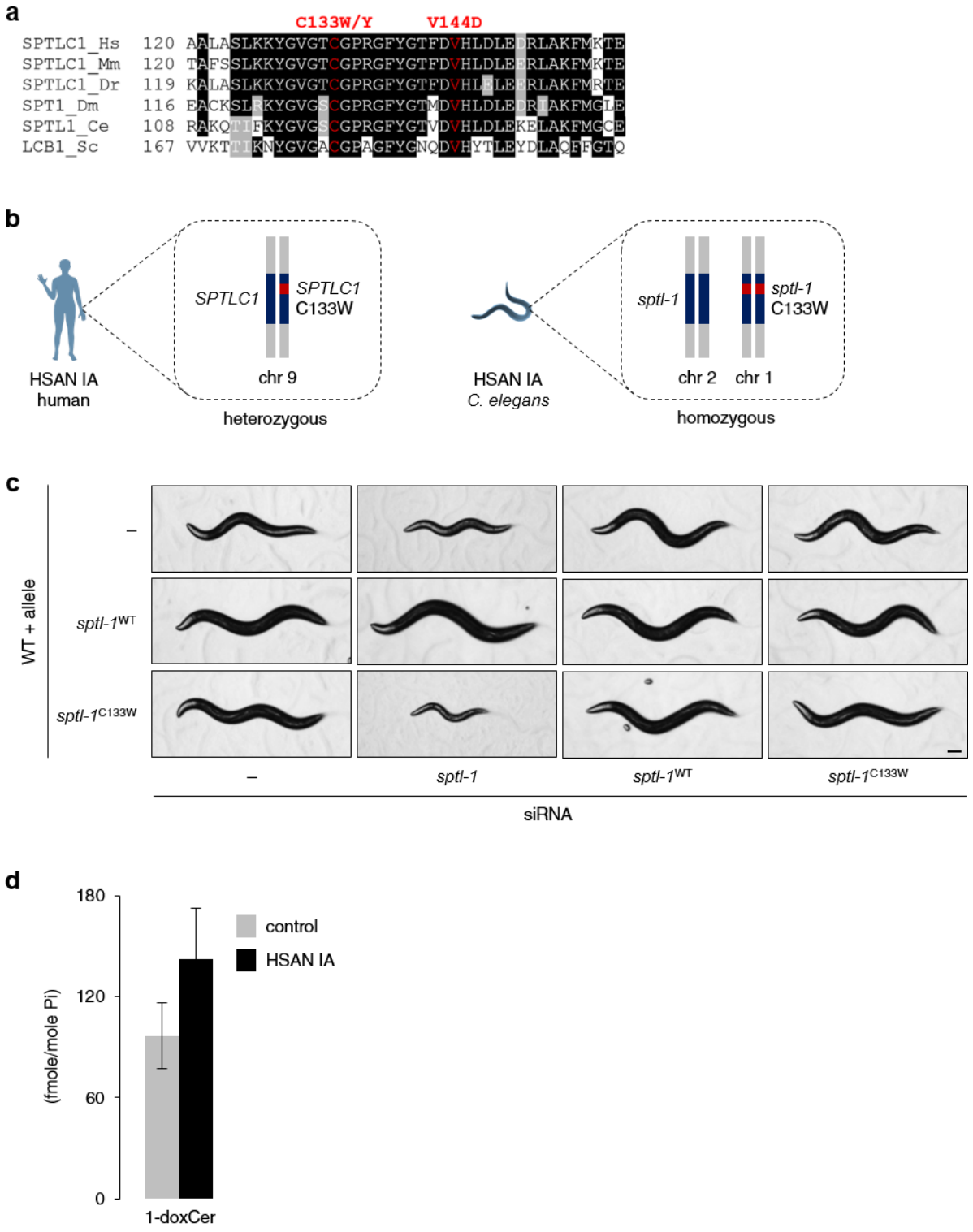

Figure 22. Establishing a *C. elegans* model of hereditary sensory and autonomic neuropathy type IA (HSAN IA). (**a**) The most common HSAN IA mutation in human (C133W) affects an amino acid residue that is conserved from the budding yeast to human. (**b**) Comparison between the genotype of human with HSAN IA and the genotype of *C. elegans* model of HSAN IA. (**c**) The mutant allele *sptl-1*^{C133W} has a dominant negative effect on worm development. WT (N2) worms bearing an additional allele of *sptl-1* were treated with siRNA targeted to different alleles of *sptl-1*. Scale bar is 100 µm. (**d**) Level of 1-deoxy-ceramide (1-doxCer) in the worm model. The amounts of lipids in young adult worms were determined by mass spectrometry.

The gene silencing also showed that worms carrying *sptl-1*^{C133W} allele treated with siRNA targeting the endogenous allele were smaller than WT worms after the same treatment. Moreover, those treated with siRNA targeting the integrated allele had similar normal body sizes to WT worms treated with the same siRNA. This result indicates that the *sptl-1*^{C133W} allele has a dominant negative effect on worm development analogous to the human HSAN IA allele. Moreover, the two alleles could also be silenced independently as designed (**Fig. 22c**). Mass spectrometry analysis showed that the level of 1-doxCer in the HSAN IA worms was slightly higher than that in control, indicating that the worms only modestly accumulates 1-doxCer when they were reared under standard laboratory conditions (**Fig. 22d**).

The HSAN IA worms do not display noticeable aberrant morphology, development, or behavior under standard laboratory rearing conditions. However, the worms might show particular phenotypes under particular conditions. This quality allows in-depth studies of the phenotypes since the physiological processes associated with the phenotypes are likely not due to global perturbation of the physiology of the worms. Therefore, we characterized the phenotypes of the worms, particularly those that are reminiscent of the hallmark of HSAN IA in humans.

First, we tested whether increased alanine or glycine intake interferes with the development of the HSAN IA worms. L1 worms fed with *E. coli* overexpressing proteins that are rich in serine (*Sc* SRp40, 48.3% of serine), alanine (*Dm* MS57A_DROME, 36% of alanine), or glycine (*At* GRP1_ARATH, 70.2% of glycine) for 3 days had comparable body sizes regardless of the HSAN IA allele (**Fig. 23a**). In addition, L1 worms fed with standard *E. coli* on agar supplemented with alanine for 3 days also had comparable body sizes regardless of the HSAN IA allele (**Fig. 23b**). These results indicate that the methods to increase alanine or glycine intake cannot be used to selectively inhibit the development of the HSAN IA worms.

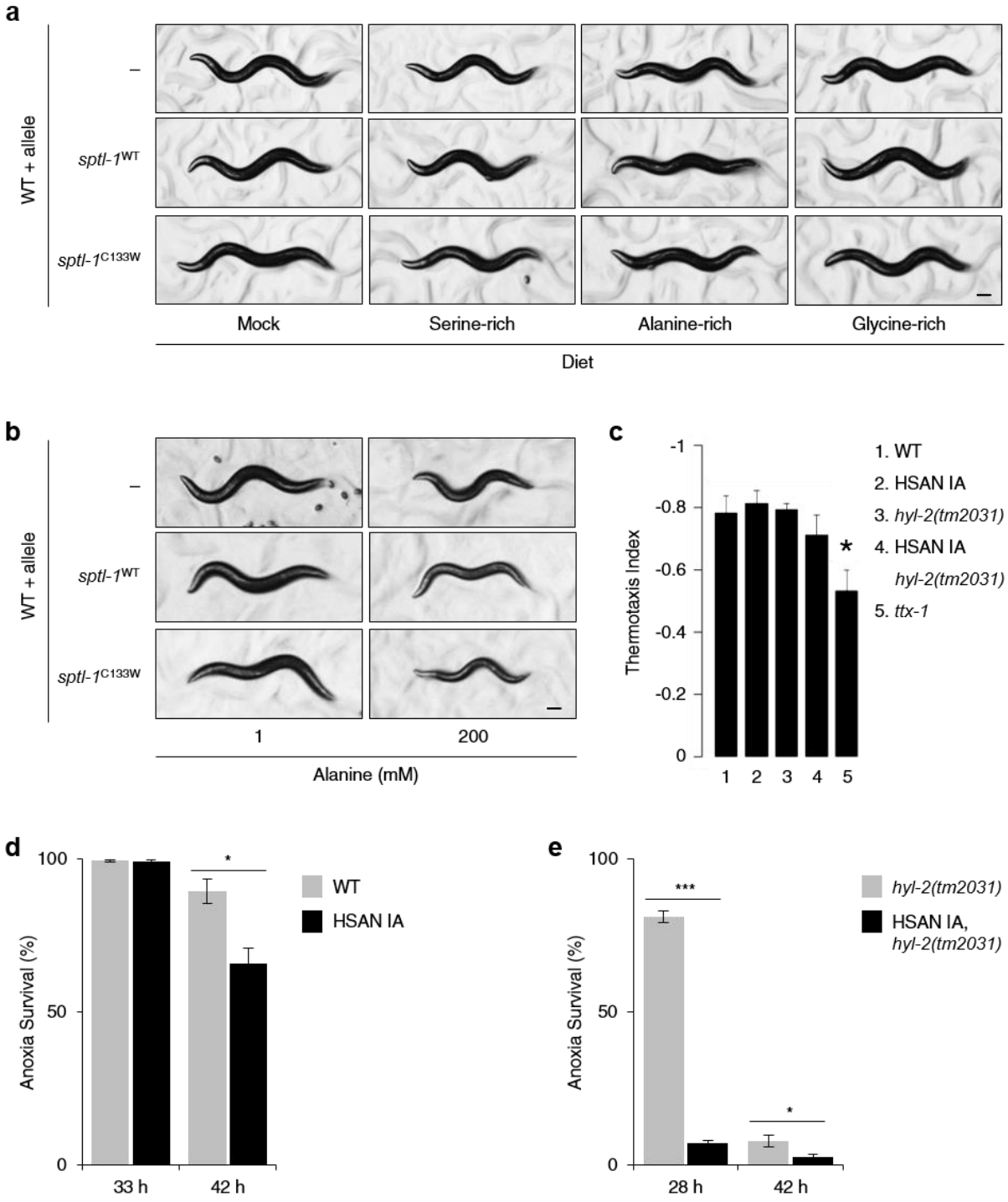

Figure 23. Phenotypes of the *C. elegans* model of HSAN IA. (**a**) Impact of diets on the development of the worm model. WT (N2) worms bearing an additional allele of *sptl-1* were fed with *E. coli* overexpressing different proteins rich in serine, alanine, or glycine. Scale bar is 100 μm. (**b**) Impact of direct alanine supplementation into the agar on the development of the worm model. Scale bar is 100 μm. (**c**) Impact of the HSAN IA allele (*sptl-1*^{C133W}) on the thermotaxis of WT and (*hyl2(tm2031)*) worms. The thermotaxis assay was performed according to [200]. The HSAN IA allele sensitizes WT (**d**) and (*hyl2(tm2031)*) (**e**) worms. The anoxia experiments were performed according to [201].

Second, we tested whether the HSAN IA worms exhibit a thermotaxis defect which reflects their inability to sense heat in the environment. A thermotaxis assay was performed by Dominique Glauser (University of Fribourg) according to [200]. Briefly, young adult worms were acclimatized at 20°C for 3-4 hours prior to the assay. Then, they were placed on the center of a thermotaxis plate with a thermal slope of 0.67°C/cm. The temperature at the center of the plate was 23°C. The worms were allowed to move around the plate for 10 minutes. The thermotaxis index was calculated as (number of worms above starting temperature – number of worms below starting temperature) / total number of worms. The assay showed that the HSAN IA worms had a comparable thermotaxis index to WT. However, introduction of a mutation that enhances the accumulation of 1-doxCer (*hyl2(tm2031)*) increased the thermotaxis index of the HSAN IA worms (**Fig. 23c**). These results suggest that increased accumulation of 1-doxCer reduces the ability of the HSAN IA worms to sense heat in the environment.

Third, we tested if the HSAN IA worms are sensitive to oxygen depletion. Anoxia sensitivity tests were performed by Thomas Hannich (University of Geneva) according to [201]. Briefly, L1 worms were placed inside an anoxic chamber for a period of time and then transferred into the normal incubator for 24 h before the survival rate was scored. The assay showed that the survival rate of the HSAN IA worms was significantly lower than that of WT following 42 hours of anoxia (**Fig. 23d**). Moreover, the survival rate of the worms bearing *hyl2(tm2031)* mutation was much lower than that of *hyl2(tm2031)* worms after 28 hours of anoxia (**Fig. 23e**). These results indicate that the HSAN IA worms are sensitive to oxygen depletion and that their sensitivity is markedly increased when the accumulation of 1-doxCer is also increased. This phenotypes allowed us to employ the HSAN IA worms to study the role of 1-doxSphs in the survival of worms during anoxia. The manuscript of the study is in preparation.

General Discussion

HSAN IA/IC are inherited neurological diseases that affect the peripheral nervous system particularly on its sensory and autonomic functions. The hallmarks of the diseases are marked loss of pain and heat sensation in the distal parts of the limbs and reduced ability to sweat. As the diseases advance, affected individuals may experience severe shooting, burning, and lancinating pains; ulcerative mutilations; muscle weakness and wasting; and reduced motor functions [178,176,167]. These complex diseases are caused by dominant mutations in the genes encoding for serine palmitoyltransferase (SPT), leading to increased synthesis of atypical sphingolipids, 1-deoxy-sphingolipids (1-doxSphs). The levels of 1-doxSphs correlate positively with the severity of the diseases [172]. Once synthesized, 1-doxSphs are metabolically trapped since they cannot be metabolized further and degraded via the canonical sphingolipid degradation pathway. Therefore, 1-doxSphs tend to accumulate over time. This gradual accumulation of 1-doxSphs might explain the late onset of the diseases in most cases. How elevated levels of 1-doxSphs cause complex perturbations of various organ systems in individuals with HSAN IA/IC, however, is not known. It is possible that the complex clinical manifestations might originate from a common perturbation at the cellular level, which emerges as various perturbations at the higher levels. Therefore, understanding the mode of action of 1-doxSphs in the cell is key to understanding of the pathogenesis of the diseases and to design better therapeutic interventions.

The ability of SPT to naturally produce 1-doxSphs at low levels appears to be conserved from the budding yeast to human since we found that the yeast also produces 1-doxSphs. The level of 1-deoxy-ceramide (1-doxCer) is about a half of that of ceramide in yeast grown under standard laboratory culture conditions. This steady state level suggests a much lower rate of synthesis since the 1-doxCers cannot be converted to more complex sphingolipids nor be

degraded. The production of 1-doxSphs during its normal growth suggests that 1-doxSphs might perform physiological functions in the cell. It also suggests that the cell might have mechanisms to prevent 1-doxSphs toxicity during its normal growth. One possible mechanism is to set the production rate of 1-doxSphs proportional to the growth rate. As a consequence, the cell would be able to maintain the amount of 1-doxSphs per unit volume of the cell or per unit area of the membranes, preventing the accumulation of 1-doxSphs to toxic levels. Despite their unclear metabolic fates and regulation, the fact that the yeast synthesizes 1-doxSphs during its normal growth allows us to employ the yeast as a model system to study the mechanism of action of 1-doxSphs at the cellular level.

1-doxSphs comprise two interconvertible groups of metabolites, 1-deoxy-sphingoid bases (1-doxSB) and 1-deoxy-ceramides (1-doxCers). 1-doxSB can be acylated by ceramide synthase to produce 1-doxCers which then can be deacylated by ceramidase to release 1-doxSB. Therefore, the first step in elucidating the mechanism of action of 1-doxSphs is determining the relative contribution of 1-doxSB and 1-doxCers to the toxicity. To this end, we increased the total amount of 1-doxSphs in the cell by supplementing the growth medium with 1-doxSB and enhanced the conversion of 1-doxSB to 1-doxCers by overexpressing yeast ceramide synthase, thereby accentuating the contribution of 1-doxCers. This strategy allows a consistent and convenient way to increase the total amount of 1-doxSphs in the cell since 1-doxSB are more water-soluble than 1-doxCers. In addition, overexpressing yeast ceramide synthase is more practical and less detrimental to the cell than other genetic modifications to accentuate the contribution of 1-doxSB. With the strategy, we found that 1-doxCers are more toxic than 1-doxSB, suggesting that 1-doxCers are the major contributors to the toxicity. This finding is consistent with that in mammalian cells [185,187,188], adding a similarity between the mechanism of action of 1-doxSphs in yeast cells and that in mammalian cells.

We expected that the length of acyl chain influences the toxicity of 1-doxCers as it has been shown to be critical for the function of sphingolipids [160,201]. We made use of the six mammalian ceramide synthases that have different preferences towards different lengths of acyl-CoA to produce 1-doxCers bearing different lengths of acyl chain in the cell. Expression of each mammalian ceramide synthase rescues the depletion of the endogenous enzyme, indicating that mammalian ceramide synthases expressed in yeast are functional. Moreover, they retain their acyl-CoA preferences. Following 1-deoxy-sphinganine (1-doxSa) supplementation to the growth medium of yeast expressing different mammalian ceramide synthases, the levels of 1-deoxy-ceramide (1-doxCer) with different lengths of acyl chain increase and the growth rate of yeast reduces depending on the mammalian ceramide synthase that is expressed in the cell. By evaluating the levels and the growth inhibitory effects of different 1-doxCer species, we concluded that C_{26} 1-doxCer is the most toxic 1-doxCer species in yeast. Furthermore, C_{16} 1-doxCer is more toxic than C_{18} 1-doxCer. These findings suggest that the toxicity of 1-doxCer depends on the length of its acyl chain. However, different 1-doxCer species might have different mechanisms of action since there is no positive correlation between the length of the acyl chain and the toxicity of 1-doxCer. Furthermore, C_{26} 1-doxCer might not be the most toxic lipid in mammals. Unfortunately, we could not evaluate the contribution of acyl chain length to the toxicity of 1-deoxymethyl-ceramide (1-doxmetCer) since mammalian ceramide synthases are not able to use 1-deoxymethyl-sphinganine (1-doxmetSa) as a substrate or 1-doxmetCer is not toxic to yeast. Therefore, we focused our investigation on 1-doxCer.

We found that high levels (up to 13.9% of the level of phosphatidylcholine) of 1-doxCer do not significantly alter the lipidome of the cell. It might suggest that 1-doxCer does not interfere with the metabolism of most lipids. Considering the biophysical properties of 1-doxCer, high levels of 1-doxCer were expected to markedly disrupt the structure of the

membrane where it resides [190]. If this is the case, the finding might also suggest that changes in membrane structure caused by high levels of 1-doxCer cannot be recognized and therefore cannot be resolved by the cell. However, we cannot rule out the possibility that 1-doxCer might be accumulated in particular cellular membranes and that the cell changes membrane lipid distribution accordingly without substantially changing its lipidome. We also discovered that 1-doxCer may accumulate up to 24.3 times the level of ceramide. Given that increased levels of C_{26} ceramide by about 2.5 fold are sufficient to significantly inhibit the growth of yeast [217], C_{26} 1-doxCer can be considered less toxic than C_{26} ceramide. It also indicates that their mechanisms of toxicity are different. This notion is supported by the fact that the biological properties of 1-doxCer do not mimic those of typical sphingolipids. Consequently, modulating the amounts of typical sphingolipids cannot be applied as a strategy to alleviate the toxicity of 1-doxCer.

We performed three different genome-wide genetic screens to reveal the mechanism of toxicity of 1-doxSphs. The first two screens evaluated the effects of depletion or reduction of gene products on the toxicity of 1-doxSphs. The library of the first screen was a collection of knockout and hypomorphic (DAmP) mutants. The inclusion of the hypomorphic mutants allowed us to evaluate the roles of many essential genes in the toxicity [218]. The library of the second screen (SATAY) was a large collection of mutants freshly generated by inserting a transposon into the genome. Compared to the library used in the first screen, it is superior in several ways; (1) it has larger coverage for non-essential genes, (2) it has more informative alleles other than simple deletion alleles, (3) it has less chances of accumulating secondary mutations since it is freshly generated, and (4) it prevents incorrect assignment of a mutant to its phenotype as the identities of the mutants are determined at the end of the screen [194]. However, we found that it had less coverage for essential genes. Therefore, the libraries in the two screens were complementary. In contrast to the first two screens, the third screen evaluated

the effects of overproduction of gene products on the toxicity of 1-doxSphs. The library of the third screen was a pool of plasmids carrying different fragments of the yeast genome. Each plasmid carries 4-5 genes as an insert and a 2-micron sequence to maintain a high copy number in yeast cells [215]. The main function of the third screen was to evaluate essential genes that were not covered in the other two screens. Therefore, the three screens should provide more complete insights into the mechanism of toxicity of 1-doxSphs. Nevertheless, the screens are not able to reveal the mechanism of toxicity if it involves inhibition of a multisubunit essential protein, inhibition of multiple essential proteins, or perturbations of the structure of cellular membranes.

The datasets obtained from the first two screens revealed a set of genes whose disruption confers CerS3 cell very strong resistance to 1-doxSphs. These genes are required for efficient synthesis of very long-chain (C_{24-26}) fatty acyl-CoA or import of sphingoid bases in yeast. Since the conversion of 1-doxSa to the much more toxic lipid C_{26} 1-doxCer requires very long-chain fatty acyl-CoA, this finding demonstrates that the screens were able to chart the capacities of the strains to cope with the toxicity of 1-doxSphs, particularly of C_{26} 1-doxCer. Moreover, it suggests that the most effective way to alleviate the toxicity of 1-doxSphs is to prevent the formation of C_{26} 1-doxCer in the cell. Analyses of the datasets showed that; (1) the overlaps of top 200 genes between the screens were 8.5% for resistant genes and 9.5% for hypersensitive genes, (2) there was no gene ontology (GO) enrichment of particular molecular functions, cellular components, or cellular processes implicated in the toxicity in the resistant genes of both screens, (3) higher doses of 1-doxSa only caused the loss of complexity of the libraries and failed to reveal resistant genes that are not involved in the production of C_{26} 1-doxCer, and (4) freshly generated the most hypersensitive mutants found in the second screen only showed mild hypersensitivity to 1-doxSphs on a spot assay. These findings point out that 1-doxSphs inhibit more than one essential cellular processes.

The cellular process revealed most by GO enrichment analysis of the hypersensitive genes of the second screen is nuclear migration. This cellular process consists of two sequential and partially redundant pathways, the early and the late pathways [203]. There are six hypersensitive genes that constitute the GO term. All of them encode for proteins that operate in the late pathway. Since all of them are not essential and the two pathways are partially redundant, the result indicates that 1-doxSphs inhibit the early pathway of nuclear migration. The key component for the functioning of the early pathway is actin cables which serve as tracks for myosin V to ferry the plus ends of cytoplasmic microtubules towards the bud tip. It is corroborated by the fact that all of the six hypersensitive genes have negative genetic interactions with *Act1* (encodes for actin), *Myo2* (encodes for type V myosin motor), *Pfy1* (encodes for profilin), and *Tpm1* (encodes for the major isoform of tropomyosin). Freshly generated deletion mutants of the six genes, however, only showed mild hypersensitivity to 1-doxSphs. This result indicates that inhibition of nuclear migration is one of events in the toxicity of 1-doxSphs and that it is not the main toxicity event that terminates cell growth.

In addition to reveal the mechanism of action of 1-doxSphs, the first two screens also have a potential to reveal novel proteins that are involved in efficient conversion of exogenous sphingoid bases to ceramides in yeast. The process includes the import of sphingoid bases from the medium, the production of C_{26} fatty acyl-CoA, and the acylation of the sphingoid bases by ceramide synthase to form ceramides. Disruption of individual genes required for the processes mostly does not lead to a noticeable growth defect since most steps of the processes are mediated by non-essential proteins or functionally redundant proteins. However, it confers a growth advantage in the presence of 1-doxSa in the medium and mammalian CerS3 in the cell since the processes are also required for efficient conversion of exogenous 1-doxSa to a toxic lipid C_{26} 1-doxCer. This potential was demonstrated by the fact that many resistant mutants

found by the screens are defective in various known steps for efficient synthesis of very long-chain fatty acyl-CoA or import of sphingoid bases from the medium.

The import of sphingoid bases from the medium into yeast cells is facilitated by two redundant long chain fatty acyl-CoA synthetases, Faa1 and Faa4 [219]. The first screen showed that CerS3 *faa1Δ* mutant was resistant to 1-doxSa, indicating that the import of 1-doxSa into the cell is also mediated by Faa1. The efficient incorporation of exogenous sphingoid bases into ceramides requires a cycle of phosphorylation by sphingoid long-chain base kinase Lcb4 and dephosphorylation by long-chain base 1-phosphate phosphatase Lcb3 on the ER membrane [220]. In contrast, the efficient incorporation of 1-doxSa into 1-doxCer does not require the phosphorylation-dephosphorylation cycle since it cannot be phosphorylated at the first carbon. However, the screens revealed that efficient conversion of 1-doxSa to 1-doxCer requires Cka2 which might phosphorylate mammalian CerS3 and thereby enhancing its activity. The screens also revealed that Sap190 is required to ensure the normal proportion of C_{24} to C_{26} fatty acyl-CoA. This function of Sap190 is novel. How Sap190 achieves this function remains to be investigated.

Examinations of the impacts of 1-doxSphs on the organization of actin, the functions of mitochondria, and the formation of hydrophobic bodies provided insights into the features of the toxicity in yeast cells compared to that in mammalian cells. We found that 1-doxSphs disrupt the organization of actin including depleting actin cables and actin patches. Such disruptions are expected to inhibit cellular processes such as polarized growth and endocytosis, leading to some inhibition of cell growth. These disruptions, however, are independent of the ability of the cell to synthesize C_{26} 1-doxCer which is the main toxic lipid. Therefore, we argue that the disruptions are not the main deleterious events of the toxicity of 1-doxSphs. Depletion of actin cables might also lead to inhibition of nuclear migration. Therefore, the inhibition is likely caused by 1-doxSa, which is consistent with the fact that it only has a minor negative

impact on yeast growth. Another abnormality that we observed is the presence of round intracellular bodies stained with phalloidin-Atto488, which could be aggregates of F-actin. In mammalian cells, 1-doxSa treatments also cause rearrangements of actin organization including the loss of actin stress fibers [184] and the aggregation of F-actin [188]. However, it is not clear if the rearrangements are caused by 1-doxSa or 1-doxCer. Moreover, it is not known if the mechanisms underlying alterations of actin organization in yeast and mammalian cells are analogous, considering the different natures of actin stress fibers [221] and actin cables [222] as well as the different appearances of the F-actin aggregates in yeast and in mammalian cells.

We also found that 1-doxSphs alter the shape of mitochondria from tubular to spherical, without affecting their inheritance from the mother cell to the bud. The alteration might be an indication of inhibition of mitochondrial fission, or mitochondrial tethering to the cell cortex [206,207] or to the ER [208]. Similar to that of actin, the alteration is independent of the ability of the cell to convert 1-doxSa to C_{26} 1-doxCer, indicating that the alteration is caused by 1-doxSa and that it is not sufficient to induce toxicity to the cell. Although the alteration of the shape of mitochondria appears dramatic, it is not accompanied by marked defects in the key functions of mitochondria such as the assembly of iron-sulfur clusters and mitochondrial respiration. Furthermore, we demonstrated that the toxicity of 1-doxSphs in yeast cells is independent of oxygen and the mitochondrial genome. Therefore, we could exclude the involvement of ROS in the toxicity. Collectively, these findings suggest that the main action of 1-doxCer is not inhibiting essential mitochondrial functions in yeast cells. Different from that in yeast cells, alteration of the shape of mitochondria in mammalian cells is accompanied by defects in mitochondrial respiration. Moreover, the defects could be reversed by inhibiting the conversion of 1-doxSa to 1-doxCer with fumonisin B1 [185], indicating the defects are

caused by 1-doxCer. Therefore, inhibition of mitochondrial respiration might be one of the key toxicity events in mammalian cells.

Besides inducing rearrangements of actin organization and alteration of mitochondrial shape, 1-doxSa is also sufficient to induce the formation of hydrophobic bodies. Nile Red staining of the bodies showed that the edges of the bodies appear blurry, suggesting that they are not enclosed by membranes. They are distinct from the canonical lipid droplets in term of size, shape, subcellular localization, and lipid composition. Since 1-doxSa is sufficient to induce their formation, 1-doxSa might be the main constituent of the bodies. Moreover, we do not expect that the presence of the bodies have substantial negative impacts on yeast survival. Similar hydrophobic bodies have been observed in HSAN IA patient-derived lymphoblasts [213] and a mammalian cell line that accumulates 1-doxSphs due to disruption of the *de novo* biosynthesis of L-serine [214]. The bodies appear to be different from the canonical lipid droplets since they are generally bigger and have lamellar inclusions. Moreover, they have significantly higher levels of 1-doxCer and lower levels of ceramide, sphingomyelin, and hexosyl ceramide [214]. However, whether 1-doxSa is also sufficient to induce their formation and whether they play major roles in the toxicity of 1-doxSphs in mammalian cells are not known.

Considering that; (1) the first two genetic screens point out pleiotropic effects of 1-doxCer, (2) there is no individual gene whose overexpression can alleviate the toxicity of 1-doxCer in the third genetic screen, and (3) the growth inhibitory effect of 1-doxSphs can be reversed by removing 1-doxSa from the medium, we hypothesize that the targets of 1-doxCer might be a multisubunit essential protein whose inhibition leads to failures in multiple cellular processes or multiple essential proteins implicated in diverse cellular processes. Furthermore, the physical interactions between 1-doxCer and its targets are not mediated by covalent bonds. To hunt for the targets, we took a chemical proteomics approach using photocrosslinkable and

clickable lipid analogs which have been demonstrated to be suitable for a global profiling of lipid-protein interactions [223]. The approach revealed two multisubunit proteins that are consistent with our hypothesis. They are COPII vesicle coat and chaperonin-containing T-complex (CCT). Follow-up experiments to validate this finding are ongoing.

Taken all the findings together, we could recapitulate the toxicity of 1-doxSphs in CerS3 cells as the following sequence of events. The cells import 1-doxSa supplemented in the medium using the same machinery for other sphingoid bases. High levels of 1-doxSa in the cells are sufficient to form micron-sized hydrophobic bodies and to increase the surface area of cellular membranes. Its accumulation causes disruption of actin organization including the loss of actin cables, which leads to inhibition of many cellular processes including nuclear migration. In addition, its accumulation alters the shape of mitochondria from tubular to spherical. Although its negative impacts appear dramatic, they are not sufficient to stop cell growth. As soon as 1-doxSa is available for CerS3, it is converted to 1-doxCer which is the main toxic lipid. Since CerS3 is a mammalian protein, it might not be subjected to a feedback regulation. Therefore, it keeps producing 1-doxCer as long as 1-doxSa is available and the cell can still cope with the toxicity of 1-doxCer. The toxicity has pleiotropic effects, although it does not involve inhibition of oxygen-dependent functions of mitochondria or the mitochondrial genome. We hypothesize that 1-doxCer directly inhibits a multisubunit essential protein, such as COPII vesicle coat or chaperonin-containing T-complex (CCT).

To study important factors in HSAN IA in an animal with a simple nervous system, I established a *C. elegans* model of HSAN IA. The HSAN IA worms were designed to have a homozygous genotype with an equal copy number of WT and HSAN IA alleles, in contrast to humans with HSAN IA that have a heterozygous genotype. The main advantage of homozygous worm lines is that they do not require constant sorting of individual worms with the desired genotype in the population for worm line maintenance or analyses that require large

numbers of worms, such as biochemical analyses, genetic screens, or chemical screens. Another motivation to establish the worm line is to study the roles of 1-doxSphs in various physiological processes in the worm. Such studies require flexibilities in modulating the levels of 1-doxSphs. However, most sphingoid bases in the worm are iso-branched sphingoid bases [224], which are not commercially available to date. Therefore, such studies are more practical with a worm line that has elevated levels of iso-branched 1-doxSphs that can be modulated by genetic manipulations, such as introducing another mutation or silencing a gene with siRNA. The HSAN IA worms have a slightly higher level of 1-doxCer than WT worms. The worms do not exhibit noticeable phenotypes. However, when another mutation (*hyl2(tm2031)*) that enhances the accumulation of 1-doxCer, the worms become less responsive to heat in the environment and sensitivity to anoxia.

Conclusions

HSAN IA/IC are inherited neurological diseases caused by aberrant sphingolipid metabolism that leads to the accumulation of atypical sphingolipids, 1-deoxy-sphingolipids (1-doxSphs). 1-doxSphs comprise two groups of interconvertible metabolites, 1-deoxy-sphingoid bases (1-doxSB) and 1-deoxy-ceramides (1-doxCers). Our study in the budding yeast revealed that the cytotoxicity of 1-doxSphs consists of two sequential and overlapping toxicity events.

The first event is the toxicity of 1-doxSB which are the first metabolites synthesized by the cell. Elevated levels of 1-deoxy-sphinganine (1-doxSa) cause disruptions of actin organization, alteration of the shape of mitochondrial, and accumulation of hydrophobic bodies. Although these effects appear dramatic, they only have minor impacts on cell growth.

The second event is the toxicity of 1-doxCers which has major impacts on cell growth. 1-doxCers are synthesized as soon as 1-doxSB are available for ceramide synthase. Elevated levels of 1-deoxy-ceramide (1-doxCer) negatively affect multiple cellular processes. Its mechanism of action is dependent on the length of its acyl chain, distinct from those of other lipids, and independent of oxygen and the mitochondrial genome. We hypothesize that 1-doxCer inhibits a multisubunit essential protein whose inhibition leads to failures in multiple cellular processes. We propose COPII vesicle coat or chaperonin-containing T-complex (CCT) as a potential target of 1-doxCer.

Perspectives

Further efforts should be focused on; (1) validating whether COPII vesicle coat or chaperonin-containing T-complex (CCT) is the direct target of 1-doxCer, (2) mapping the subcellular localization of 1-doxCer, and (3) investigating how Sap190 ensures the normal proportion of C_{24} to C_{26} fatty acyl-CoA.

One additional genetic test may provide supporting data for the involvement of COPII vesicle coat or CCT. Haploid insufficiency profiling, which uses diploid cells heterozygous for the essential genes, should show differences in sensitivity to 1-doxSphs if these complexes are involved in the mechanism of action.

Studies in mammalian cells showed that elevated levels of 1-doxSphs are accompanied by various phenotypes which might complicate our understanding about the mechanism of toxicity of 1-doxSphs. Our study showed that the toxicity of 1-doxSphs in yeast cells is mainly due to elevated levels of 1-doxCer, the same as that in mammalian cells. Moreover, our study showed that 1-doxSa could induce dramatic phenotypes without significantly affecting cell growth. Therefore, care must be taken for further studies in mammalian cells to dissect the contributions of various phenotypes to the inhibition of cell growth.

References

1. Astudillo L, Sabourdy F, Therville N, Bode H, Segui B, Andrieu-Abadie N, Hornemann T, and Levade T. 2015. Human genetic disorders of sphingolipid biosynthesis. *J Inherit Metab Dis*. **38**, 65-76. (doi:10.1007/s10545-014-9736-1).

2. Platt F M. 2014. Sphingolipid lysosomal storage disorders. *Nature*. **510**, 68-75. (doi:10.1038/nature13476).

3. Yamaji T and Hanada K. 2015. Sphingolipid metabolism and interorganellar transport: localization of sphingolipid enzymes and lipid transfer proteins. *Traffic*. **16**, 101-22. (doi:10.1111/tra.12239).

4. Aguilera-Romero A, Gehin C, and Riezman H. 2014. Sphingolipid homeostasis in the web of metabolic routes. *Biochim Biophys Acta*. **1841**, 647-56. (doi:10.1016/j.bbalip.2013.10.014).

5. Kihara A. 2014. Sphingosine 1-phosphate is a key metabolite linking sphingolipids to glycerophospholipids. *Biochim Biophys Acta*. **1841**, 766-72. (doi:10.1016/j.bbalip.2013.08.014).

6. Merrill A H, Jr. 2011. Sphingolipid and glycosphingolipid metabolic pathways in the era of sphingolipidomics. *Chem Rev*. **111**, 6387-422. (doi:10.1021/cr2002917).

7. Hannun Y A and Obeid L M. 2017. Sphingolipids and their metabolism in physiology and disease. *Nat Rev Mol Cell Biol*. (doi:10.1038/nrm.2017.107).

8. Hanada K. 2003. Serine palmitoyltransferase, a key enzyme of sphingolipid metabolism. *Biochim Biophys Acta*. **1632**, 16-30.

9. Megyeri M, Riezman H, Schuldiner M, and Futerman A H. 2016. Making Sense of the Yeast Sphingolipid Pathway. *J Mol Biol*. **428**, 4765-4775. (doi:10.1016/j.jmb.2016.09.010).

10. Levy M and Futerman A H. 2010. Mammalian ceramide synthases. *IUBMB Life*. **62**, 347-56. (doi:10.1002/iub.319).

11. Hanada K, Kumagai K, Yasuda S, Miura Y, Kawano M, Fukasawa M, and Nishijima M. 2003. Molecular machinery for non-vesicular trafficking of ceramide. *Nature*. **426**, 803-9. (doi:10.1038/nature02188).

12. Bornancin F. 2011. Ceramide kinase: the first decade. *Cell Signal*. **23**, 999-1008. (doi:10.1016/j.cellsig.2010.11.012).

13. Holthuis J C and Luberto C. 2010. Tales and mysteries of the enigmatic sphingomyelin synthase family. *Adv Exp Med Biol*. **688**, 72-85.

14. D'Angelo G, Polishchuk E, Di Tullio G, Santoro M, Di Campli A, Godi A, West G, Bielawski J, Chuang C C, van der Spoel A C, Platt F M, Hannun Y A, Polishchuk R, Mattjus P, and De Matteis M A. 2007. Glycosphingolipid synthesis requires FAPP2 transfer of glucosylceramide. *Nature*. **449**, 62-7. (doi:10.1038/nature06097).

15. D'Angelo G, Uemura T, Chuang C C, Polishchuk E, Santoro M, Ohvo-Rekila H, Sato T, Di Tullio G, Varriale A, D'Auria S, Daniele T, Capuani F, Johannes L, Mattjus P, Monti M, Pucci P, Williams R L, Burke J E, Platt F M, Harada A, and De Matteis M A. 2013. Vesicular and non-vesicular transport feed distinct glycosylation pathways in the Golgi. *Nature*. **501**, 116-20. (doi:10.1038/nature12423).

16. Sandhoff K and Kolter T. 2003. Biosynthesis and degradation of mammalian glycosphingolipids. *Philos Trans R Soc Lond B Biol Sci*. **358**, 847-61. (doi:10.1098/rstb.2003.1265).

17. Simanshu D K, Kamlekar R K, Wijesinghe D S, Zou X, Zhai X, Mishra S K, Molotkovsky J G, Malinina L, Hinchcliffe E H, Chalfant C E, Brown R E, and Patel D J. 2013. Non-vesicular trafficking by a ceramide-1-phosphate transfer protein regulates eicosanoids. *Nature*. **500**, 463-7. (doi:10.1038/nature12332).

18. Cao X, Surma M A, and Simons K. 2012. Polarized sorting and trafficking in epithelial cells. *Cell Res*. **22**, 793-805. (doi:10.1038/cr.2012.64).

19. Henry B, Ziobro R, Becker K A, Kolesnick R, and Gulbins E. 2013. Acid sphingomyelinase. *Handb Exp Pharmacol*. 77-88. (doi:10.1007/978-3-7091-1368-4_4).

20. Clarke C J, Wu B X, and Hannun Y A. 2011. The neutral sphingomyelinase family: identifying biochemical connections. *Adv Enzyme Regul*. **51**, 51-8. (doi:10.1016/j.advenzreg.2010.09.016).

21. Duan R D. 2006. Alkaline sphingomyelinase: an old enzyme with novel implications. *Biochim Biophys Acta*. **1761**, 281-91. (doi:10.1016/j.bbalip.2006.03.007).

22. Coant N, Sakamoto W, Mao C, and Hannun Y A. 2017. Ceramidases, roles in sphingolipid metabolism and in health and disease. *Adv Biol Regul*. **63**, 122-131. (doi:10.1016/j.jbior.2016.10.002).

23. Adams D R, Pyne S, and Pyne N J. 2016. Sphingosine Kinases: Emerging Structure-Function Insights. *Trends Biochem Sci*. **41**, 395-409. (doi:10.1016/j.tibs.2016.02.007).

24. Serra M and Saba J D. 2010. Sphingosine 1-phosphate lyase, a key regulator of sphingosine 1-phosphate signaling and function. *Adv Enzyme Regul*. **50**, 349-62. (doi:10.1016/j.advenzreg.2009.10.024).

25. Breslow D K, Collins S R, Bodenmiller B, Aebersold R, Simons K, Shevchenko A, Ejsing C S, and Weissman J S. 2010. Orm family proteins mediate sphingolipid homeostasis. *Nature*. **463**, 1048-53. (doi:10.1038/nature08787).

26. Shimobayashi M, Oppliger W, Moes S, Jeno P, and Hall M N. 2013. TORC1-regulated protein kinase Npr1 phosphorylates Orm to stimulate complex sphingolipid synthesis. *Mol Biol Cell*. **24**, 870-81. (doi:10.1091/mbc.E12-10-0753).

27. Roelants F M, Breslow D K, Muir A, Weissman J S, and Thorner J. 2011. Protein kinase Ypk1 phosphorylates regulatory proteins Orm1 and Orm2 to control sphingolipid homeostasis in Saccharomyces cerevisiae. *Proc Natl Acad Sci U S A*. **108**, 19222-7. (doi:10.1073/pnas.1116948108).

28. Sun Y, Miao Y, Yamane Y, Zhang C, Shokat K M, Takematsu H, Kozutsumi Y, and Drubin D G. 2012. Orm protein phosphoregulation mediates transient sphingolipid biosynthesis response to heat stress via the Pkh-Ypk and Cdc55-PP2A pathways. *Mol Biol Cell*. **23**, 2388-98. (doi:10.1091/mbc.E12-03-0209).

29. Siow D L and Wattenberg B W. 2012. Mammalian ORMDL proteins mediate the feedback response in ceramide biosynthesis. *J Biol Chem*. **287**, 40198-204. (doi:10.1074/jbc.C112.404012).

30. Moffatt M F, Kabesch M, Liang L, Dixon A L, Strachan D, Heath S, Depner M, von Berg A, Bufe A, Rietschel E, Heinzmann A, Simma B, Frischer T, Willis-Owen S A, Wong K C, Illig T, Vogelberg C, Weiland S K, von Mutius E, Abecasis G R, Farrall M, Gut I G, Lathrop G M, and Cookson W O. 2007. Genetic variants regulating ORMDL3 expression contribute to the risk of childhood asthma. *Nature*. **448**, 470-3. (doi:10.1038/nature06014).

31. Siow D, Sunkara M, Dunn T M, Morris A J, and Wattenberg B. 2015. ORMDL/serine palmitoyltransferase stoichiometry determines effects of ORMDL3 expression on sphingolipid biosynthesis. *J Lipid Res*. **56**, 898-908. (doi:10.1194/jlr.M057539).

32. Zhakupova A, Debeuf N, Krols M, Toussaint W, Vanhoutte L, Alecu I, Kutalik Z, Vollenweider P, Ernst D, von Eckardstein A, Lambrecht B N, Janssens S, and Hornemann T. 2016. ORMDL3 expression levels have no influence on the activity of serine palmitoyltransferase. *FASEB J*. **30**, 4289-4300. (doi:10.1096/fj.201600639R).

33. Cantalupo A, Zhang Y, Kothiya M, Galvani S, Obinata H, Bucci M, Giordano F J, Jiang X C, Hla T, and Di Lorenzo A. 2015. Nogo-B regulates endothelial sphingolipid homeostasis to control vascular function and blood pressure. *Nat Med*. **21**, 1028-1037. (doi:10.1038/nm.3934).

34. Zhang Y, Huang Y, Cantalupo A, Azevedo P S, Siragusa M, Bielawski J, Giordano F J, and Di Lorenzo A. 2016. Endothelial Nogo-B regulates sphingolipid biosynthesis to promote pathological cardiac hypertrophy during chronic pressure overload. *JCI Insight*. **1**. (doi:10.1172/jci.insight.85484).

35. Schorling S, Vallee B, Barz W P, Riezman H, and Oesterhelt D. 2001. Lag1p and Lac1p are essential for the Acyl-CoA-dependent ceramide synthase reaction in Saccharomyces cerevisae. *Mol Biol Cell*. **12**, 3417-27.

36. Vallee B and Riezman H. 2005. Lip1p: a novel subunit of acyl-CoA ceramide synthase. *EMBO J*. **24**, 730-41. (doi:10.1038/sj.emboj.7600562).

37. Kobayashi S D and Nagiec M M. 2003. Ceramide/long-chain base phosphate rheostat in Saccharomyces cerevisiae: regulation of ceramide synthesis by Elo3p and Cka2p. *Eukaryot Cell*. **2**, 284-94.

38. Fresques T, Niles B, Aronova S, Mogri H, Rakhshandehroo T, and Powers T. 2015. Regulation of ceramide synthase by casein kinase 2-dependent phosphorylation in Saccharomyces cerevisiae. *J Biol Chem*. **290**, 1395-403. (doi:10.1074/jbc.M114.621086).

39. Muir A, Ramachandran S, Roelants F M, Timmons G, and Thorner J. 2014. TORC2-dependent protein kinase Ypk1 phosphorylates ceramide synthase to stimulate synthesis of complex sphingolipids. *Elife*. **3**. (doi:10.7554/eLife.03779).

40. Laviad E L, Albee L, Pankova-Kholmyansky I, Epstein S, Park H, Merrill A H, Jr., and Futerman A H. 2008. Characterization of ceramide synthase 2: tissue distribution, substrate specificity, and inhibition by sphingosine 1-phosphate. *J Biol Chem*. **283**, 5677-84. (doi:10.1074/jbc.M707386200).

41. Pewzner-Jung Y, Ben-Dor S, and Futerman A H. 2006. When do Lasses (longevity assurance genes) become CerS (ceramide synthases)?: Insights into the regulation of ceramide synthesis. *J Biol Chem*. **281**, 25001-5. (doi:10.1074/jbc.R600010200).

42. Sridevi P, Alexander H, Laviad E L, Pewzner-Jung Y, Hannink M, Futerman A H, and Alexander S. 2009. Ceramide synthase 1 is regulated by proteasomal mediated turnover. *Biochim Biophys Acta*. **1793**, 1218-27. (doi:10.1016/j.bbamcr.2009.04.006).

43. Sassa T, Hirayama T, and Kihara A. 2016. Enzyme Activities of the Ceramide Synthases CERS2-6 Are Regulated by Phosphorylation in the C-terminal Region. *J Biol Chem*. **291**, 7477-87. (doi:10.1074/jbc.M115.695858).

44. Newton J, Lima S, Maceyka M, and Spiegel S. 2015. Revisiting the sphingolipid rheostat: Evolving concepts in cancer therapy. *Exp Cell Res*. **333**, 195-200. (doi:10.1016/j.yexcr.2015.02.025).

45. Alvarez S E, Milstien S, and Spiegel S. 2007. Autocrine and paracrine roles of sphingosine-1-phosphate. *Trends Endocrinol Metab*. **18**, 300-7. (doi:10.1016/j.tem.2007.07.005).

46. Mendelson K, Evans T, and Hla T. 2014. Sphingosine 1-phosphate signalling. *Development*. **141**, 5-9. (doi:10.1242/dev.094805).

47. Chan H and Pitson S M. 2013. Post-translational regulation of sphingosine kinases. *Biochim Biophys Acta*. **1831**, 147-56. (doi:10.1016/j.bbalip.2012.07.005).

48. Pitson S M, Moretti P A, Zebol J R, Lynn H E, Xia P, Vadas M A, and Wattenberg B W. 2003. Activation of sphingosine kinase 1 by ERK1/2-mediated phosphorylation. *EMBO J*. **22**, 5491-500. (doi:10.1093/emboj/cdg540).

49. Jarman K E, Moretti P A, Zebol J R, and Pitson S M. 2010. Translocation of sphingosine kinase 1 to the plasma membrane is mediated by calcium- and integrin-binding protein 1. *J Biol Chem*. **285**, 483-92. (doi:10.1074/jbc.M109.068395).

50. Stahelin R V, Hwang J H, Kim J H, Park Z Y, Johnson K R, Obeid L M, and Cho W. 2005. The mechanism of membrane targeting of human sphingosine kinase 1. *J Biol Chem*. **280**, 43030-8. (doi:10.1074/jbc.M507574200).

51. Barr R K, Lynn H E, Moretti P A, Khew-Goodall Y, and Pitson S M. 2008. Deactivation of sphingosine kinase 1 by protein phosphatase 2A. *J Biol Chem*. **283**, 34994-5002. (doi:10.1074/jbc.M804658200).

52. Hait N C, Bellamy A, Milstien S, Kordula T, and Spiegel S. 2007. Sphingosine kinase type 2 activation by ERK-mediated phosphorylation. *J Biol Chem*. **282**, 12058-65. (doi:10.1074/jbc.M609559200).

53. Ding G, Sonoda H, Yu H, Kajimoto T, Goparaju S K, Jahangeer S, Okada T, and Nakamura S. 2007. Protein kinase D-mediated phosphorylation and nuclear export of sphingosine kinase 2. *J Biol Chem*. **282**, 27493-502. (doi:10.1074/jbc.M701641200).

54. Igarashi N, Okada T, Hayashi S, Fujita T, Jahangeer S, and Nakamura S. 2003. Sphingosine kinase 2 is a nuclear protein and inhibits DNA synthesis. *J Biol Chem*. **278**, 46832-9. (doi:10.1074/jbc.M306577200).

55. Kumagai K, Kawano M, Shinkai-Ouchi F, Nishijima M, and Hanada K. 2007. Interorganelle trafficking of ceramide is regulated by phosphorylation-dependent cooperativity between the PH and START domains of CERT. *J Biol Chem*. **282**, 17758-66. (doi:10.1074/jbc.M702291200).

56. Prashek J, Bouyain S, Fu M, Li Y, Berkes D, and Yao X. 2017. Interaction between the PH and START domains of ceramide transfer protein competes with phosphatidylinositol 4-phosphate binding by the PH domain. *J Biol Chem*. **292**, 14217-14228. (doi:10.1074/jbc.M117.780007).

57. Fugmann T, Hausser A, Schoffler P, Schmid S, Pfizenmaier K, and Olayioye M A. 2007. Regulation of secretory transport by protein kinase D-mediated phosphorylation of the ceramide transfer protein. *J Cell Biol*. **178**, 15-22. (doi:10.1083/jcb.200612017).

58. Tomishige N, Kumagai K, Kusuda J, Nishijima M, and Hanada K. 2009. Casein kinase I{gamma}2 down-regulates trafficking of ceramide in the synthesis of sphingomyelin. *Mol Biol Cell*. **20**, 348-57. (doi:10.1091/mbc.E08-07-0669).

59. Saito S, Matsui H, Kawano M, Kumagai K, Tomishige N, Hanada K, Echigo S, Tamura S, and Kobayashi T. 2008. Protein phosphatase 2Cepsilon is an endoplasmic reticulum integral membrane protein that dephosphorylates the ceramide transport protein CERT to enhance its association with organelle membranes. *J Biol Chem*. **283**, 6584-93. (doi:10.1074/jbc.M707691200).

60. Kumagai K, Kawano-Kawada M, and Hanada K. 2014. Phosphoregulation of the ceramide transport protein CERT at serine 315 in the interaction with VAMP-associated protein (VAP) for inter-organelle trafficking of ceramide in mammalian cells. *J Biol Chem*. **289**, 10748-60. (doi:10.1074/jbc.M113.528380).

61. Gillard B K, Clement R G, and Marcus D M. 1998. Variations among cell lines in the synthesis of sphingolipids in de novo and recycling pathways. *Glycobiology*. **8**, 885-90.

62. Tettamanti G, Bassi R, Viani P, and Riboni L. 2003. Salvage pathways in glycosphingolipid metabolism. *Biochimie*. **85**, 423-37.

63. Alvarez-Vasquez F, Sims K J, Voit E O, and Hannun Y A. 2007. Coordination of the dynamics of yeast sphingolipid metabolism during the diauxic shift. *Theor Biol Med Model*. **4**, 42. (doi:10.1186/1742-4682-4-42).

64. Chen P W, Fonseca L L, Hannun Y A, and Voit E O. 2013. Coordination of rapid sphingolipid responses to heat stress in yeast. *PLoS Comput Biol*. **9**, e1003078. (doi:10.1371/journal.pcbi.1003078).

65. Loizides-Mangold U, Perrin L, Vandereycken B, Betts J A, Walhin J P, Templeman I, Chanon S, Weger B D, Durand C, Robert M, Paz Montoya J, Moniatte M, Karagounis L G, Johnston J D, Gachon F, Lefai E, Riezman H, and Dibner C. 2017. Lipidomics reveals diurnal lipid oscillations in human skeletal muscle persisting in cellular myotubes cultured in vitro. *Proc Natl Acad Sci U S A*. **114**, E8565-E8574. (doi:10.1073/pnas.1705821114).

66. Ferlinz K, Hurwitz R, Moczall H, Lansmann S, Schuchman E H, and Sandhoff K. 1997. Functional characterization of the N-glycosylation sites of human acid sphingomyelinase by site-directed mutagenesis. *Eur J Biochem*. **243**, 511-7.

67. Jenkins R W, Canals D, Idkowiak-Baldys J, Simbari F, Roddy P, Perry D M, Kitatani K, Luberto C, and Hannun Y A. 2010. Regulated secretion of acid sphingomyelinase: implications for selectivity of ceramide formation. *J Biol Chem*. **285**, 35706-18. (doi:10.1074/jbc.M110.125609).

68. Rhein C, Reichel M, Muhle C, Rotter A, Schwab S G, and Kornhuber J. 2014. Secretion of acid Sphingomyelinase is affected by its polymorphic signal peptide. *Cell Physiol Biochem*. **34**, 1385-401. (doi:10.1159/000366345).

69. Zeidan Y H and Hannun Y A. 2007. Activation of acid sphingomyelinase by protein kinase Cdelta-mediated phosphorylation. *J Biol Chem*. **282**, 11549-61. (doi:10.1074/jbc.M609424200).

70. Hofmann K, Tomiuk S, Wolff G, and Stoffel W. 2000. Cloning and characterization of the mammalian brain-specific, Mg2+-dependent neutral sphingomyelinase. *Proc Natl Acad Sci U S A*. **97**, 5895-900.

71. Shamseddine A A, Airola M V, and Hannun Y A. 2015. Roles and regulation of neutral sphingomyelinase-2 in cellular and pathological processes. *Adv Biol Regul*. **57**, 24-41. (doi:10.1016/j.jbior.2014.10.002).

72. Coroneos E, Martinez M, McKenna S, and Kester M. 1995. Differential regulation of sphingomyelinase and ceramidase activities by growth factors and cytokines. Implications for cellular proliferation and differentiation. *J Biol Chem*. **270**, 23305-9.

73. Philipp S, Puchert M, Adam-Klages S, Tchikov V, Winoto-Morbach S, Mathieu S, Deerberg A, Kolker L, Marchesini N, Kabelitz D, Hannun Y A, Schutze S, and Adam D. 2010. The Polycomb group protein EED couples TNF receptor 1 to neutral sphingomyelinase. *Proc Natl Acad Sci U S A*. **107**, 1112-7. (doi:10.1073/pnas.0908486107).

74. Filosto S, Fry W, Knowlton A A, and Goldkorn T. 2010. Neutral sphingomyelinase 2 (nSMase2) is a phosphoprotein regulated by calcineurin (PP2B). *J Biol Chem*. **285**, 10213-22. (doi:10.1074/jbc.M109.069963).

75. Filosto S, Ashfaq M, Chung S, Fry W, and Goldkorn T. 2012. Neutral sphingomyelinase 2 activity and protein stability are modulated by phosphorylation of five conserved serines. *J Biol Chem*. **287**, 514-22. (doi:10.1074/jbc.M111.315481).

76. Marchesini N, Luberto C, and Hannun Y A. 2003. Biochemical properties of mammalian neutral sphingomyelinase 2 and its role in sphingolipid metabolism. *J Biol Chem*. **278**, 13775-83. (doi:10.1074/jbc.M212262200).

77. Wu B X, Clarke C J, Matmati N, Montefusco D, Bartke N, and Hannun Y A. 2011. Identification of novel anionic phospholipid binding domains in neutral sphingomyelinase 2 with selective binding preference. *J Biol Chem*. **286**, 22362-71. (doi:10.1074/jbc.M110.156471).

78. Airola M V, Shanbhogue P, Shamseddine A A, Guja K E, Senkal C E, Maini R, Bartke N, Wu B X, Obeid L M, Garcia-Diaz M, and Hannun Y A. 2017. Structure of human nSMase2 reveals an interdomain allosteric activation mechanism for ceramide generation. *Proc Natl Acad Sci U S A*. **114**, E5549-E5558. (doi:10.1073/pnas.1705134114).

79. Boulgaropoulos B, Amenitsch H, Laggner P, and Pabst G. 2010. Implication of sphingomyelin/ceramide molar ratio on the biological activity of sphingomyelinase. *Biophys J*. **99**, 499-506. (doi:10.1016/j.bpj.2010.04.028).

80. Cheng Y, Ohlsson L, and Duan R D. 2004. Psyllium and fat in diets differentially affect the activities and expressions of colonic sphingomyelinases and caspase in mice. *Br J Nutr*. **91**, 715-23. (doi:10.1079/BJN20041107).

81. Liu J J, Nilsson A, and Duan R D. 2000. Effects of phospholipids on sphingomyelin hydrolysis induced by intestinal alkaline sphingomyelinase: an in vitro study. *J Nutr Biochem*. **11**, 192-7.

82. Liu J J, Nilsson A, and Duan R D. 2002. In vitro effects of fat, FA, and cholesterol on sphingomyelin hydrolysis induced by rat intestinal alkaline sphingomyelinase. *Lipids*. **37**, 469-74.

83. Bernardo K, Hurwitz R, Zenk T, Desnick R J, Ferlinz K, Schuchman E H, and Sandhoff K. 1995. Purification, characterization, and biosynthesis of human acid ceramidase. *J Biol Chem*. **270**, 11098-102.

84. Shtraizent N, Eliyahu E, Park J H, He X, Shalgi R, and Schuchman E H. 2008. Autoproteolytic cleavage and activation of human acid ceramidase. *J Biol Chem*. **283**, 11253-9. (doi:10.1074/jbc.M709166200).

85. Kishimoto Y, Hiraiwa M, and O'Brien J S. 1992. Saposins: structure, function, distribution, and molecular genetics. *J Lipid Res*. **33**, 1255-67.

86. Azuma N, O'Brien J S, Moser H W, and Kishimoto Y. 1994. Stimulation of acid ceramidase activity by saposin D. *Arch Biochem Biophys*. **311**, 354-7.

87. Linke T, Wilkening G, Sadeghlar F, Mozcall H, Bernardo K, Schuchman E, and Sandhoff K. 2001. Interfacial regulation of acid ceramidase activity. Stimulation of ceramide degradation by lysosomal lipids and sphingolipid activator proteins. *J Biol Chem*. **276**, 5760-8. (doi:10.1074/jbc.M006846200).

88. Tani M, Iida H, and Ito M. 2003. O-glycosylation of mucin-like domain retains the neutral ceramidase on the plasma membranes as a type II integral membrane protein. *J Biol Chem*. **278**, 10523-30. (doi:10.1074/jbc.M207932200).

89. Tani M, Okino N, Sueyoshi N, and Ito M. 2004. Conserved amino acid residues in the COOH-terminal tail are indispensable for the correct folding and localization and enzyme activity of neutral ceramidase. *J Biol Chem*. **279**, 29351-8. (doi:10.1074/jbc.M404012200).

90. Franzen R, Pfeilschifter J, and Huwiler A. 2002. Nitric oxide induces neutral ceramidase degradation by the ubiquitin/proteasome complex in renal mesangial cell cultures. *FEBS Lett*. **532**, 441-4.

91. Franzen R, Fabbro D, Aschrafi A, Pfeilschifter J, and Huwiler A. 2002. Nitric oxide induces degradation of the neutral ceramidase in rat renal mesangial cells and is counterregulated by protein kinase C. *J Biol Chem*. **277**, 46184-90. (doi:10.1074/jbc.M204034200).

92. Sun W, Jin J, Xu R, Hu W, Szulc Z M, Bielawski J, Obeid L M, and Mao C. 2010. Substrate specificity, membrane topology, and activity regulation of human alkaline ceramidase 2 (ACER2). *J Biol Chem*. **285**, 8995-9007. (doi:10.1074/jbc.M109.069203).

93. Sasaki H, Toyomura K, Matsuzaki W, Okamoto A, Yamaguchi N, Nakamura H, and Murayama T. 2014. Regulation of alkaline ceramidase activity by the c-Src-mediated pathway. *Arch Biochem Biophys*. **550-551**, 12-9. (doi:10.1016/j.abb.2014.03.012).

94. Holland W L, Miller R A, Wang Z V, Sun K, Barth B M, Bui H H, Davis K E, Bikman B T, Halberg N, Rutkowski J M, Wade M R, Tenorio V M, Kuo M S, Brozinick J T, Zhang B B, Birnbaum M J, Summers S A, and Scherer P E. 2011. Receptor-mediated activation of ceramidase activity initiates the pleiotropic actions of adiponectin. *Nat Med*. **17**, 55-63. (doi:10.1038/nm.2277).

95. Vasiliauskaite-Brooks I, Sounier R, Rochaix P, Bellot G, Fortier M, Hoh F, De Colibus L, Bechara C, Saied E M, Arenz C, Leyrat C, and Granier S. 2017. Structural insights into adiponectin receptors suggest ceramidase activity. *Nature*. **544**, 120-123. (doi:10.1038/nature21714).

96. van Meer G and de Kroon A I. 2011. Lipid map of the mammalian cell. *J Cell Sci*. **124**, 5-8. (doi:10.1242/jcs.071233).

97. Sonnino S, Prinetti A, Mauri L, Chigorno V, and Tettamanti G. 2006. Dynamic and structural properties of sphingolipids as driving forces for the formation of membrane domains. *Chem Rev*. **106**, 2111-25. (doi:10.1021/cr0100446).

98. Slotte J P. 2016. The importance of hydrogen bonding in sphingomyelin's membrane interactions with co-lipids. *Biochim Biophys Acta*. **1858**, 304-10. (doi:10.1016/j.bbamem.2015.12.008).

99. Goni F M, Sot J, and Alonso A. 2014. Biophysical properties of sphingosine, ceramides and other simple sphingolipids. *Biochem Soc Trans*. **42**, 1401-8. (doi:10.1042/BST20140159).

100. Carreira A C, Ventura A E, Varela A R, and Silva L C. 2015. Tackling the biophysical properties of sphingolipids to decipher their biological roles. *Biol Chem*. **396**, 597-609. (doi:10.1515/hsz-2014-0283).

101. Al Sazzad M A, Yasuda T, Murata M, and Slotte J P. 2017. The Long-Chain Sphingoid Base of Ceramides Determines Their Propensity for Lateral Segregation. *Biophys J*. **112**, 976-983. (doi:10.1016/j.bpj.2017.01.016).

102. Clay L, Caudron F, Denoth-Lippuner A, Boettcher B, Buvelot Frei S, Snapp E L, and Barral Y. 2014. A sphingolipid-dependent diffusion barrier confines ER stress to the yeast mother cell. *Elife*. **3**, e01883. (doi:10.7554/eLife.01883).

103. Simons K and van Meer G. 1988. Lipid sorting in epithelial cells. *Biochemistry*. **27**, 6197-202.

104. Oertel S, Scholich K, Weigert A, Thomas D, Schmetzer J, Trautmann S, Wegner M S, Radeke H H, Filmann N, Brune B, Geisslinger G, Tegeder I, and Grosch S. 2017. Ceramide synthase 2 deficiency aggravates AOM-DSS-induced colitis in mice: role of colon barrier integrity. *Cell Mol Life Sci*. **74**, 3039-3055. (doi:10.1007/s00018-017-2518-9).

105. Breiden B and Sandhoff K. 2014. The role of sphingolipid metabolism in cutaneous permeability barrier formation. *Biochim Biophys Acta*. **1841**, 441-52. (doi:10.1016/j.bbalip.2013.08.010).

106. Borodzicz S, Rudnicka L, Mirowska-Guzel D, and Cudnoch-Jedrzejewska A. 2016. The role of epidermal sphingolipids in dermatologic diseases. *Lipids Health Dis*. **15**, 13. (doi:10.1186/s12944-016-0178-7).

107. Li W, Sandhoff R, Kono M, Zerfas P, Hoffmann V, Ding B C, Proia R L, and Deng C X. 2007. Depletion of ceramides with very long chain fatty acids causes defective skin permeability barrier function, and neonatal lethality in ELOVL4 deficient mice. *Int J Biol Sci*. **3**, 120-8.

108. Jennemann R, Rabionet M, Gorgas K, Epstein S, Dalpke A, Rothermel U, Bayerle A, van der Hoeven F, Imgrund S, Kirsch J, Nickel W, Willecke K, Riezman H, Grone H J, and Sandhoff R. 2012. Loss of ceramide synthase 3 causes lethal skin barrier disruption. *Hum Mol Genet*. **21**, 586-608. (doi:10.1093/hmg/ddr494).

109. Aldahmesh M A, Mohamed J Y, Alkuraya H S, Verma I C, Puri R D, Alaiya A A, Rizzo W B, and Alkuraya F S. 2011. Recessive mutations in ELOVL4 cause ichthyosis, intellectual disability, and spastic quadriplegia. *Am J Hum Genet*. **89**, 745-50. (doi:10.1016/j.ajhg.2011.10.011).

110. Simons K and Ikonen E. 1997. Functional rafts in cell membranes. *Nature*. **387**, 569-72. (doi:10.1038/42408).

111. Klemm R W, Ejsing C S, Surma M A, Kaiser H J, Gerl M J, Sampaio J L, de Robillard Q, Ferguson C, Proszynski T J, Shevchenko A, and Simons K. 2009. Segregation of sphingolipids and sterols during formation of secretory vesicles at the trans-Golgi network. *J Cell Biol*. **185**, 601-12. (doi:10.1083/jcb.200901145).

112. Surma M A, Klose C, Klemm R W, Ejsing C S, and Simons K. 2011. Generic sorting of raft lipids into secretory vesicles in yeast. *Traffic*. **12**, 1139-47. (doi:10.1111/j.1600-0854.2011.01221.x).

113. Deng Y, Rivera-Molina F E, Toomre D K, and Burd C G. 2016. Sphingomyelin is sorted at the trans Golgi network into a distinct class of secretory vesicle. *Proc Natl Acad Sci U S A*. **113**, 6677-82. (doi:10.1073/pnas.1602875113).

114. Zhang H, Abraham N, Khan L A, Hall D H, Fleming J T, and Gobel V. 2011. Apicobasal domain identities of expanding tubular membranes depend on glycosphingolipid biosynthesis. *Nat Cell Biol*. **13**, 1189-201. (doi:10.1038/ncb2328).

115. Munro S. 2003. Lipid rafts: elusive or illusive? *Cell*. **115**, 377-88.

116. Varma R and Mayor S. 1998. GPI-anchored proteins are organized in submicron domains at the cell surface. *Nature*. **394**, 798-801. (doi:10.1038/29563).

117. Sharma P, Varma R, Sarasij R C, Ira, Gousset K, Krishnamoorthy G, Rao M, and Mayor S. 2004. Nanoscale organization of multiple GPI-anchored proteins in living cell membranes. *Cell*. **116**, 577-89.

118. Raghupathy R, Anilkumar A A, Polley A, Singh P P, Yadav M, Johnson C, Suryawanshi S, Saikam V, Sawant S D, Panda A, Guo Z, Vishwakarma R A, Rao M, and Mayor S. 2015. Transbilayer lipid interactions mediate nanoclustering of lipid-anchored proteins. *Cell*. **161**, 581-594. (doi:10.1016/j.cell.2015.03.048).

119. Fujiwara T, Ritchie K, Murakoshi H, Jacobson K, and Kusumi A. 2002. Phospholipids undergo hop diffusion in compartmentalized cell membrane. *J Cell Biol*. **157**, 1071-81. (doi:10.1083/jcb.200202050).

120. Dietrich C, Yang B, Fujiwara T, Kusumi A, and Jacobson K. 2002. Relationship of lipid rafts to transient confinement zones detected by single particle tracking. *Biophys J*. **82**, 274-84. (doi:10.1016/S0006-3495(02)75393-9).

121. Eggeling C, Ringemann C, Medda R, Schwarzmann G, Sandhoff K, Polyakova S, Belov V N, Hein B, von Middendorff C, Schonle A, and Hell S W. 2009. Direct observation of the nanoscale dynamics of membrane lipids in a living cell. *Nature*. **457**, 1159-62. (doi:10.1038/nature07596).

122. Schneider F, Waithe D, Clausen M P, Galiani S, Koller T, Ozhan G, Eggeling C, and Sezgin E. 2017. Diffusion of lipids and GPI-anchored proteins in actin-free plasma membrane vesicles measured by STED-FCS. *Mol Biol Cell*. **28**, 1507-1518. (doi:10.1091/mbc.E16-07-0536).

123. Kusumi A, Suzuki K G, Kasai R S, Ritchie K, and Fujiwara T K. 2011. Hierarchical mesoscale domain organization of the plasma membrane. *Trends Biochem Sci*. **36**, 604-15. (doi:10.1016/j.tibs.2011.08.001).

124. Rao M and Mayor S. 2014. Active organization of membrane constituents in living cells. *Curr Opin Cell Biol*. **29**, 126-32. (doi:10.1016/j.ceb.2014.05.007).

125. Sezgin E, Levental I, Mayor S, and Eggeling C. 2017. The mystery of membrane organization: composition, regulation and roles of lipid rafts. *Nat Rev Mol Cell Biol*. **18**, 361-374. (doi:10.1038/nrm.2017.16).

126. Bastiani M and Parton R G. 2010. Caveolae at a glance. *J Cell Sci*. **123**, 3831-6. (doi:10.1242/jcs.070102).

127. Parton R G and del Pozo M A. 2013. Caveolae as plasma membrane sensors, protectors and organizers. *Nat Rev Mol Cell Biol*. **14**, 98-112. (doi:10.1038/nrm3512).

128. Martinez-Outschoorn U E, Sotgia F, and Lisanti M P. 2015. Caveolae and signalling in cancer. *Nat Rev Cancer*. **15**, 225-37. (doi:10.1038/nrc3915).

129. Sinha B, Koster D, Ruez R, Gonnord P, Bastiani M, Abankwa D, Stan R V, Butler-Browne G, Vedie B, Johannes L, Morone N, Parton R G, Raposo G, Sens P, Lamaze C, and Nassoy P. 2011. Cells respond to mechanical stress by rapid disassembly of caveolae. *Cell*. **144**, 402-13. (doi:10.1016/j.cell.2010.12.031).

130. Nassoy P and Lamaze C. 2012. Stressing caveolae new role in cell mechanics. *Trends Cell Biol*. **22**, 381-9. (doi:10.1016/j.tcb.2012.04.007).

131. Malinska K, Malinsky J, Opekarova M, and Tanner W. 2003. Visualization of protein compartmentation within the plasma membrane of living yeast cells. *Mol Biol Cell*. **14**, 4427-36. (doi:10.1091/mbc.E03-04-0221).

132. Walther T C, Brickner J H, Aguilar P S, Bernales S, Pantoja C, and Walter P. 2006. Eisosomes mark static sites of endocytosis. *Nature*. **439**, 998-1003. (doi:10.1038/nature04472).

133. Kabeche R, Howard L, and Moseley J B. 2015. Eisosomes provide membrane reservoirs for rapid expansion of the yeast plasma membrane. *J Cell Sci*. **128**, 4057-62. (doi:10.1242/jcs.176867).

134. Berchtold D, Piccolis M, Chiaruttini N, Riezman I, Riezman H, Roux A, Walther T C, and Loewith R. 2012. Plasma membrane stress induces relocalization of Slm proteins and activation of TORC2 to promote sphingolipid synthesis. *Nat Cell Biol*. **14**, 542-7. (doi:10.1038/ncb2480).

135. Pyne S, Adams D R, and Pyne N J. 2016. Sphingosine 1-phosphate and sphingosine kinases in health and disease: Recent advances. *Prog Lipid Res*. **62**, 93-106. (doi:10.1016/j.plipres.2016.03.001).

136. Van Brocklyn J R, Lee M J, Menzeleev R, Olivera A, Edsall L, Cuvillier O, Thomas D M, Coopman P J, Thangada S, Liu C H, Hla T, and Spiegel S. 1998. Dual actions of sphingosine-1-phosphate: extracellular through the Gi-coupled receptor Edg-1 and intracellular to regulate proliferation and survival. *J Cell Biol*. **142**, 229-40.

137. Mitra P, Oskeritzian C A, Payne S G, Beaven M A, Milstien S, and Spiegel S. 2006. Role of ABCC1 in export of sphingosine-1-phosphate from mast cells. *Proc Natl Acad Sci U S A*. **103**, 16394-9. (doi:10.1073/pnas.0603734103).

138. Kawahara A, Nishi T, Hisano Y, Fukui H, Yamaguchi A, and Mochizuki N. 2009. The sphingolipid transporter spns2 functions in migration of zebrafish myocardial precursors. *Science*. **323**, 524-7. (doi:10.1126/science.1167449).

139. Hisano Y, Kobayashi N, Yamaguchi A, and Nishi T. 2012. Mouse SPNS2 functions as a sphingosine-1-phosphate transporter in vascular endothelial cells. *PLoS One*. **7**, e38941. (doi:10.1371/journal.pone.0038941).

140. Kobayashi N, Kobayashi N, Yamaguchi A, and Nishi T. 2009. Characterization of the ATP-dependent sphingosine 1-phosphate transporter in rat erythrocytes. *J Biol Chem*. **284**, 21192-200. (doi:10.1074/jbc.M109.006163).

141. Vu T M, Ishizu A N, Foo J C, Toh X R, Zhang F, Whee D M, Torta F, Cazenave-Gassiot A, Matsumura T, Kim S, Toh S E S, Suda T, Silver D L, Wenk M R, and Nguyen L N. 2017. Mfsd2b is essential for the sphingosine-1-phosphate export in erythrocytes and platelets. *Nature*. **550**, 524-528. (doi:10.1038/nature24053).

142. Galvani S, Sanson M, Blaho V A, Swendeman S L, Obinata H, Conger H, Dahlback B, Kono M, Proia R L, Smith J D, and Hla T. 2015. HDL-bound sphingosine 1-phosphate acts as a biased agonist for the endothelial cell receptor S1P1 to limit vascular inflammation. *Sci Signal*. **8**, ra79. (doi:10.1126/scisignal.aaa2581).

143. Takabe K, Paugh S W, Milstien S, and Spiegel S. 2008. "Inside-out" signaling of sphingosine-1-phosphate: therapeutic targets. *Pharmacol Rev*. **60**, 181-95. (doi:10.1124/pr.107.07113).

144. Ogretmen B. 2018. Sphingolipid metabolism in cancer signalling and therapy. *Nat Rev Cancer*. **18**, 33-50. (doi:10.1038/nrc.2017.96).

145. Izawa K, Kitaura J, Yamanishi Y, Matsuoka T, Kaitani A, Sugiuchi M, Takahashi M, Maehara A, Enomoto Y, Oki T, Takai T, and Kitamura T. 2009. An activating and inhibitory signal from an inhibitory receptor LMIR3/CLM-1: LMIR3 augments lipopolysaccharide response through association with FcRgamma in mast cells. *J Immunol*. **183**, 925-36. (doi:10.4049/jimmunol.0900552).

146. Izawa K, Yamanishi Y, Maehara A, Takahashi M, Isobe M, Ito S, Kaitani A, Matsukawa T, Matsuoka T, Nakahara F, Oki T, Kiyonari H, Abe T, Okumura K, Kitamura T, and Kitaura J. 2012. The receptor LMIR3 negatively regulates mast cell activation and allergic responses by binding to extracellular ceramide. *Immunity*. **37**, 827-39. (doi:10.1016/j.immuni.2012.08.018).

147. Matsukawa T, Izawa K, Isobe M, Takahashi M, Maehara A, Yamanishi Y, Kaitani A, Okumura K, Teshima T, Kitamura T, and Kitaura J. 2016. Ceramide-CD300f binding suppresses experimental colitis by inhibiting ATP-mediated mast cell activation. *Gut*. **65**, 777-87. (doi:10.1136/gutjnl-2014-308900).

148. Shiba E, Izawa K, Kaitani A, Isobe M, Maehara A, Uchida K, Maeda K, Nakano N, Ogawa H, Okumura K, Kitamura T, Shimizu T, and Kitaura J. 2017. Ceramide-CD300f Binding Inhibits Lipopolysaccharide-induced Skin Inflammation. *J Biol Chem*. **292**, 2924-2932. (doi:10.1074/jbc.M116.768366).

149. Alvarez S E, Harikumar K B, Hait N C, Allegood J, Strub G M, Kim E Y, Maceyka M, Jiang H, Luo C, Kordula T, Milstien S, and Spiegel S. 2010. Sphingosine-1-phosphate is a missing cofactor for the E3 ubiquitin ligase TRAF2. *Nature*. **465**, 1084-8. (doi:10.1038/nature09128).

150. Park E S, Choi S, Shin B, Yu J, Yu J, Hwang J M, Yun H, Chung Y H, Choi J S, Choi Y, and Rho J. 2015. Tumor necrosis factor (TNF) receptor-associated factor (TRAF)-interacting protein (TRIP) negatively regulates the TRAF2 ubiquitin-dependent pathway by suppressing the TRAF2-sphingosine 1-phosphate (S1P) interaction. *J Biol Chem*. **290**, 9660-73. (doi:10.1074/jbc.M114.609685).

151. Adada M M, Orr-Gandy K A, Snider A J, Canals D, Hannun Y A, Obeid L M, and Clarke C J. 2013. Sphingosine kinase 1 regulates tumor necrosis factor-mediated RANTES induction through p38 mitogen-activated protein kinase but independently of nuclear factor kappaB activation. *J Biol Chem*. **288**, 27667-79. (doi:10.1074/jbc.M113.489443).

152. Xiong Y, Lee H J, Mariko B, Lu Y C, Dannenberg A J, Haka A S, Maxfield F R, Camerer E, Proia R L, and Hla T. 2013. Sphingosine kinases are not required for inflammatory responses in macrophages. *J Biol Chem*. **288**, 32563-73. (doi:10.1074/jbc.M113.483750).

153. Etemadi N, Chopin M, Anderton H, Tanzer M C, Rickard J A, Abeysekera W, Hall C, Spall S K, Wang B, Xiong Y, Hla T, Pitson S M, Bonder C S, Wong W W, Ernst M, Smyth G K, Vaux D L, Nutt S L, Nachbur U, and Silke J. 2015. TRAF2 regulates TNF and NF-kappaB signalling to suppress apoptosis and skin inflammation independently of Sphingosine kinase 1. *Elife*. **4**. (doi:10.7554/eLife.10592).

154. Hait N C, Allegood J, Maceyka M, Strub G M, Harikumar K B, Singh S K, Luo C, Marmorstein R, Kordula T, Milstien S, and Spiegel S. 2009. Regulation of histone acetylation in the nucleus by sphingosine-1-phosphate. *Science*. **325**, 1254-7. (doi:10.1126/science.1176709).

155. Panneer Selvam S, De Palma R M, Oaks J J, Oleinik N, Peterson Y K, Stahelin R V, Skordalakes E, Ponnusamy S, Garrett-Mayer E, Smith C D, and Ogretmen B. 2015. Binding of the sphingolipid S1P to hTERT stabilizes telomerase at the nuclear periphery by allosterically mimicking protein phosphorylation. *Sci Signal*. **8**, ra58. (doi:10.1126/scisignal.aaa4998).

156. Bourbon N A, Yun J, and Kester M. 2000. Ceramide directly activates protein kinase C zeta to regulate a stress-activated protein kinase signaling complex. *J Biol Chem*. **275**, 35617-23. (doi:10.1074/jbc.M007346200).

157. Takasugi N, Sasaki T, Suzuki K, Osawa S, Isshiki H, Hori Y, Shimada N, Higo T, Yokoshima S, Fukuyama T, Lee V M, Trojanowski J Q, Tomita T, and Iwatsubo T. 2011. BACE1 activity is modulated by cell-associated sphingosine-1-phosphate. *J Neurosci*. **31**, 6850-7. (doi:10.1523/JNEUROSCI.6467-10.2011).

158. Schonauer S, Korschen H G, Penno A, Rennhack A, Breiden B, Sandhoff K, Gutbrod K, Dormann P, Raju D N, Haberkant P, Gerl M J, Brugger B, Zigdon H, Vardi A, Futerman A H, Thiele C, and Wachten D. 2017. Identification of a feedback loop involving beta-glucosidase 2 and its product sphingosine sheds light on the molecular mechanisms in Gaucher disease. *J Biol Chem*. **292**, 6177-6189. (doi:10.1074/jbc.M116.762831).

159. Brugger B, Sandhoff R, Wegehingel S, Gorgas K, Malsam J, Helms J B, Lehmann W D, Nickel W, and Wieland F T. 2000. Evidence for segregation of sphingomyelin and cholesterol during formation of COPI-coated vesicles. *J Cell Biol*. **151**, 507-18.

160. Contreras F X, Ernst A M, Haberkant P, Bjorkholm P, Lindahl E, Gonen B, Tischer C, Elofsson A, von Heijne G, Thiele C, Pepperkok R, Wieland F, and Brugger B. 2012. Molecular recognition of a single sphingolipid species by a protein's transmembrane domain. *Nature*. **481**, 525-9. (doi:10.1038/nature10742).

161. Chipuk J E, McStay G P, Bharti A, Kuwana T, Clarke C J, Siskind L J, Obeid L M, and Green D R. 2012. Sphingolipid metabolism cooperates with BAK and BAX to promote the mitochondrial pathway of apoptosis. *Cell*. **148**, 988-1000. (doi:10.1016/j.cell.2012.01.038).

162. Sentelle R D, Senkal C E, Jiang W, Ponnusamy S, Gencer S, Selvam S P, Ramshesh V K, Peterson Y K, Lemasters J J, Szulc Z M, Bielawski J, and Ogretmen B. 2012. Ceramide targets autophagosomes to mitochondria and induces lethal mitophagy. *Nat Chem Biol*. **8**, 831-8. (doi:10.1038/nchembio.1059).

163. Adams E J. 2014. Lipid presentation by human CD1 molecules and the diverse T cell populations that respond to them. *Curr Opin Immunol*. **26**, 1-6. (doi:10.1016/j.coi.2013.09.005).

164. Huang S, Cheng T Y, Young D C, Layre E, Madigan C A, Shires J, Cerundolo V, Altman J D, and Moody D B. 2011. Discovery of deoxyceramides and diacylglycerols as CD1b scaffold lipids among diverse groove-blocking lipids of the human CD1 system. *Proc Natl Acad Sci U S A*. **108**, 19335-40. (doi:10.1073/pnas.1112969108).

165. Bejaoui K, Wu C, Scheffler M D, Haan G, Ashby P, Wu L, de Jong P, and Brown R H, Jr. 2001. SPTLC1 is mutated in hereditary sensory neuropathy, type 1. *Nat Genet*. **27**, 261-2. (doi:10.1038/85817).

166. Dawkins J L, Hulme D J, Brahmbhatt S B, Auer-Grumbach M, and Nicholson G A. 2001. Mutations in SPTLC1, encoding serine palmitoyltransferase, long chain base subunit-1, cause hereditary sensory neuropathy type I. *Nat Genet*. **27**, 309-12. (doi:10.1038/85879).

167. Rotthier A, Auer-Grumbach M, Janssens K, Baets J, Penno A, Almeida-Souza L, Van Hoof K, Jacobs A, De Vriendt E, Schlotter-Weigel B, Loscher W, Vondracek P, Seeman P, De Jonghe P, Van Dijck P, Jordanova A, Hornemann T, and Timmerman V. 2010. Mutations in the SPTLC2 subunit of serine palmitoyltransferase cause hereditary sensory and autonomic neuropathy type I. *Am J Hum Genet*. **87**, 513-22. (doi:10.1016/j.ajhg.2010.09.010).

168. Ernst D, Murphy S M, Sathiyanadan K, Wei Y, Othman A, Laura M, Liu Y T, Penno A, Blake J, Donaghy M, Houlden H, Reilly M M, and Hornemann T. 2015. Novel HSAN1 mutation in serine palmitoyltransferase resides at a putative phosphorylation site that is involved in regulating substrate specificity. *Neuromolecular Med*. **17**, 47-57. (doi:10.1007/s12017-014-8339-1).

169. Suriyanarayanan S, Auranen M, Toppila J, Paetau A, Shcherbii M, Palin E, Wei Y, Lohioja T, Schlotter-Weigel B, Schon U, Abicht A, Rautenstrauss B, Tyynismaa H, Walter M C, Hornemann T, and Ylikallio E. 2016. The Variant p.(Arg183Trp) in SPTLC2 Causes Late-Onset Hereditary Sensory Neuropathy. *Neuromolecular Med*. **18**, 81-90. (doi:10.1007/s12017-015-8379-1).

170. Penno A, Reilly M M, Houlden H, Laura M, Rentsch K, Niederkofler V, Stoeckli E T, Nicholson G, Eichler F, Brown R H, Jr., von Eckardstein A, and Hornemann T. 2010. Hereditary sensory neuropathy type 1 is caused by the accumulation of two neurotoxic sphingolipids. *J Biol Chem*. **285**, 11178-87. (doi:10.1074/jbc.M109.092973).

171. Gable K, Gupta S D, Han G, Niranjanakumari S, Harmon J M, and Dunn T M. 2010. A disease-causing mutation in the active site of serine palmitoyltransferase causes catalytic promiscuity. *J Biol Chem*. **285**, 22846-52. (doi:10.1074/jbc.M110.122259).

172. Bode H, Bourquin F, Suriyanarayanan S, Wei Y, Alecu I, Othman A, Von Eckardstein A, and Hornemann T. 2016. HSAN1 mutations in serine palmitoyltransferase reveal a close structure-function-phenotype relationship. *Hum Mol Genet*. **25**, 853-65. (doi:10.1093/hmg/ddv611).

173. Zitomer N C, Mitchell T, Voss K A, Bondy G S, Pruett S T, Garnier-Amblard E C, Liebeskind L S, Park H, Wang E, Sullards M C, Merrill A H, Jr., and Riley R T. 2009. Ceramide synthase inhibition by fumonisin B1 causes accumulation of 1-deoxysphinganine: a novel category of bioactive 1-deoxysphingoid bases and 1-deoxydihydroceramides biosynthesized by mammalian cell lines and animals. *J Biol Chem*. **284**, 4786-95. (doi:10.1074/jbc.M808798200).

174. Steiner R, Saied E M, Othman A, Arenz C, Maccarone A T, Poad B L, Blanksby S J, von Eckardstein A, and Hornemann T. 2016. Elucidating the chemical structure of native 1-deoxysphingosine. *J Lipid Res*. **57**, 1194-203. (doi:10.1194/jlr.M067033).

175. Rotthier A, Baets J, De Vriendt E, Jacobs A, Auer-Grumbach M, Levy N, Bonello-Palot N, Kilic S S, Weis J, Nascimento A, Swinkels M, Kruyt M C, Jordanova A, De Jonghe P, and Timmerman V. 2009. Genes for hereditary sensory and autonomic neuropathies: a genotype-phenotype correlation. *Brain*. **132**, 2699-711. (doi:10.1093/brain/awp198).

176. Auer-Grumbach M. 2008. Hereditary sensory neuropathy type I. *Orphanet J Rare Dis*. **3**, 7. (doi:10.1186/1750-1172-3-7).

177. Suh B C, Hong Y B, Nakhro K, Nam S H, Chung K W, and Choi B O. 2014. Early-onset severe hereditary sensory and autonomic neuropathy type 1 with S331F SPTLC1 mutation. *Mol Med Rep*. **9**, 481-6. (doi:10.3892/mmr.2013.1808).

178. Houlden H, King R, Blake J, Groves M, Love S, Woodward C, Hammans S, Nicoll J, Lennox G, O'Donovan D G, Gabriel C, Thomas P K, and Reilly M M. 2006. Clinical, pathological and genetic characterization of hereditary sensory and autonomic neuropathy type 1 (HSAN I). *Brain*. **129**, 411-25. (doi:10.1093/brain/awh712).

179. Garofalo K, Penno A, Schmidt B P, Lee H J, Frosch M P, von Eckardstein A, Brown R H, Hornemann T, and Eichler F S. 2011. Oral L-serine supplementation reduces production of neurotoxic deoxysphingolipids in mice and humans with hereditary sensory autonomic neuropathy type 1. *J Clin Invest*. **121**, 4735-45. (doi:10.1172/JCI57549).

180. Auranen M, Toppila J, Suriyanarayanan S, Lone M A, Paetau A, Tyynismaa H, Hornemann T, and Ylikallio E. 2017. Clinical and metabolic consequences of L-serine supplementation in hereditary sensory and autonomic neuropathy type 1C. *Cold Spring Harb Mol Case Stud*. **3**. (doi:10.1101/mcs.a002212).

181. Nicholson G A, *Hereditary Sensory Neuropathy Type IA*, in *GeneReviews((R))*, M.P. Adam, et al., Editors. 1993: Seattle (WA).

182. Alecu I, Othman A, Penno A, Saied E M, Arenz C, von Eckardstein A, and Hornemann T. 2017. Cytotoxic 1-deoxysphingolipids are metabolized by a cytochrome P450-dependent pathway. *J Lipid Res*. **58**, 60-71. (doi:10.1194/jlr.M072421).

183. Duan J and Merrill A H, Jr. 2015. 1-Deoxysphingolipids Encountered Exogenously and Made de Novo: Dangerous Mysteries inside an Enigma. *J Biol Chem*. **290**, 15380-9. (doi:10.1074/jbc.R115.658823).

184. Cuadros R, Montejo de Garcini E, Wandosell F, Faircloth G, Fernandez-Sousa J M, and Avila J. 2000. The marine compound spisulosine, an inhibitor of cell proliferation, promotes the disassembly of actin stress fibers. *Cancer Lett*. **152**, 23-9.

185. Alecu I, Tedeschi A, Behler N, Wunderling K, Lamberz C, Lauterbach M A, Gaebler A, Ernst D, Van Veldhoven P P, Al-Amoudi A, Latz E, Othman A, Kuerschner L, Hornemann T, Bradke F, Thiele C, and Penno A. 2017. Localization of 1-deoxysphingolipids to mitochondria induces mitochondrial dysfunction. *J Lipid Res*. **58**, 42-59. (doi:10.1194/jlr.M068676).

186. Salcedo M, Cuevas C, Alonso J L, Otero G, Faircloth G, Fernandez-Sousa J M, Avila J, and Wandosell F. 2007. The marine sphingolipid-derived compound ES 285 triggers an atypical cell death pathway. *Apoptosis*. **12**, 395-409. (doi:10.1007/s10495-006-0573-z).

187. Sanchez A M, Malagarie-Cazenave S, Olea N, Vara D, Cuevas C, and Diaz-Laviada I. 2008. Spisulosine (ES-285) induces prostate tumor PC-3 and LNCaP cell death by de novo synthesis of ceramide and PKCzeta activation. *Eur J Pharmacol*. **584**, 237-45. (doi:10.1016/j.ejphar.2008.02.011).

188. Zuellig R A, Hornemann T, Othman A, Hehl A B, Bode H, Guntert T, Ogunshola O O, Saponara E, Grabliauskaite K, Jang J H, Ungethuem U, Wei Y, von Eckardstein A, Graf R, and Sonda S. 2014. Deoxysphingolipids, novel biomarkers for type 2 diabetes, are cytotoxic for insulin-producing cells. *Diabetes*. **63**, 1326-39. (doi:10.2337/db13-1042).

189. Kramer R, Bielawski J, Kistner-Griffin E, Othman A, Alecu I, Ernst D, Kornhauser D, Hornemann T, and Spassieva S. 2015. Neurotoxic 1-deoxysphingolipids and paclitaxel-induced peripheral neuropathy. *FASEB J*. **29**, 4461-72. (doi:10.1096/fj.15-272567).

190. Jimenez-Rojo N, Sot J, Busto J V, Shaw W A, Duan J, Merrill A H, Jr., Alonso A, and Goni F M. 2014. Biophysical properties of novel 1-deoxy-(dihydro)ceramides occurring in mammalian cells. *Biophys J*. **107**, 2850-9. (doi:10.1016/j.bpj.2014.10.010).

191. da Silveira Dos Santos A X, Riezman I, Aguilera-Romero M A, David F, Piccolis M, Loewith R, Schaad O, and Riezman H. 2014. Systematic lipidomic analysis of yeast protein kinase and phosphatase mutants reveals novel insights into regulation of lipid homeostasis. *Mol Biol Cell*. **25**, 3234-46. (doi:10.1091/mbc.E14-03-0851).

192. Baryshnikova A, Costanzo M, Dixon S, Vizeacoumar F J, Myers C L, Andrews B, and Boone C. 2010. Synthetic genetic array (SGA) analysis in Saccharomyces cerevisiae and Schizosaccharomyces pombe. *Methods Enzymol*. **470**, 145-79. (doi:10.1016/S0076-6879(10)70007-0).

193. Young B P and Loewen C J. 2013. Balony: a software package for analysis of data generated by synthetic genetic array experiments. *BMC Bioinformatics*. **14**, 354. (doi:10.1186/1471-2105-14-354).

194. Michel A H, Hatakeyama R, Kimmig P, Arter M, Peter M, Matos J, De Virgilio C, and Kornmann B. 2017. Functional mapping of yeast genomes by saturated transposition. *Elife*. **6**. (doi:10.7554/eLife.23570).

195. Bauer C, Herzog V, and Bauer M F. 2001. Improved Technique for Electron Microscope Visualization of Yeast Membrane Structure. *Microsc Microanal*. **7**, 530-534. (doi:10.1017.S1431927601010522).

196. Haberkant P, Raijmakers R, Wildwater M, Sachsenheimer T, Brugger B, Maeda K, Houweling M, Gavin A C, Schultz C, van Meer G, Heck A J, and Holthuis J C. 2013. In vivo profiling and visualization of cellular protein-lipid interactions using bifunctional fatty acids. *Angew Chem Int Ed Engl*. **52**, 4033-8. (doi:10.1002/anie.201210178).

197. Bockelmann S, Mina J G M, Korneev S, Hassan D G, Muller D, Hilderink A, Vlieg H C, Raijmakers R, Heck A J R, Haberkant P, and Holthuis J C M. 2018. A search for ceramide binding proteins using bifunctional lipid analogs yields CERT-related protein StarD7. *J Lipid Res*. **59**, 515-530. (doi:10.1194/jlr.M082354).

198. Frokjaer-Jensen C, Davis M W, Hopkins C E, Newman B J, Thummel J M, Olesen S P, Grunnet M, and Jorgensen E M. 2008. Single-copy insertion of transgenes in Caenorhabditis elegans. *Nat Genet*. **40**, 1375-83. (doi:10.1038/ng.248).

199. Kamath R S, Martinez-Campos M, Zipperlen P, Fraser A G, and Ahringer J. 2001. Effectiveness of specific RNA-mediated interference through ingested double-stranded RNA in Caenorhabditis elegans. *Genome Biol*. **2**, RESEARCH0002. (doi:10.1186/gb-2000-2-1-research0002).

200. Glauser D A, Chen W C, Agin R, Macinnis B L, Hellman A B, Garrity P A, Tan M W, and Goodman M B. 2011. Heat avoidance is regulated by transient receptor potential (TRP) channels and a neuropeptide signaling pathway in Caenorhabditis elegans. *Genetics*. **188**, 91-103. (doi:10.1534/genetics.111.127100).

201. Menuz V, Howell K S, Gentina S, Epstein S, Riezman I, Fornallaz-Mulhauser M, Hengartner M O, Gomez M, Riezman H, and Martinou J C. 2009. Protection of C. elegans from anoxia by HYL-2 ceramide synthase. *Science*. **324**, 381-4. (doi:10.1126/science.1168532).

202. Kolaczkowski M, Kolaczkowska A, Gaigg B, Schneiter R, and Moye-Rowley W S. 2004. Differential regulation of ceramide synthase components LAC1 and LAG1 in Saccharomyces cerevisiae. *Eukaryot Cell*. **3**, 880-92. (doi:10.1128/EC.3.4.880-892.2004).

203. McNally F J. 2013. Mechanisms of spindle positioning. *J Cell Biol*. **200**, 131-40. (doi:10.1083/jcb.201210007).

204. Mao C, Xu R, Bielawska A, and Obeid L M. 2000. Cloning of an alkaline ceramidase from Saccharomyces cerevisiae. An enzyme with reverse (CoA-independent) ceramide synthase activity. *J Biol Chem*. **275**, 6876-84.

205. Mao C, Xu R, Bielawska A, Szulc Z M, and Obeid L M. 2000. Cloning and characterization of a Saccharomyces cerevisiae alkaline ceramidase with specificity for dihydroceramide. *J Biol Chem*. **275**, 31369-78. (doi:10.1074/jbc.M003683200).

206. Lackner L L. 2013. Determining the shape and cellular distribution of mitochondria: the integration of multiple activities. *Curr Opin Cell Biol*. **25**, 471-6. (doi:10.1016/j.ceb.2013.02.011).

207. Lackner L L. 2014. Shaping the dynamic mitochondrial network. *BMC Biol*. **12**, 35. (doi:10.1186/1741-7007-12-35).

208. Kornmann B, Currie E, Collins S R, Schuldiner M, Nunnari J, Weissman J S, and Walter P. 2009. An ER-mitochondria tethering complex revealed by a synthetic biology screen. *Science*. **325**, 477-81. (doi:10.1126/science.1175088).

209. Lill R and Muhlenhoff U. 2005. Iron-sulfur-protein biogenesis in eukaryotes. *Trends Biochem Sci*. **30**, 133-41. (doi:10.1016/j.tibs.2005.01.006).

210. Lill R, Fekete Z, Sipos K, and Rotte C. 2005. Is there an answer? Why are mitochondria essential for life? *IUBMB Life*. **57**, 701-3. (doi:10.1080/15216540500305860).

211. Dikalov S I and Harrison D G. 2014. Methods for detection of mitochondrial and cellular reactive oxygen species. *Antioxid Redox Signal*. **20**, 372-82. (doi:10.1089/ars.2012.4886).

212. Foury F, Roganti T, Lecrenier N, and Purnelle B. 1998. The complete sequence of the mitochondrial genome of Saccharomyces cerevisiae. *FEBS Lett*. **440**, 325-31.

213. Marshall L L, Stimpson S E, Hyland R, Coorssen J R, and Myers S J. 2014. Increased lipid droplet accumulation associated with a peripheral sensory neuropathy. *J Chem Biol*. **7**, 67-76. (doi:10.1007/s12154-014-0108-y).

214. Esaki K, Sayano T, Sonoda C, Akagi T, Suzuki T, Ogawa T, Okamoto M, Yoshikawa T, Hirabayashi Y, and Furuya S. 2015. L-Serine Deficiency Elicits Intracellular Accumulation of Cytotoxic

Deoxysphingolipids and Lipid Body Formation. *J Biol Chem*. **290**, 14595-609. (doi:10.1074/jbc.M114.603860).

215. Jones G M, Stalker J, Humphray S, West A, Cox T, Rogers J, Dunham I, and Prelich G. 2008. A systematic library for comprehensive overexpression screens in Saccharomyces cerevisiae. *Nat Methods*. **5**, 239-41. (doi:10.1038/nmeth.1181).

216. Abegg D, Frei R, Cerato L, Prasad Hari D, Wang C, Waser J, and Adibekian A. 2015. Proteome-Wide Profiling of Targets of Cysteine reactive Small Molecules by Using Ethynyl Benziodoxolone Reagents. *Angew Chem Int Ed Engl*. **54**, 10852-7. (doi:10.1002/anie.201505641).

217. Epstein S, Castillon G A, Qin Y M, and Riezman H. 2012. An essential function of sphingolipids in yeast cell division. *Molecular Microbiology*. **84**, 1018-1032. (doi:10.1111/j.1365-2958.2012.08087.x).

218. Breslow D K, Cameron D M, Collins S R, Schuldiner M, Stewart-Ornstein J, Newman H W, Braun S, Madhani H D, Krogan N J, and Weissman J S. 2008. A comprehensive strategy enabling high-resolution functional analysis of the yeast genome. *Nat Methods*. **5**, 711-8. (doi:10.1038/nmeth.1234).

219. Narita T, Naganuma T, Sase Y, and Kihara A. 2016. Long-chain bases of sphingolipids are transported into cells via the acyl-CoA synthetases. *Sci Rep*. **6**, 25469. (doi:10.1038/srep25469).

220. Funato K, Lombardi R, Vallee B, and Riezman H. 2003. Lcb4p is a key regulator of ceramide synthesis from exogenous long chain sphingoid base in Saccharomyces cerevisiae. *J Biol Chem*. **278**, 7325-34. (doi:10.1074/jbc.M209925200).

221. Tojkander S, Gateva G, and Lappalainen P. 2012. Actin stress fibers--assembly, dynamics and biological roles. *J Cell Sci*. **125**, 1855-64. (doi:10.1242/jcs.098087).

222. Goode B L, Eskin J A, and Wendland B. 2015. Actin and endocytosis in budding yeast. *Genetics*. **199**, 315-58. (doi:10.1534/genetics.112.145540).

223. Haberkant P and Holthuis J C. 2014. Fat & fabulous: bifunctional lipids in the spotlight. *Biochim Biophys Acta*. **1841**, 1022-30. (doi:10.1016/j.bbalip.2014.01.003).

224. Hannich J T, Mellal D, Feng S, Zumbuehl A, and Riezman H. 2017. Structure and conserved function of iso-branched sphingoid bases from the nematode Caenorhabditis elegans. *Chemical Science*. **8**, 3676-3686. (doi:10.1039/C6SC04831E).

Acknowledgements

Foremost, I would like to express my sincere gratitude to my supervisor, Prof. Howard Riezman for the opportunity to develop myself to become a scientist by allowing me to work on this project, for his trust, patience, immense knowledge, constant support, motivation, and enthusiasm trough the study. I am afraid that I will not have such a privilege again in my next steps. I would also like to thank all members of Riezman Lab who help me personally and technically during my study. If I have to single out, I wish to present my special thanks to Thomas Hannich with whom I worked closely on the project.

I would like to extend my gratitude to our collaborators who made this study possible; Prof. Maya Schuldiner and Marton Megyeri at Weizmann Institute of Science for assisting me with the first genetic screen, Prof. Benoit Kornmann and Agnes Michel at ETH Zurich for helping me with the second genetic screen, Per Haberkant at EMBL Heidelberg for the pac-fatty acid, Michaël Plank at University of Geneva for the proteomic analysis, Prof. Dominique Glauser at University of Fribourg for the thermotaxis assay, Fabrice David at EPFL for the bioinformatic work, the bioimaging and genomic platforms, and ACCESS Geneva at the university.

I am also grateful to our funding bodies; NCCR chemical biology, Marie Curie ITN Sphingonet, and iGE3.